The Redoxchemistry of Azobenzene Photoswitches for Energy Storage

---

Inauguraldissertation zur Erlangung des Doktorgrades (Dr. rer. nat.)
der Naturwissenschaftlichen Fachbereiche im Fachgebiet Chemie
der Justus-Liebig-Universität Gießen

vorgelegt von

Dominic Schatz

Betreuer: Prof. Dr. Hermann A. Wegner

Gießen 2025

Versicherung Nach §17 der Promotionsordnung

Ich erkläre: Ich habe die vorgelegte Dissertation selbstständig und ohne unerlaubte fremde Hilfe und nur mit den Hilfen angefertigt, die ich in der Dissertation angegeben habe. Alle Textstellen, die wörtlich oder sinngemäß aus veröffentlichten Schriften entnommen sind, und alle Angaben, die auf mündlichen Auskünften beruhen, sind als solche kenntlich gemacht. Ich stimme einer evtl. Überprüfung meiner Dissertation durch eine Antiplagiat-Software zu. Bei den von mir durchgeführten und in der Dissertation erwähnten Untersuchungen habe ich die Grundsätze guter wissenschaftlicher Praxis, wie sie in der „Satzung der Justus-Liebig-Universität Gießen zur Sicherung guter wissenschaftlicher Praxis“ niedergelegt sind, eingehalten.

Dominic Schatz Ort, Datum

Dekan: Prof. Dr. Holger Zorn
Erstgutachter: Prof. Dr. Hermann A. Wegner
Zweitgutachter: Prof. Dr. Richard Göttlich

If I am guilty of anything it is the simple pursuit of knowledge.

— Magnus the Red

There is nothing like looking, if you want to find something. You certainly usually find something, if you look, but it is not always quite the something you were after.

— Thorin Oakenshield

You are not prepared!

— Illidan Stormrage

Table of Content

Abstract

There is a variety of applications for azobenzenes (AB) that can be traced back to mainly three properties: Their bright coloration, their reversible photoisomerization, and their redox chemistry. These inherent properties are the foundation for most of AB use cases, ranging from simple dye stuff to photopharmacology. An additional topic that emerged in the recent years is their application in energy storage materials.

On one hand, the reversible isomerization from the stable (*E*)-isomer to the metastable (*Z*)-isomer can be used in molecular solar thermal energy storage (MOST). Hereby, the energy difference between both isomers is stored upon irradiation, and is released as useable heat during back isomerization. Ideally, a MOST candidate should show efficient isomerization under solar irradiation, possess a thermal half-life that is suitable for the intent storage application, and demonstrate a large energy density. We established a 2,6-difluoro substituted AB for MOST as a thermally stable switch, that can be charged with green light. One of the most important features of this AB is the low viscosity resulting in an easy to handle, pumpable, and storable liquid MOST material. Due to the low molecular weight of this compound, it shows the highest energy density in comparison to known liquid ABs. We were able to prepare efficiently large quantities of this AB in a continuous flow reactor (3.7 g h^{-1}), and also realized the isomerization in a flow photoreactor. The liquid AB can act as a MOST-active solvent carrying higher energy density norbornadienes and can also dissolve organic salts to increase its electric conductivity. The observable conductivity allows to trigger the heat release electro-catalytically thereby harvesting the total stored heat energy.

On the other hand, their reversible redox behaviour can be used in electrochemical energy storage. Due to the reversible reduction to a radical anion, ABs have been employed as anolytes in, for example, redox flow batteries. Herein, we introduced AB as a catholyte material. The addition of dialkyl amino substituents at the *para*-positions opens the potential of a reversible oxidative behaviour. This property is ascribed to the formation of a quinoidal system that is stable over the time scale of a cyclic voltammetry experiment. The underlying mechanism of this oxidation reaction was confirmed by the isolation of a quinoidal solid state structure after chemical oxidation. Furthermore, we expanded the range of suitable 4,4’-diamino AB to their azoxybenzene (AOB) derivatives, and showed that they possess similar redox behaviour. In charge/discharge cycling experiments of the oxidation, decomposition of AB and AOB compounds were observed over multiple cycles. This hinders their successful application in large scale electro chemical energy storages. An intermediate radical cation was presumed as a possible decomposition pathway.

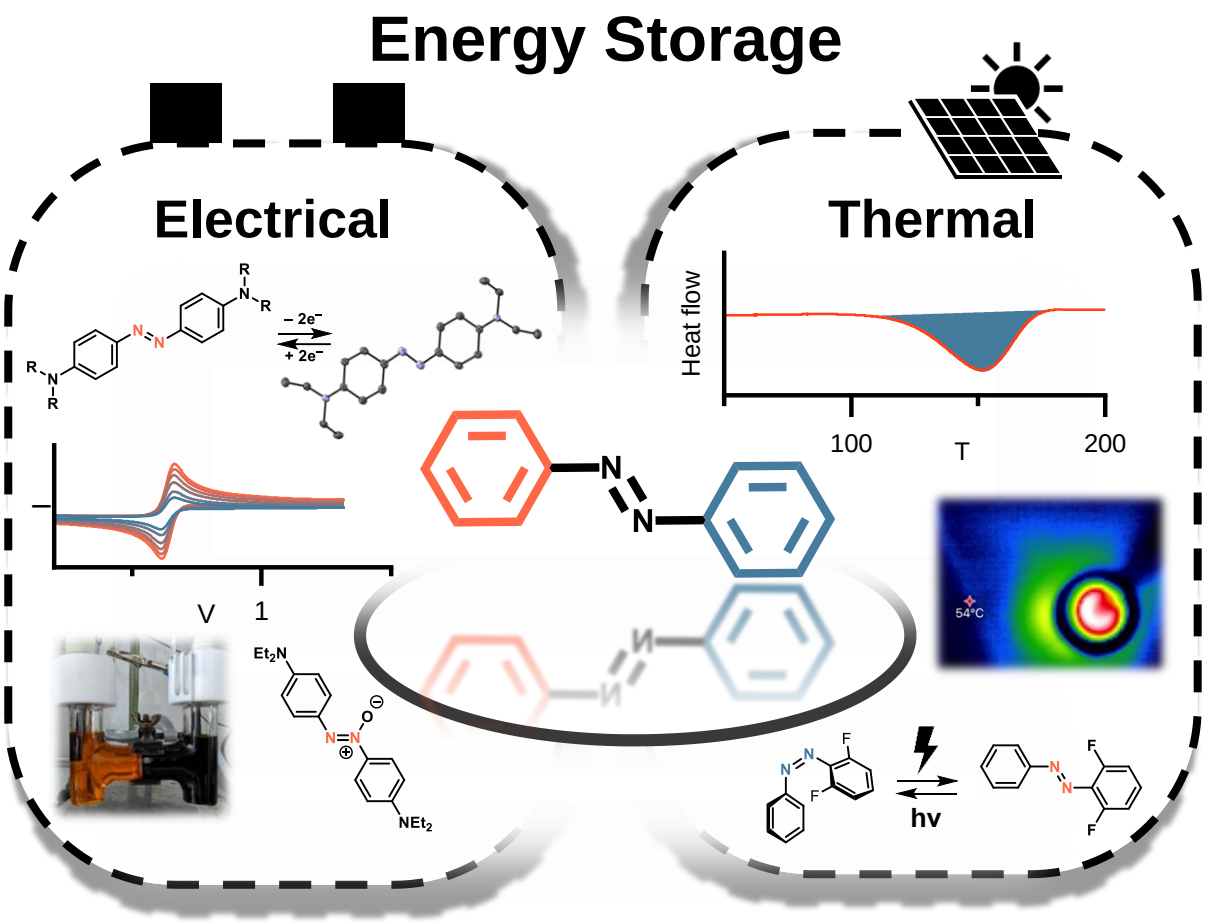

Understanding the redox behaviour of AB is crucial for their electrochemical storage solutions, and also for their electro-catalytic isomerization in MOST materials. We hereby give an introduction to ABs, their different redox properties, and their respective applications for energy storage solutions.

Zusammenfassung

Azobenzole (AB) finden in einer Vielzahl von Anwendungen Verwendung, was sich hauptsächlich auf drei grundlegenden Eigenschaften zurückführen lässt: Ihre intensive Farbgebung, ihre reversible Photoisomerisierung und ihre Redoxchemie. Diese Merkmale bilden die Basis für die meisten Applikationen von AB, die von einfachen Farbstoffen bis hin zur Photopharmakologie reichen. Ein zusätzliches Thema, das sich in den letzten Jahren als wichtiger Gegenstand der Forschung herausgestellt hat, ist ihre Anwendung als Energiespeichermaterialien.

Einerseits kann die reversible Isomerisierung vom stabilen (*E*)- zum metastabilen (*Z*)-Isomer in molekularen Solarthermiespeichern (MOST) genutzt werden. Dabei wird die Energiedifferenz zwischen beiden Isomeren während der Bestrahlung gespeichert, und bei der Rückisomerisierung als nutzbare Wärmeenergie freigesetzt. Idealerweise sollte ein MOST-Kandidat eine effiziente Isomerisierung unter Sonneneinstrahlung zeigen, eine thermische Halbwertszeit besitzen, die für die beabsichtige Speicheranwendung geeignet ist, und eine möglichst hohe Energiedichte aufweisen. Wir haben 2,6-difluoriertes AB für eine mögliche MOST-Anwendung eingeführt. Diese Verbindung besitzt eine hohe Halbwertszeit und kann mit grünem Licht in das (*Z*)-Isomer überführt werden. Aufgrund des geringen Molekulargewichts unserer Verbindung weist sie die höchste Energiedichte im Vergleich zu bekannten flüssigen ABs auf. Wir waren in der Lage, den Photoschalter in einem kontinuierlichen Durchflussreaktor in großem Maßstab (3,7 g h^{-1}) herzustellen, sowie die Isomerisierung in einem kontinuierlichen Durchflussphotoreaktor effizient durchzuführen. Das flüssige AB kann als MOST-aktives Lösungsmittel fungieren und Norbornadiene mit höherer Energiedichte, sowie organische Salze zur Erhöhung der elektrischen Leitfähigkeit lösen. Die beobachtete Leitfähigkeit ermöglicht es, die Wärmefreisetzung elektro-katalytisch auszulösen und so die gesamte gespeicherte Wärmeenergie zu erhalten.

Andererseits kann das reversible Redoxverhalten bei der elektrochemischen Energiespeicherung genutzt werden. Aufgrund der reversiblen Reduktion zu einem Radikalanion wird AB als Anolyt z.B. in Redox-Fluss-Batterien eingesetzt. Durch Substitution des AB Gerüsts mit Dialkylamino-Gruppen an den *para*-Positionen kann auch ein reversibles oxidatives Verhalten beobachtet werden. Dies wird auf die Bildung eines chinoidalen Systems zurückgeführt, welches auf der Zeitskala eines Cyclovoltammetrieexperiments stabil ist. Der zugrundeliegende Mechanismus dieser Oxidationsreaktion wurde durch die Isolierung einer chinoidalen Festkörperstruktur nach chemischer Oxidation bekräftigt. Wir haben die 4,4‘-diamino-substituierten ABs mit den strukturell ähnlichen Azoxybenzolen (AOBs) verglichen und haben gezeigt, dass sie ein ähnliches Redoxverhalten aufweisen. Bei Lade-Entlade-Zyklisierexperimenten der Oxidation wurde eine Zersetzung beider Strukturklassen über mehrere Zyklen hinweg beobachtet. Diese Instabilität hemmt ihre erfolgreiche Anwendung in elektrochemischen Energiespeichern. Ein möglicher Zersetzungsweg über ein intermediäres Radikalkation wird vermutet.

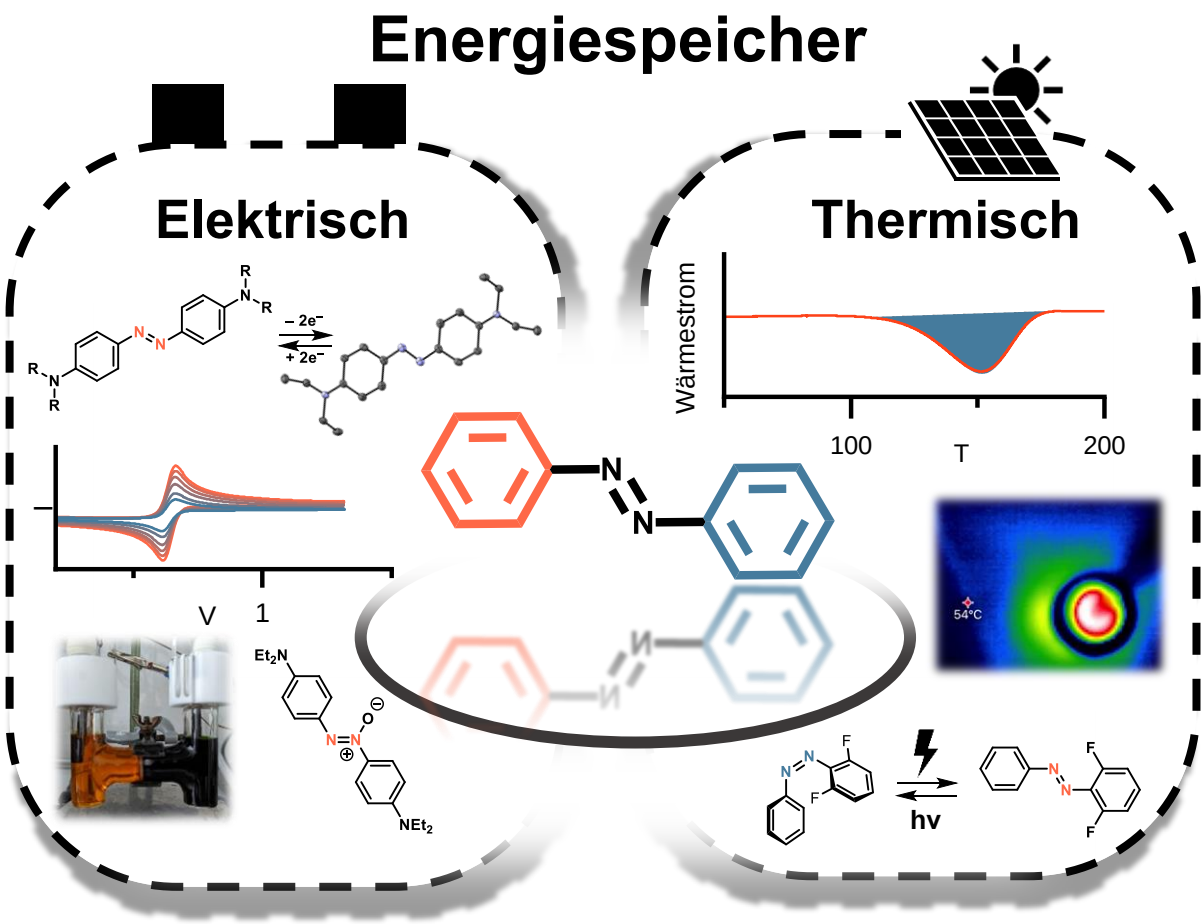

Da das Verständnis des Redoxverhalten von ABs für elektrochemische Speichertechnologien, aber auch für die elektrokatalytische Isomerisierung in MOST Anwendungen von entscheidender Bedeutung ist, stellen wir hier eine Einführung von ABs, ihren verschiedene Redoxeigenschaften sowie ihrer jeweiligen Anwendungen für Energiespeicherlösungen vor.

1 Azobenzene Photoswitches

Undoubtedly, azobenzenes (AB) belong to a class of privileged structures, which have been studied extensively in the literature, be it their synthesis, properties, or their versatile application. ABs have been an important research topic since their discovery by Mitscherlich in the middle of the 19th century.[1] Due to their intense colour, their scalable production, and their straightforward preparation, they became an important class in the dye industry.[2] Colour and textile industries were complemented by the prodrug behaviour of sulfonamide AB,[3,4] until Hartley observed the (*E*)- and (*Z*)-isomerism during solubility measurements using photometry.[5] The ability to switch between both states *via* light, together with their intrinsic photoresistance, made ABs promising candidates for molecular photoswitches.[6] Since Hartley's seminal discovery, they have found their way into nearly every subtopic in chemistry or material science.

1.1 Fundamentals of Azobenzene Photochemistry

Pristine (*E*)-AB **1** shows an absorption maximum at around 325 nm, which can be assigned to the π-π* transition. A weaker n-π* transition can be observed at 425 nm. (*Z*)-AB **1** on the other hand displays a decrease in the π-π* transition intensity, and an increase in the n-π* transition, with both absorptions being slightly shifted in comparison to the (*E*)-isomer (Figure 1).[7] Generally, excitation of the (*E*)-π-π* band leads to formation of (*Z*)-isomer, and irradiation in the n-π* transition leads to formation of (*E*)-isomer. As the (*Z*)-isomer of unsubstituted AB is thermodynamically less stable, it can thermally isomerize back to the ground state. The half-life of the (*Z*)-isomer is dependent on the considered derivative, solvent, additives and temperature, and can be everywhere between the nanosecond[8] and thousands of years timescale.[9] The switching of AB does not only change its absorption properties, but also its solubility,[10,11] dipole moment,[12] basicity,[13,14] volume and the end-to-end distance.[15,16] These switchable properties allowed ABs to be *inter alia* used in lithography,[17,18] as actuators in polymers,[19,20] in photopharmacology,[21,22] as molecular wind-up meters,[23–26] or as molecular machines.[27,28]

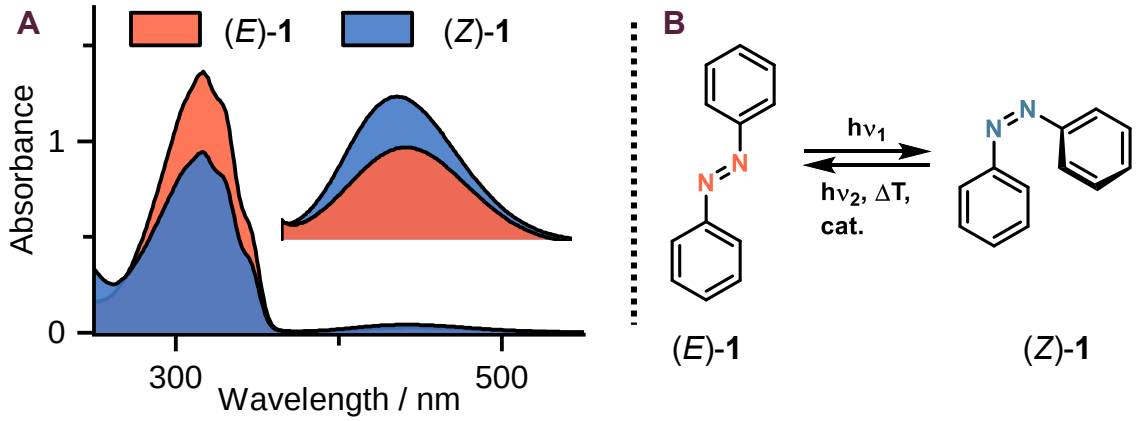

Figure 1. A) UV-Vis spectra of pristine AB **1** in *n*-decane.[7] B) The photoisomerization of AB **1**.

An additional application of ABs that emerged in recent years, most probably due to the rise in renewable energy production, is the storage of energy.[29] As the generation of energy from sun or wind is intermittent and decoupled from energy consumption, energy storage solutions are necessary to ensure a stable power grid.[30] The majority of the required energy types are electrical and thermal energy. As interconversions between energy types are not perfectly efficient, it would be advantageous to store energy in the later required form.[31]

ABs can be used in both types of storage, highlighting again the versatility of this privileged compound. The reversible redox chemistry of ABs, which allows them to be used in batteries as an electrochemical storage, will be discussed in a section below. The photoisomerization to an energetically higher metastable state can be used as a solar thermal energy storage. The technology behind this is called molecular solar thermal energy storage (MOST),[32] and the idea of storing solar irradiation as thermal energy in photoswitches originates from the early 20th century by Weigert, who investigated the photodimerization of anthracene.[33–35] Since then, multiple possible structures have been introduced, all exhibiting different advantages and disadvantages. Various extensive reviews deal with in-depth comparison of these photoswitchable molecules,[36–43] but herein we will mainly focus on AB, and how to optimize its MOST properties.

1.2 Azobenzene in Molecular Solar Thermal Energy Storage Systems

A MOST cycle typically consist of four consecutive steps that a mostophore undergoes during a store/release, or charge/discharge cycle (Figure 2).

A) A photoswitchable molecule in its groundstate is irradiated with light of a specific wavelength to an excited state.

B) The excited state relaxes into a metastable state, which is generated in a high percentage.

C) The metastable state is significantly higher in energy than the ground state, but has an activation barrier for the back isomerization that is suitable for the storage duration.

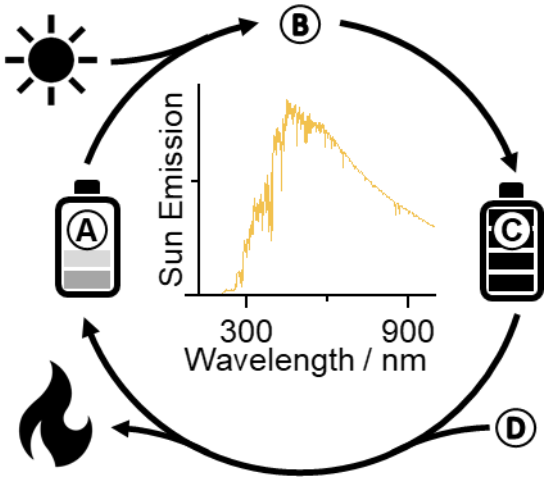

Figure 2. Schematic representation of a typical MOST cycle from **A** to **D**, and the AM 1.5 standard solar emission spectrum.

D) An external stimulus, e.g. thermally, photochemically or catalytically, triggers the back isomerization to release the stored energy. The resulting thermal energy is collected and used. The ground state is generated back without decomposition, and the molecule is available for an additional cycle.

Each of these steps is sensitive to molecular engineering of the employed molecule, and offers the possibility to optimize MOST properties.

As the maximum of the solar emission spectrum is in the visible range (Figure 2), and the absorption maximum of unsubstituted AB is in the UV region, red-shifting is an important step to increase the solar match. The introduction of electron-donating or electron-withdrawing substituents at one or both phenyl rings leads to “push-pull” or “push-push” ABs. These show a significant red-shift in comparison to unsubstituted AB but at the cost of their half-lives. Additionally, they often show overlapping π-π* and n-π* transitions that make individual addressing of (*E*)- and (*Z*)-states difficult. An additional possibility to allow solar switching is to increase the gap between the n-π* transition of (*E*)- and (*Z*)-isomers, so that efficient switching can be achieved by irradiation in these usually overlapping bands (Figure 3). Wooley introduced bulky electron-rich substituents in the *ortho*-positions, which force the phenyl rings of the (*E*)-isomer out of planarity and result in destabilizing interactions between the substituent and the nitrogen lone pairs.[44] This leads to a red-shift of the n-π* transition of the (*E*)-isomer, while the (*Z*)-isomer is less affected. A gap of the absorption maxima of 28 nm for the model compound **2** can be observed. Substitution with ethers[45] or thioethers[46] diminish the half-lives of their (*Z*)-isomer, and are therefore not ideal for energy storage. Hecht pioneered the introduction of electron-withdrawing substituents, like fluorine, in the *ortho*-positions.[47–49] These stabilize the π* orbital of both isomers, and the n orbitals of the (*Z*)-isomer, which overall results in a red shift of the n-π* transition of the (*E*)-isomer, and a blue shift of n-π* transition of the (*Z*)-isomer, which leads to well-separated bands. The model substrate **3** shows a maximum gap of 42 nm, which allows the efficient switching with green light.

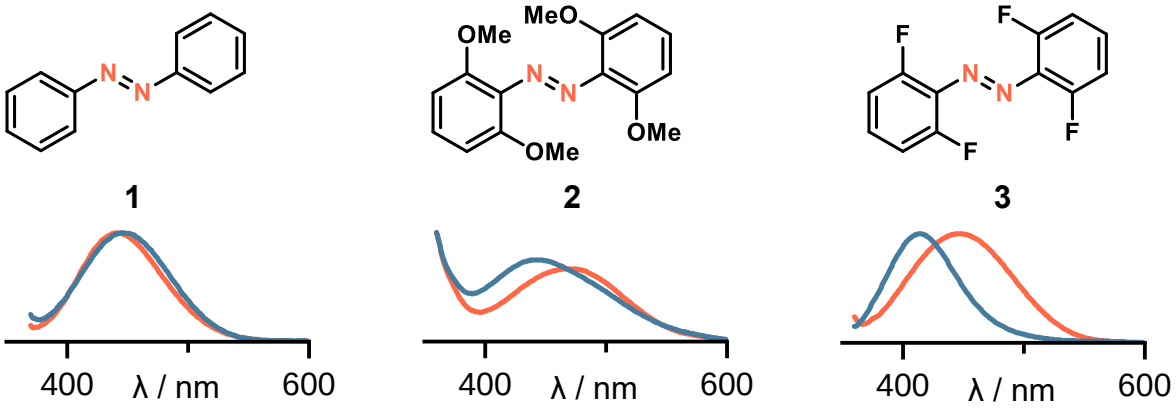

$\Delta\lambda_{n-\pi^*}$ = 14 nm

$\Delta\lambda_{n-\pi^*}$ = 28 nm
$PSS_{530\ nm}$ = 17:83
$PSS_{365\ nm}$ = 67:33

$\Delta\lambda_{n-\pi^*}$ = 42 nm
$PSS_{>500\ nm}$ = 14:86
$PSS_{410\ nm}$ = 91:9

Figure 3. The n-π* bands of (*E*)- and (*Z*)-isomers of pristine AB **1 ,** di-*ortho*-substituted methoxy AB **2** by Wooley,[45] and fluorine AB **3** by Hecht.[47] The larger peak separation allows the isomerization to proceed under green light irradiation. Photostationary states (PSS) given as (*E*):(*Z*)-isomer ratio. The orange trace corresponds to the (*E*)-isomer, the blue to the (*Z*)-isomer.[48,50]

Displacement of one phenyl ring in AB with electron rich heterocycles can also alter the isomerization wavelength, by changing the electronic nature of one side of the diazo unit, forming a “push-pull” motif, with very tuneable half-lives.[51–54] The obtained (*E*)/(*Z*)-ratio in the photostationary state (PSS) is an important characteristic for MOST systems as well. High (*Z*)-content during charging is important to achieve the highest possible energy density, while high (*E*)-content during (photochemical)-discharging is important for the complete heat release of the stored energy.

In addition to the absorption wavelength of the photoswitch, the efficiency of the isomerization process, the obtained (*E*)/(*Z*)-ratio and the half-life are important parameters. The PSS obtained at any given wavelength is *inter alia* dependent on the excitation coefficient and the quantum yield at this wavelength.[55] Hence, a large band separation between both isomers is necessary for an efficient MOST compound, as observed in the examples above. Consequentially, another possibility to increase the PSS during charging is to decrease the absorption of the (*Z*)-isomer. One way to achieve this is to exploit the T-shaped (*Z*)-isomer of some selected azoheteroarenes.[56] This highly symmetrical geometry significantly lowers the absorption of the symmetry-forbidden n-π* transition.[57] Complementary, *ortho*-amino substituents add additional π-π* transitions in the (*E*)-isomer, allowing very efficient solar irradiation uptake.[58–60] Combining a bis-azoheteroarene and *ortho*-amino groups can shift the maximal wavelength for (*E*)- to (*Z*)-isomerization even further.[61]

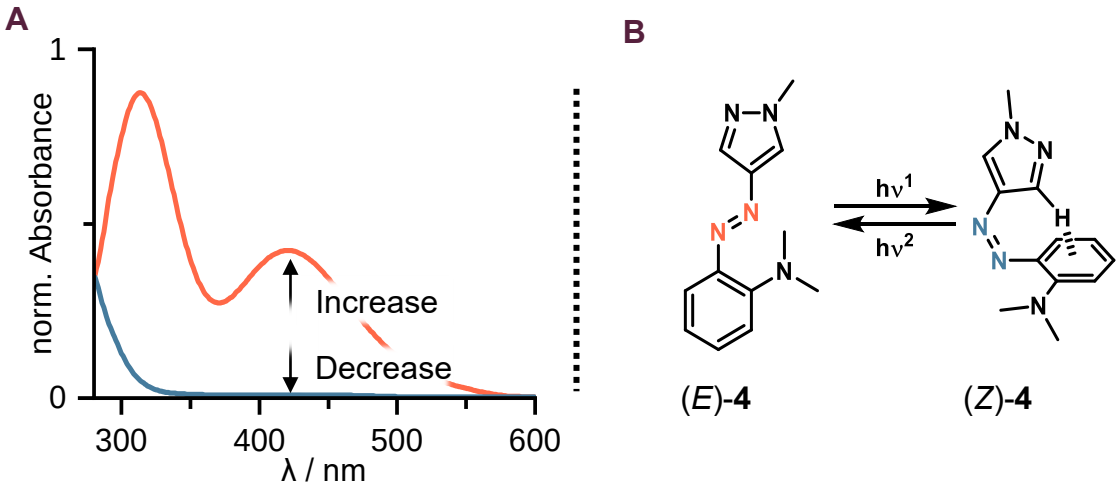

Figure 4. A) A schematic representation of the photochemical modification strategy that allows for high (*Z*)-content at the PSS upon solar irradiation.[56] B) The geometry change to a highly symmetrical T-shaped (*Z*)-isomer of azoheteroarene **4** upon photoisomerization. The orange trace corresponds to the (*E*)-isomer, the blue to the (*Z*)-isomer. Reproduced under terms of the CC BY license.

Even if a MOST compound shows great solar absorption, a high PSS and an appropriate half-life, their practical usage is dependent on the maximum amount of possibly stored energy. In previous literature, the minimal heat energy that a potential storage material needs is specified as over 300 kJ kg^{-1}, as these are the storage values of conventional systems.[62,39] The stored energy is directly proportional to the energy difference between (*E*)- and (*Z*)-isomer. Conceptually, increasing the energy gap between ground- and metastable state is straightforward: Either by destabilizing the

storage state (**B**), or by stabilizing the ground state (**A**, Figure 5). The (*Z*)-state can be destabilized by incorporation of the switching unit into a (macro)cyclic scaffold, so that upon photoisomerization, the induced strain increases the energy level of the switch.[63] It is important to fine-tune the scaffold, as a twisted conformation of the (*Z*)-isomer can result in less observed strain,[64] or can even become the thermodynamically more stable isomer.[65,66] By densely packing multiple ABs on a rigid backbone, the more spacious (*Z*)-isomers can show repulsive interactions with each other, destabilizing the storage state.[67–69] Strategies for stabilizing the ground state can be based on intermolecular London Dispersion interactions in the (*E*)-state,[70] or by π-stacking.[71]

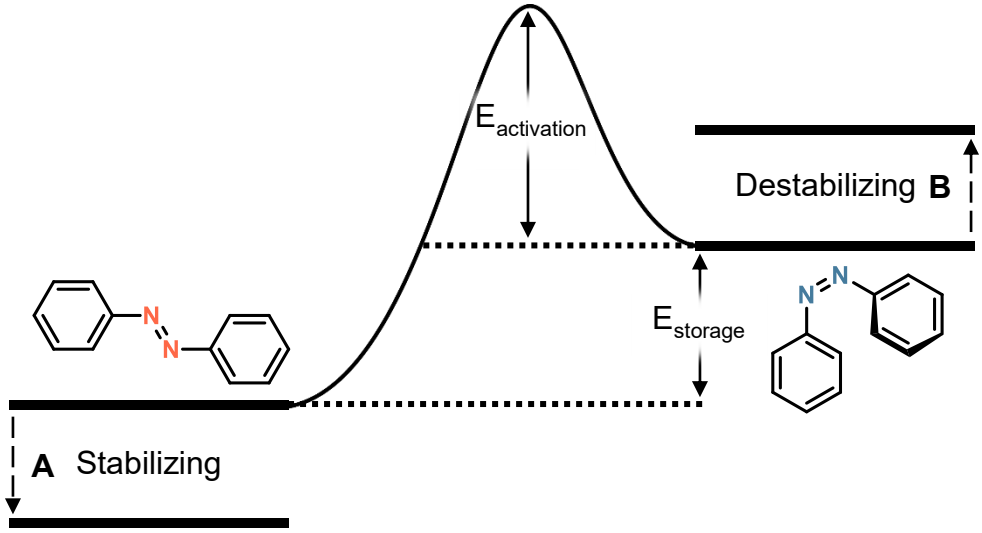

Figure 5. Energy scheme that presents the energy difference of AB photoisomers, and the strategies to improve the energy difference between storage and metastable state. **A**) Stabilization of the ground state. **B**) Destabilization of the metastable state.

If the melting point of the (*E*)-isomer is higher than of the corresponding (*Z*)-isomer, photoisomerization can be accompanied by a phase change from solid to liquid of the employed compound.[72,73] This means that upon back isomerization, the released isomerization enthalpy is bolstered by a release of latent heat. These phase change materials can show very promising energy densities and are currently explored for MOST applications.[74–77]

An important aspect of these compounds is that they are usually not used in the neat state. Mostly, AB (or MOST materials in general) are studied in a diluted solution in organic solvents, to allow quick and homogeneous isomerization. This drastically lowers the energy density, and is often overlooked in MOST studies. Although there are some examples of neat MOST materials,[78,79] most of their photophysical properties are still studied in solution, and even their heat release is measured diluted.[80] Additionally, most liquid ABs rely on the introduction of long, sometimes branched, alkyl chains, to add flexibility, break the symmetry, and hinder π–π interactions of the phenyl units (Figure 6). These additional groups increase the synthetic effort, lower efficiency of the storage material, and decrease the energy density due to the additional molecular weight. For genuine applications, the usage of neat samples is associated with multiple problems, *inter alia* the inner filter effect and the viscosity, making pumping and storing of the MOST material harder.[81]

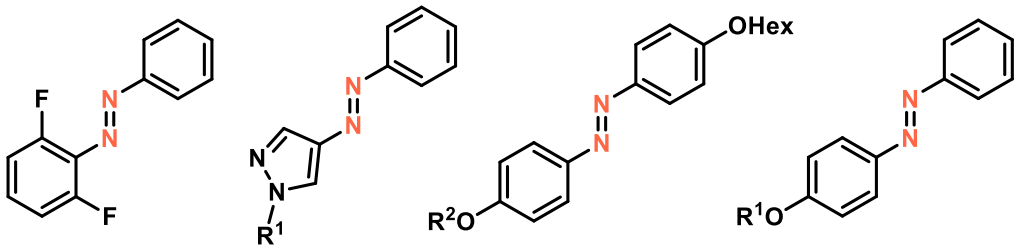

5	**6**	**7**	**8**	
218	310	957	284	MW / g mol^{-1}
218	168	48.2	144	$\Delta H_{storage}$ / kJ kg^{-1}

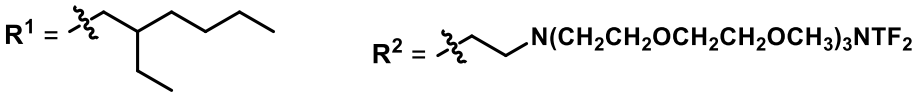

Figure 6. Structures and properties of liquid state AB in the literature. Compounds **6**-**8**[82–84] were reported by Kimizuka, compound **5** by Hecht[48] and our group.[85] The energy densities are calculate for 100% (*Z*)-isomer.

The last step in the MOST cycle is the energy release. For some applications, it may be beneficial to release heat over time following the ordinary thermal relaxation, like in heat storing fabrics,[86] or energy-saving windows.[87] However, a controlled and complete release is usually desired. This can be achieved photochemically by irradiation with a wavelength suitable for (*Z*)- to (*E*)-isomerization, or by catalytic processes involving acids or metals.[88–90] One of the most promising and efficient methods to induce rapid back isomerization is the utilization of ABs' redox chemistry, where electrons or holes are used to induce energy release.[91,92]

To tackle most of these photophysical problems, we introduced liquid 2,6-difluoro AB **5** that shows a very low viscosity (η = 9.9 mPas) and does not contain long, branched alkyl chains.[85] This results in a low molecular weight, and therefore a high energy storage density. The low viscosity allows efficient irradiation in a continuous flow reactor to ensure quick isomerization (Figure 7, A). Furthermore, this *ortho*-disubstituted compound can be isomerized using green light which enhances the spectral overlap with the emission spectra of the sun. Additionally, the liquid AB can act as a solvent and dissolve higher energy MOST materials like norbornadienes to further tune the absorption and heat storage of this mixed material. The heat release can either be started by irradiation with blue light (Figure 7, A), by addition of a catalytic amount of acid (Figure 7, B) or by an electrochemical trigger. To improve the efficiency of the electrochemical trigger, the conductivity of the MOST liquid can be improved by dissolution of an electrolyte.

As the redox chemistry of AB is the basis for its application in electrochemical energy storage and for the mentioned electro-catalytic isomerization, it will be discussed in the following chapter. Parts of the following section have been published as a review by our group beforehand.[93]

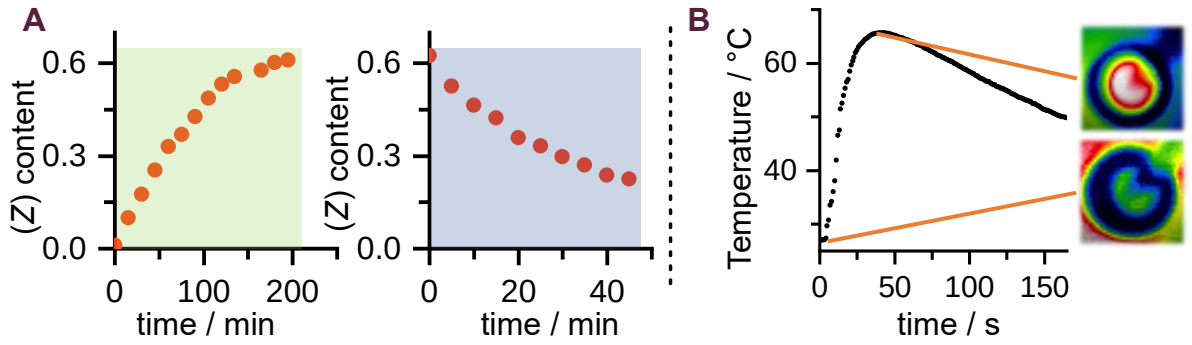

Figure 7. A) Change in the (*Z*)-isomer content during green light (left) and blue light (right) irradiation of neat AB **5** pumped through a 10 mL tube reactor. The irradiation was conducted by a simple home-made setup using an LED strip intended for ambient light irradiation. B) Macroscopic heat release of 1 mL AB **5** after addition of a catalytic amount of acid measured by an *in situ* thermometer and visualized using an IR camera.

2 Redoxchemistry of Azobenzenes

The incorporation of nitrogen atoms into a molecular scaffold significantly alters the electronic nature.[94] The HOMO and LUMO of acenes are, for example, both lowered with increasing nitrogen content.[95,96] Comparing the molecular orbitals of pentacene and diazapentacene, the HOMO is lowered from –4.6 to –5.1 eV, while the LUMO is lowered from –2.7 to –3.3 eV. Following Koopmans' theorem, these orbital properties affect photophysical and electrochemical quantities.[97,98] Similarly, 2,3-diaza-anthraquinone can be reduced by +450 mV more easily then pristine anthraquinone.[99] Comparing AB to its carbon-based derivative stilbene, shows a less facile reduction wave shifted by more than 800 mV.[100,101] The electrochemical properties of arenes can further be altered by increasing π-delocalization,[102] and in the case of oligo-stilbenes, the reduction potential can range from –2.25 to –1.97 V (vs. Ag/AgCl) depending on the number of *para*-connected stilbene units.[103] Therefore, AB as a nitrogen-containing, π-extended compound has generated interest as a redox active-material in electrochemical energy storage systems.[104]

2.1 Azobenzene Redox States

Nitrogen-containing organic compounds that are related to ABs, either by synthesis, degradation or structure, can show nearly all oxidation states in the range from –III to +III (Figure 8). Consequently, the redox chemistry of AB is complex and has been studied thoroughly. The significance of understanding and expanding AB redox chemistry can be seen in the chemistry of the Nobel prize from 1939. Domagk from IG Farben studied the effect of sulfonated ABs against bacterial infections. He observed that some azo compounds show a clear difference of their antibacterial properties between *in vivo* and *in vitro* experiments.[3] The *in vivo* effect of Prontosil, an AB molecule used as a prodrug for the first sulfonamide active ingredient, was ascribed to the metabolic reduction of the N=N bond to a free aniline.[4]

The metabolic degradation of ABs can occur oxidatively by ring hydroxylations,[105] by *N*'-demethylation of dialkylamino-ABs,[106] or reductively in the cyctochrome P-450,[107] and by azoreductases under aerobic and anaerobic conditions.[108,109] Shifting from biological media to a more controlled electrochemical environment (e.g. solvent, potential…) allows the observation of more elusive AB redox states.

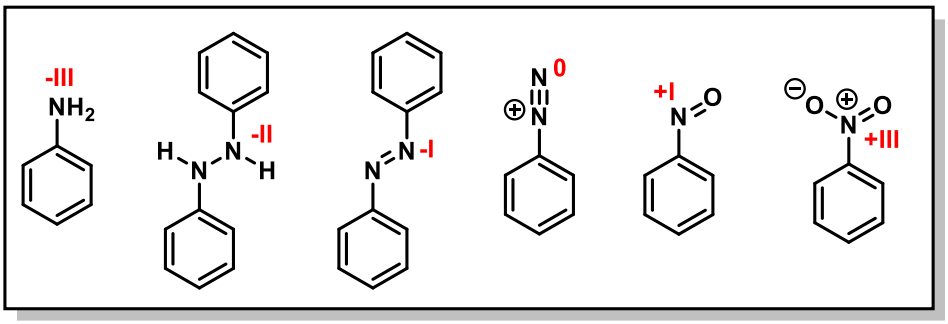

Figure 8. Compounds of interest with their redox states in AB chemistry.

2.1.1 Reductive Behaviour

One of the earliest examples of AB redox chemistry was from Wilhelm Schlenk who studied the alkali metal addition to different double bonds.[110] He observed that the combination of sodium powder with AB results in a dark purple solid, which, after quenching with water, yields equimolar amounts of hydrazobenzene and AB. The result was therefore not the expected 1e$^-$ reduction product as a mono-sodium radical anion, but a mixture of a neutral compound and the 2e$^-$ reduction product. Wittig made a contrary observation with the complete formation of the bis-lithiated hydrazobenzene with two equivalents of methyllithium, which formed the radical anion after addition of more AB.[111] The comproportionation of deprotonated hydrazobenzene was further studied and showed a strong dependence on the employed counter cation, as well as an electron paramagnetic resonance (EPR) signal that is influenced by hyperfine splitting of the alkali metal.[112] Even just the mixture of AB and hydrazobenzene yields an observable EPR radical, indicating an electron transfer between the -II and -I oxidation state compounds.[113]

The electrochemical reduction of AB can be traced back to the research by Gattermann and Haber at the start of the 20th century, when the electrochemical reduction of nitrobenzenes was studied.[114–116] AB behaves rather differently in electrochemical experiments, and the observed results are dependent on solvent, electrolyte, and electrode material. During polarography in aprotic, polar solvents, AB **1** is reduced in two consecutive 1e$^-$ waves.[117] The first wave produces the radical anion **1**$^{-\bullet}$, as observed by EPR and UV-Vis measurements, and the second wave the bis-anion **1**$^{-2}$ (Figure 9, A). Under most conditions, the first wave appears reversible on the time-scale of the electrochemical measurements, while the second wave appears irreversible. The irreversibility of the second wave can be explained by the *vide supra* discussed comproportionation, as well as the significant basicity of the electron-rich bis-anion **1**$^{-2}$. In fact, AB **1** can be used as an electrochemical generated base strong enough to deprotonate acetonitrile (ACN), and the resulting anion can be used as a nucleophile (Figure 9, C).[118] Due to the lower electron density in 4,4'-pyridine hetero-AB **9**, the second reduction can be made more reversible (Figure 9, B).[119]

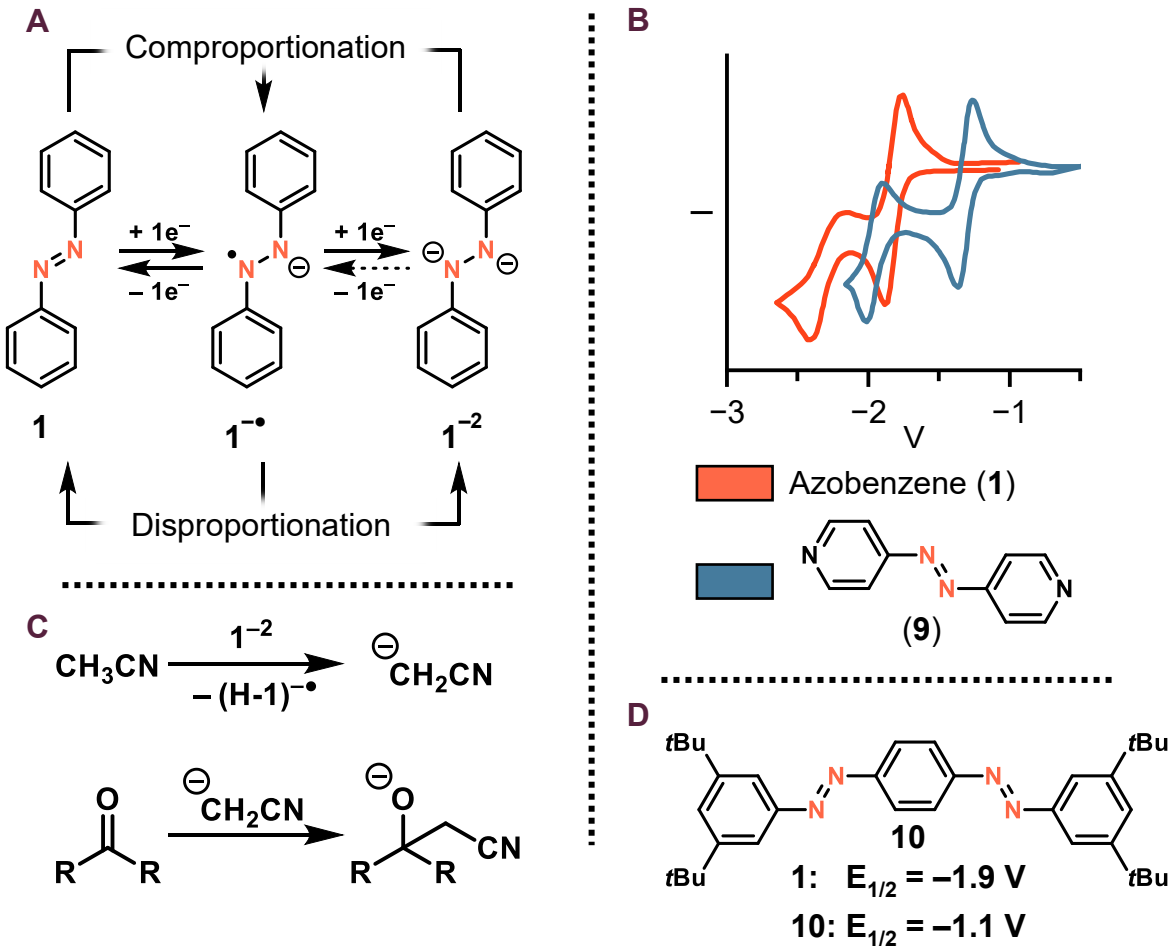

Figure 9. A) Reductive redox chemistry of AB **1** in organic solvents B) Cyclic voltammetry measurement (CV) of AB **1** and 4,4'-azopyridine (**9**) in an organic solvent referenced to ferrocene/ferrocenium (Fc/Fc^+).[119,120] The second reduction appears more reversible for the electron-poor pyridine derivative **9** than for pristine AB **1**. Reprinted with permission from Y. Xie *et. al*.[120] Copyright © 2024 American Chemical Society. C) Electrochemically generated AB $\mathbf{1^{-2}}$ base deprotonates an ACN solvent molecule, which reacts as a nucleophile.[118] D) Structure of bis-AB **10** and its reduction potential compared to the reduction potential of AB **1** vs. Fc/Fc^+.[91,121]

By extending the π-system in *para*-connected bis-AB **10**, their reduction proceeds more facile in comparison to pristine AB **1** (Figure 9, D).[121] *Para*-bis-ABs show two clearly distinct reversible $1e^-$ reductions for each azo unit that are separated by 0.5 V. This clearly shows the strong electronic communication in *para*-AB, as also demonstrated by ultrafast isomerization dynamic experiments.[122] If the azo units are separated by a biphenyl linker, the first two $1e^-$ reductions proceed at more similar potentials, as they behave more independently from each other. Increasing the dihedral angle between the biphenyl moieties by adding steric bulk (ABs **11**-**13**) results in one indistinguishable redox wave for both redox processes (Figure 10, A). The charge delocalisation of quasi planar *para*-bridged oligo-AB has also been visualized by electron paramagnetic resonance.[123] The observed delocalization is smaller than in the structurally akin stilbene compounds, which is reasoned with the large degree of spin density on the nitrogen bridge.

Furthermore, *para*-biphenylene-connected asymmetric bis-ABs like compound **14** were able to switch orthogonally by a mixture of photochemical and electrochemical stimuli (Figure 10, B).[124] This can be achieve by the discussed loss of electronic communication due to rotationally hindered biphenyl bridges, as well as two clearly different redox potentials due to different substitution on the AB rings.

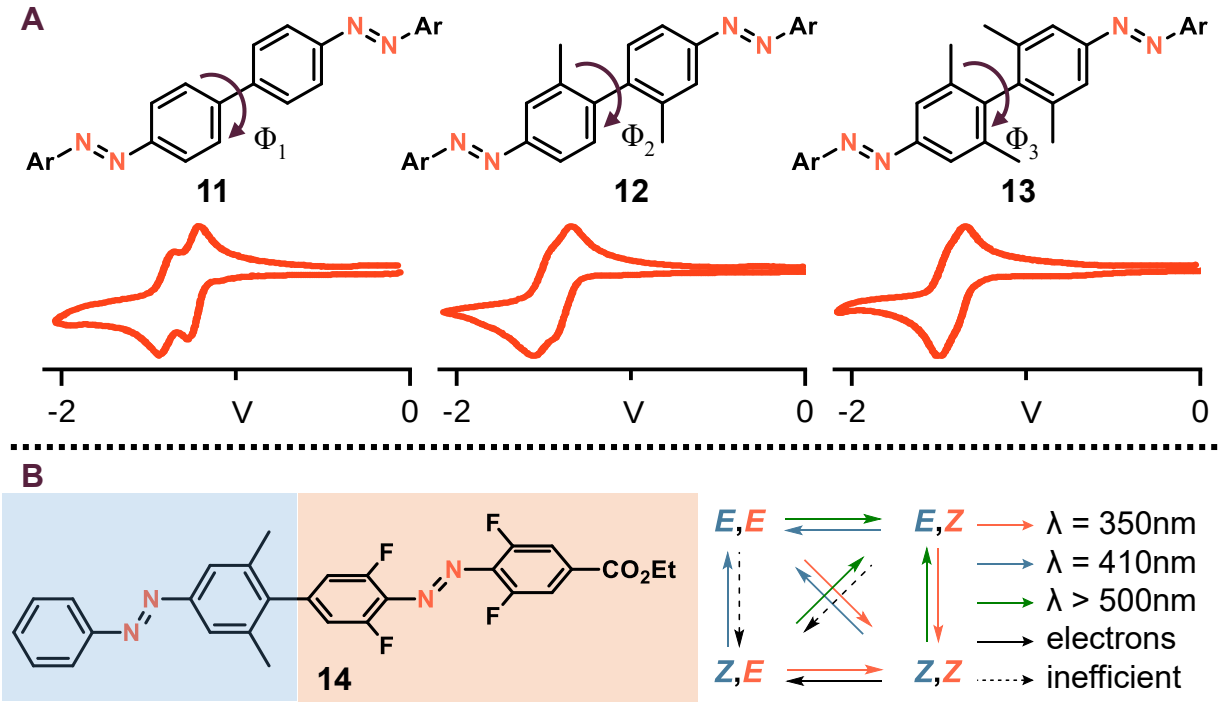

Figure 10. A) Dependence of the peak-to-peak separation in the CV of bis-azobenzenes **11**-**13** based on the dihedral angle between both photoswitches.[121] CVs are referenced to Fc/Fc^+. The higher the dihedral angle, the smaller the peak separation, as the independent redox behavior increases with increasing angle. Reprinted with permission from Bléger *et. al*.[121] Copyright © 2011 American Chemical Society. B) Asymmetric bis-azobenzene **14** and the pathways to achieve orthogonal switching, with the different reduction potential allowing selective (*Z*) to (*E*) switching of the more electron poor switch.[124]

Evidence of the structure and geometry of the reduced AB species was obtained by single-crystal X-ray diffraction (SC-XRD). In earlier studies, the electron transfer from two ABs to Re(0) yielded paramagnetic Re(II) complexed with two AB radicals.[125] In the obtained crystal, an elongation of the N–N bond in comparison to pristine AB was observed, as well as a shift in the ν_{N-N} IR band to lower wavenumbers, indicating a decrease in the double bond character of the radical in comparison to the neutral compound. The observed bond elongation and the obtainable EPR signals are in agreement with the location of the radical on and over the azo nitrogens. Similar results have been obtained in osmium[126] and ruthenium[127] complexes, or with imidazole based AB.[128] In 2020, free AB radical and bis-anion were isolated after reduction with alkali metals in the presence of a crown ether. Due to the free N–N bond in these compounds, they were able to coordinate and activate CO_2 to yield oxalic acid.[129]

2.1.2 Oxidative Behaviour

The electrochemical oxidation of ABs is less explored than the reduction. This is mainly due to the reason that most AB derivatives show irreversible and destructive oxidation behaviour.[130] Nevertheless, an EPR spectrum of AB **1** was obtained after bombardment with γ-rays in a frozen $CFCl_3$ matrix,[131] and later in a frozen cryofluorane matrix at 77 K.[132] It was shown that substitution with amino or hydroxyl groups at the *para*- or *ortho*-positions with respect to the azo bond, allows reversible oxidation reactions.[133] The observed two-electron process was rationalised by the formation of a benzoquinoneimine azine structure.[134] Evidence for this proposed structure was obtained by comparison of ^{1}H-NMR signals before and after oxidation of AB containing hydroxyl groups at both *para*-positions. The obtained signals are shifted downfield in comparison to the neutral compound, and differ from the signals of the corresponding azoxy compound, eliminating azoxy compounds as possible oxidation products.[134] Although earlier studies observed only a $1e^-$ oxidation of 4,4'-diamino ABs by electron-poor quinodimethanes, forming the corresponding 1:1 salts,[135] more recent electrochemical studies and redox titrations by the group of Hecht confirmed the $2e^-$ oxidation of 4,4'-diamino AB **15**.[92] They furthermore showed that neither the 3,3'-dimethylamino AB **16**, nor the very electron rich 3,3',4,4',5,5'-hexamethoxy AB **17** can undergo reversible oxidations, as they cannot form the proposed quinoidal structure.

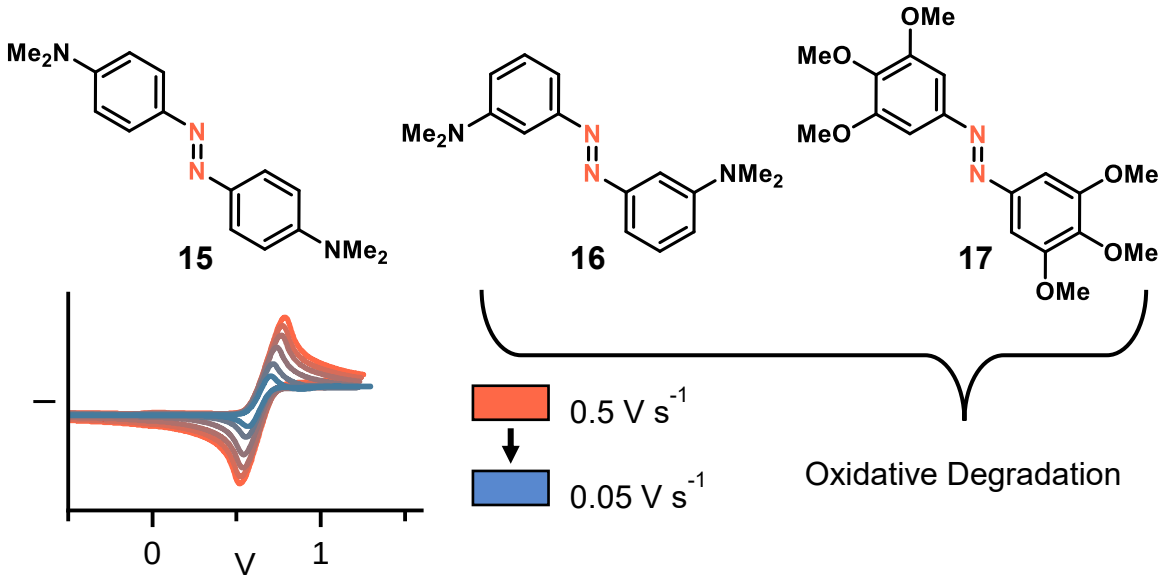

Figure 11. The reversible oxidation of 4,4'-dimethylamino AB **15** is based on the formed quinoidal oxidized species, as neither the 3,3'-dialkylamino AB **16**, nor the electron-rich hexamethoxy AB **17** show reversibility.[92,136] Copyright © 2024 The Author(s). Angewandte Chemie International Edition published by Wiley-VCH GmbH.

To get further insights into the structure of the oxidized species and the mechanisms of the reversible oxidation, we crystallised the product obtained after oxidation of 4,4'-diethylamino AB **18** with two equivalents of $NOBF_4$.[136] The obtained solid state structure revealed the, until then only predicted, quinoidal structure to be valid. A bond elongation of the N-N bond, a shortening of the N-C_{aryl} bond, and a bond alternation in the ring systems all indicate a quinoidal form over the whole AB core (Figure 12). Furthermore, calculation of the δ_r value, a value used for quantification of quinoidal character,[137] of 0.100 Å verifies fully quinoidal rings.

	a_{N-N} / Å	b_{N-C} / Å	c_{C-C} / Å	d_{C-C} / Å	e_{C-C} / Å	δ_r[137] / Å
AB **18**[138]	1.266	1.423	1.385	1.382	1.417	0.019
AB $\mathbf{18}^{2+}$[136]	1.363	1.321	1.442	1.346	1.450	0.100

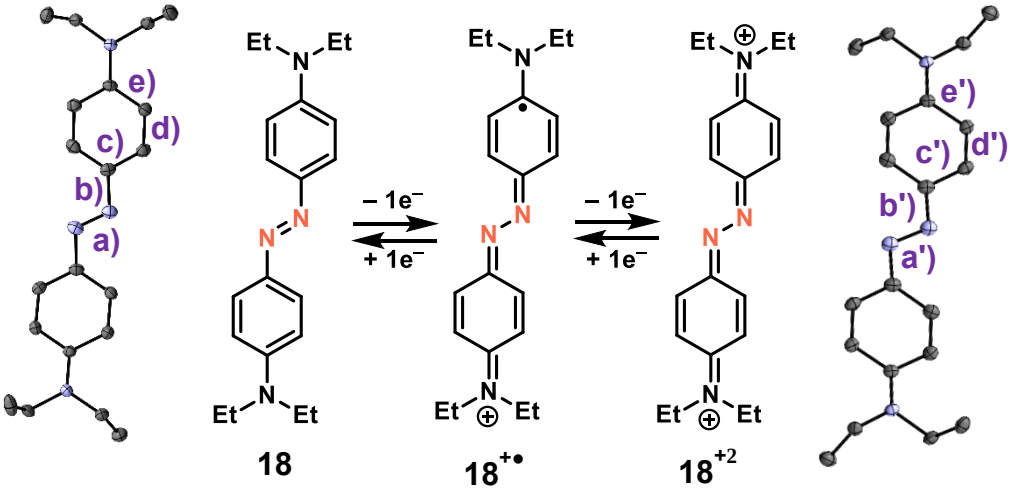

Figure 12. Solid-state structures of 4,4'-diethylamino AB **18**[138] (from CCDC: 1000644) and the quinoidal form $\mathbf{18}^{+2}$[136] (from CCDC: 2247535) after the chemical oxidation with $NOBF_4$. Solvent molecules, hydrogens and counter anions are omitted for clarity. Thermal ellipsoids are shown at 50% probability.

2.2 Redoxproperties of (*Z*)-Azobenzene

One of the most prominent features of AB is the ability to isomerize from the stable (*E*)- to the metastable (*Z*)-isomer by irradiation with the appropriate wavelength.[5] Isomerization leads to changes in properties such as basicity, end-to-end distance, solubility, and dipole moment. This raises the question of whether the electrochemical properties are also affected. The oxidation of (*E*)-AB with perbenzoic acid yields (*E*)-azoxybenzene (AOB), while the same procedure with (*Z*)-AB leads to significant formation of (*Z*)-AOB,[139] with a higher reaction rate for (*Z*)-AB than for (*E*)-AB. Upon treatment of (*Z*)-AOB with a reducing agent, only the (*E*)-AB was obtained. This highlights the formation of an intermediate, in which the rotation of the N–N bond is less hindered, which is not observed during peracid oxidation. Polarograms of *p*-methoxy AB **19** in aqueous dioxane electrolyte gave an additional signal after irradiation of the sample with UV light (Figure 13).[140]

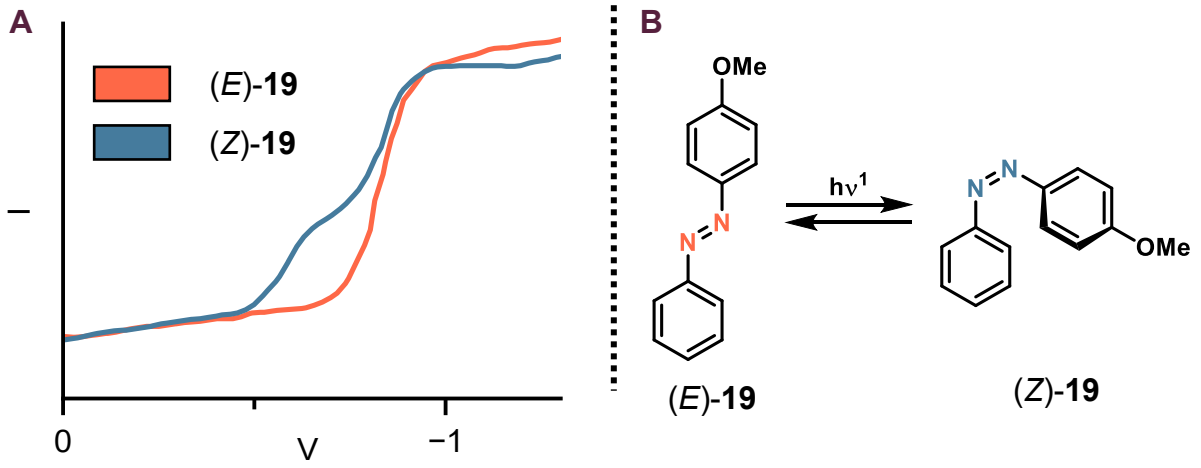

Figure 13. A) Difference between the polarograms of *para* methoxy AB **19** in 70% aqueous dioxane before and after photoisomerization.[140] The new signal corresponding to the (*Z*)-isomer is shifted to more positive potentials, and corresponds to the polarogram of a pure (*Z*)-isomer sample. Reprinted with permission from Klopman *et. al*.[140] Copyright © 1974 American Chemical Society. B) Isomerization of AB **19**.

The height ratio of both peaks was dependent on the irradiation duration, but the sum stayed constant, which correlates with photoisomerization. The metastable isomer can be reduced by nearly 200 mV more easily, and the result of the observed 2e⁻ reduction is the same starting from (*E*)- or (*Z*)-isomer. If similar experiments are carried out in DMF solutions, no difference in the redox potential of both isomers at room temperature are observed.[141] Cooling the electrolyte to –22 °C and using very high sweep rates results in distinguishable cyclic voltammograms of (*E*)- and (*Z*)-AB. Photomodulated voltammetry, a technique typically used for elusive radical species,[142,143] of *in situ* generated (*Z*)-AB in a variety of organic solvents likewise revealed a difference between both isomers.[144] The underlying problem of electrochemical analysis of the (*Z*)-isomer, is the formation of the anion radical, which has an activation energy of the isomerization of only around 8 kJ mol^{-1}.[141] Pairing the fast kinetic constant with a radical transfer to other (*Z*)-ABs in the vicinity of the electrochemically generated radical, (*Z*)-AB can only be observed in voltamogramms if the sweep rate is higher than the rate of isomerization.

There are ways to stabilize a (*Z*)-AB radical: Hecht prepared a linear AB compound (**20**) and compared it to a cyclic derivative (**21**). The cyclic compound **21** acts as a locked (*Z*)-**20** analog.[91] He observed no difference between the (*E*)- and (*Z*)-isomer of the open form AB **20** in the voltammograms, while cycle **21** showed a difference of around 250 mV to more negative potentials for the 1e⁻ reduction compared to (*E*)-**20**. Former was reasoned with the catalytic back isomerization during scanning. By addition of a small amount of generated AB anion radical to a bulk solution containing (*Z*)-AB, fast isomerization to (*E*)-AB was observed.[141,91] Using a spectro-electrochemical setup, the fast isomerization of (*Z*)-isomer to its stable isomer was observable by its change in the UV-Vis spectra during cyclic voltammetry.[92,91] Additional cyclic diazo derivatives are the 1,2-diazo rings from Herges. Their redox behaviour is strongly dependent on the length of their alkyl chains, although all show the expected 1e⁻ reduction of azo compounds.[145]

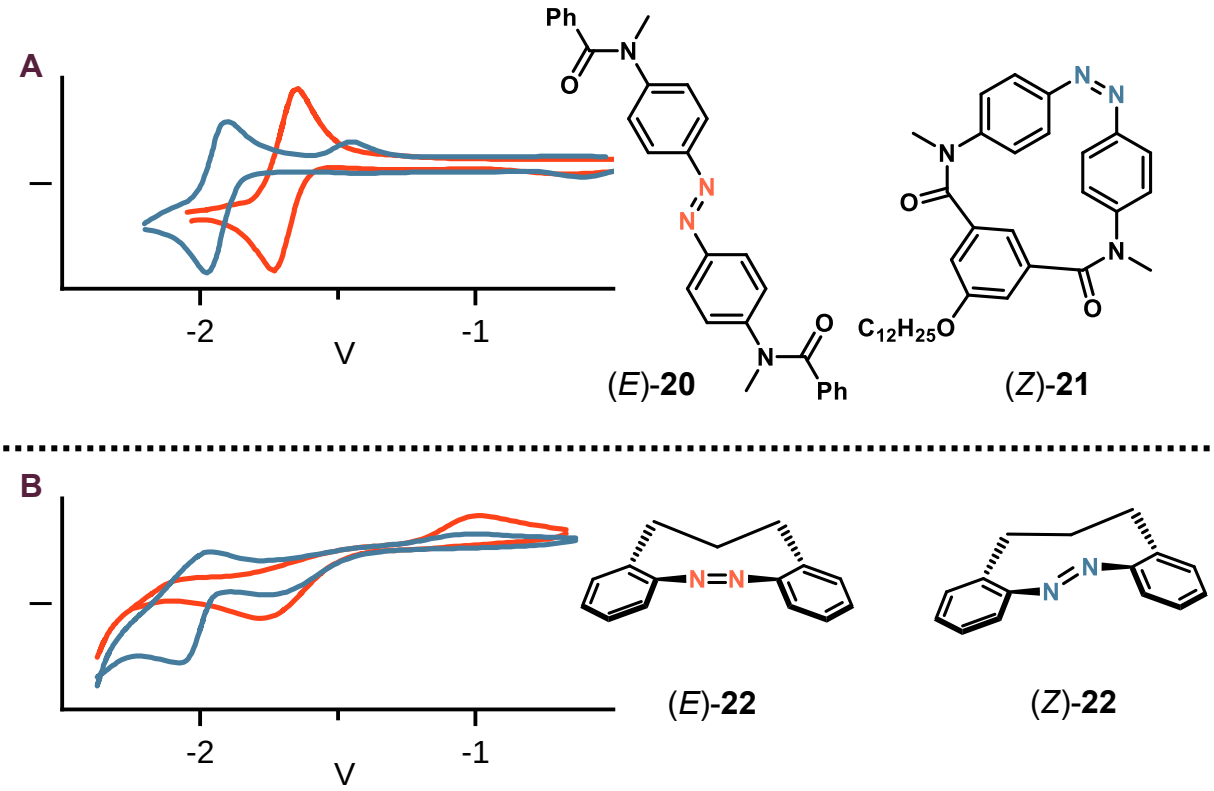

Figure 14. A) A cyclic derivative **21** of (*E*)-AB **20** as a model for its (*Z*)-isomer with different redox potentials. (*Z*)-AB **20** isomerizes due to fast radical transfer on the time scale of the CV experiment.[91] Reprinted with permission from Goulet-Hanssens *et. al*.[91] Copyright © 2017 American Chemical Society. B) Herges' diazonine **22** where the (*Z*)-isomer (thermodynamically stable) and (*E*)-isomer (metastable) show different redox potentials observable by CV measurements.[145] This is due to the stability of the formed radical anion that only undergoes slow radical transfer. The orange trace corresponds to the (*E*)-isomer, the blue to the (*Z*)-isomer. Copyright © 2023 The Authors. Chemistry - A European Journal published by Wiley-VCH GmbH.

If the linker is increased to a C3-chain, yielding a diazonine (compound **22**), reduction of metastable (*E*)-isomer does not yield the (*Z*)-isomer in a catalytic fashion, while C1- and C2-chains isomerise upon reduction. The obtained redox potentials of (*E*)-**22** are shifted 130 mV to more positive potentials compared to (*Z*)-**22**. The formed radicals are decomposing in around 100 s, probably due to disproportionation.

3 Electrochemistry of Azobenzenes in Energy Storage Applications

The versatility of ABs is based on their derivatisation and their tuneable properties. The great variety of applications makes it impossible to comprehensively cover them all in this work. One emerging technology is the usage in energy storage. Here, AB shows its versatility once again as it can be employed in the storage of electrochemical, as well as thermal energy storage. The storage of both forms of energy is essential for an efficient energy grid.

3.1 Electrical Energy Storage

Rechargeable electrochemical energy storages are employed in everyday-used handheld electronic devices, like smartphones or laptops, but are also important for large-scale, high-capacity storages. Due to the reversible reduction of most diazo units, they have been employed in rechargeable alkali-metal batteries, as well as in redox-flow batteries. A comprehensive analysis of the different technologies, AB derivatives and their application can be found in an in-depth review by Shimizu, Tanifuji and Yoshikawa.[104] Herein we want to showcase some use cases for AB redoxchemistry in the broader scope of electrical and thermal energy storage technologies.

3.1.1 Metal Batteries

During their study of aromatic nitro compounds as organic electrodes for Li batteries the group of Wang observed that a drastic capacity drop occurred after their first reductive cycle, with a good capacity retention of the following cycles (Figure 15).[146] They showed that during the first cycle their employed nitro compound **23** is irreversibly reduced (over nitrosobenzene **24** and AOB **25**) to the corresponding AB **26**, which then is the electrochemically active electrode that undergoes reversible reduction to the bis-lithiated hydrazine **27**. Similar systems based on AB electrodes were realised for Na- and K-batteries,[147,148] and Al- or Zn-based storage solutions.[149] Interestingly, alkyl azo compounds lack the reversibility of their aromatic analoga, which highlights the importance of conjugation.[150] To further increase stability, dinitro compounds can be used as an electrode material, as they polymerize to a π-conjugated azo polymer during initial cycling with a similar mechanism as for nitrobenzene **23**.[151] Other macromolecular azo compounds in alkali metal batteries are covalent-organic and metal-organic frameworks.[152,153] One of their advantages as cathode materials is their decrease in solubility, and their small volume change upon ion insertion.[154] Although they show promising properties, their electrochemical stability can be negatively influenced by less stable linkers,[155] and the accessible active material can be highly dependent on the used metal ion.[156] An often seen feature in AB electrode materials are carboxyl groups, as they improve the interactions with metal cations, and decrease solubility in the electrolyte.[157,158] These ABs can also be used in all solid-state lithium batteries, highlighting the compatibility and strong interactions with lithium sources.[159,160]

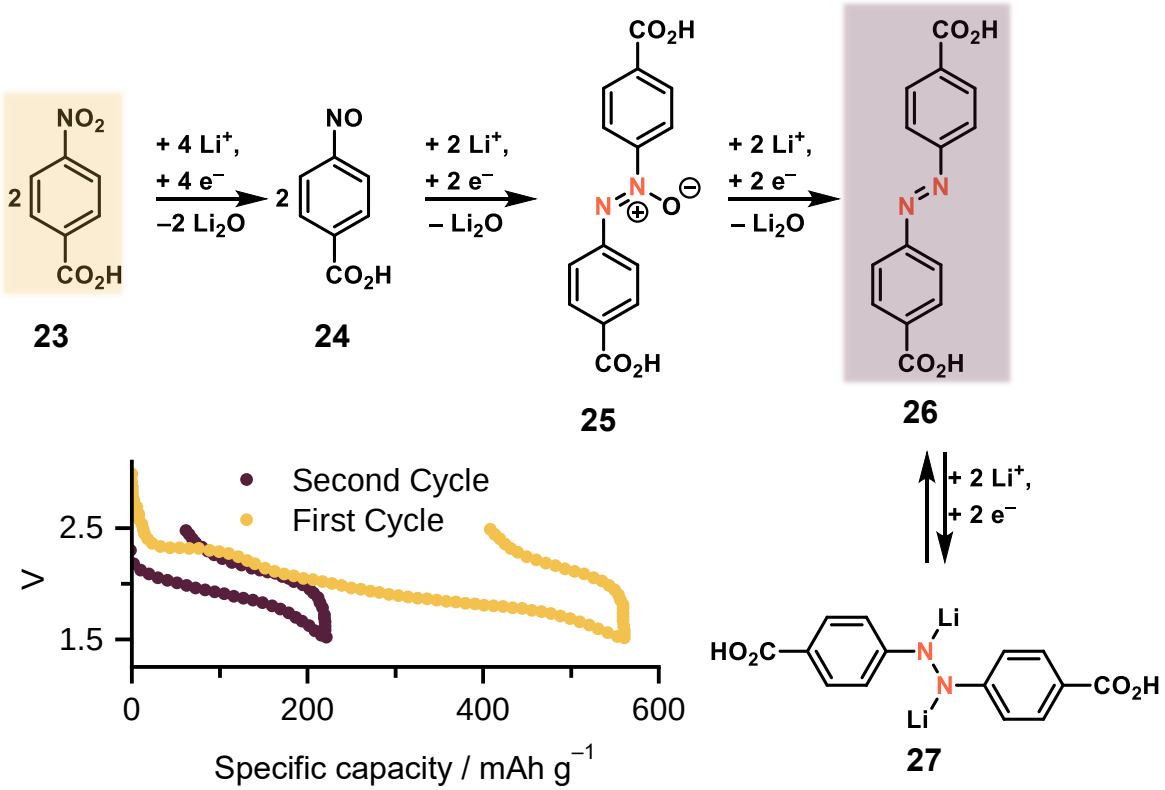

Figure 15. Galvanostatic charge/discharge curves from nitrobenzene **23**.[146] The low coulombic efficiency during the first cycle can be explained by the irreversible reduction of nitrobenzenes to AB **26**. The thereby formed AB **26** shows good capacity retention during reductive cycling. Copyright © 2018 WILEY-VCH Verlag GmbH & Co. KGaA, Weinheim.

To achieve an additional coordination side for alkali metals, AB can be substituted with AOB in electrochemical active frameworks, and thereby increase lithium storage potentials.[161] As electron-poor pyridine based AB **9** show reversibility even for their second reduction, they can be used to further increase the performance of batteries.[120] Furthermore, the reduced (discharged) azopyridines $\mathbf{9^{-2}}$ show spontaneous reoxidation to the neutral compound by ambient oxygen as oxidant, therefore offering self-charging capabilities.[162]

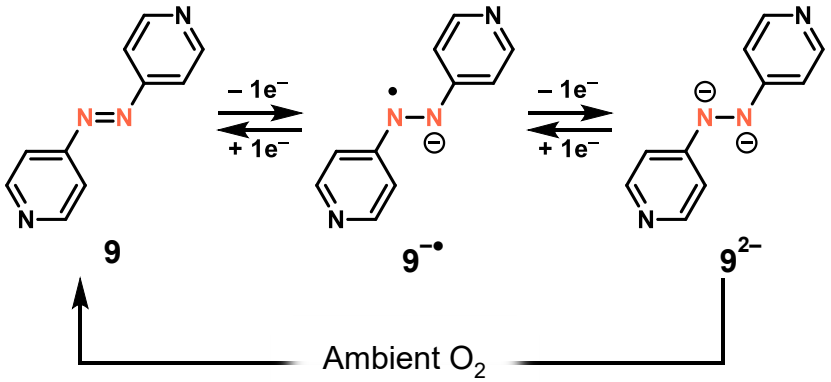

Figure 16. Reductive behaviour of 4,4'-azopyridine (**9**), and the observed reoxidation by ambient oxygen of the electrochemically generated hydrazine $\mathbf{9^{2-}}$ to the neutral state.[162]

3.1.2 Redox Flow Batteries

Due to the reversibility of the 1e⁻ reduction to the anion radical, AB can perform as the redox active material in large-scale energy storage systems, like redox-flow batteries (RFB). In a seminal study by the group of Yu, pristine AB **1** was employed as the anolyte in an organic RFB.[163] With optimization of solvent, separator, and supporting electrolyte, AB based RFBs were able to deliver the highest power density at that time.[164] To overcome the limitations of high intrinsic resistance and low conductivity of organic electrolytes, as well as to use environmental friendly solvent, aqueous AB-based RFBs are needed. As pristine AB only shows negligible solubility in water, Zu *et al*. added sulfoxide groups, which results in high solubility of the redox-active substrate **28** in basic aqueous media (Figure 17).[165] In a comparison of the anolyte before and after cycling, the hydrazine and aniline were observed during 1e⁻ reduction.[166] It was suggested that the formed anion radical can disproportionate to give a neutral AB and double deprotonated hydrazine. AOB was excluded to be a side product that is produced during reoxidation. To improve the stability of the cleaved bond and therefore increase the long term stability, skeletal rearrangement of ABs to benzo[*c*]chinnoline derivatives was employed.[167] In comparison of the cyclised di-sulfonated compound **29** with the corresponding AB, a much slower capacity decay and therefore a better cyclability was achieved.

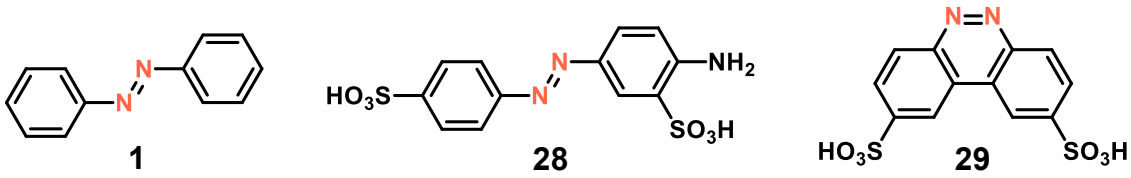

Figure 17. Molecular diazene scaffolds used in reductive RFBs. Compounds **28** and **29** can be used in aqueous electrolytes.

These systems rely on the reductive electrochemical behaviour of the employed diazenes, as they usually decompose oxidatively.[93] To nevertheless allow AB to be employed as a possible catholyte, we relied on the reversible oxidation of 4,4'-dialkylamino substituted ABs that form a quinoidal system upon the loss of 2e⁻ (Figure 18).[136]

Albeit we were able to demonstrate their cyclability in H-cell experiments, a capacity decay over multiple cycles indicates the need for further improvements. Switching from AB **18** to AOB **30** increases oxidation potential and solubility for ethyl-substituted 4,4'-dialkylamino compounds, but does not improve the cycling stability.[168] In fact, a larger capacity decay is observed for AOB, which we assumed to be caused by the instability of the cation radical intermediate, which is more pronounced in the AOB case. Nevertheless, this proof of principle shows that ABs can be employed in both half cells of a battery, further extending the applicability of this versatile compound class.

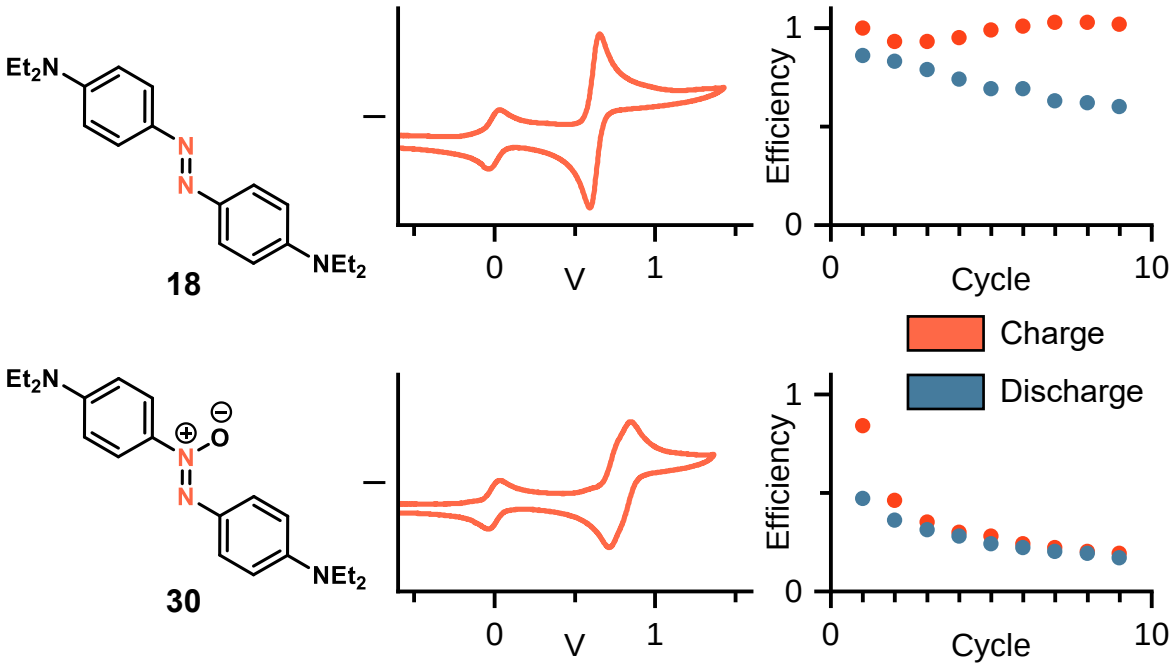

Figure 18. 4,4'-Diamino AB **18** and AOB **30** with their reversible oxidation on the time scale of an CV experiment referenced and measured with decamethylferrocene during charge/discharge cycling in a H-cell. A capacity decay over multiple cycles was observed.[136,168] Copyright © 2024 The Author(s). Angewandte Chemie International Edition published by Wiley-VCH GmbH and Copyright © 2025 The Author(s). Chemistry - A European Journal published by Wiley-VCH GmbH.

3.2 Electrochemical Heat Release in Molecular Solar Thermal Energy Storage

One of the cornerstones for a proficient and practicable MOST system is the efficient back isomerization to controllably harvest the stored thermal energy. Different strategies are discussed as possible stimuli for AB isomerization, and, among others, redox processes are one of the most efficient ones. In a study about the reductive behaviour of (*Z*)-AB **1**, Laviron *et al*. observed a fast isomerization of (*Z*)- to (*E*) upon electrochemical reduction.[141] Gescheidt *et al*. showed a catalytic (*Z*)- to (*E*)-isomerization of 1,1'-azanorbornane (**31**) upon addition of oxidant, or by electrochemical oxidation (Figure 19). In both cases, a radical (*Z*)-anion or -cation is formed, which shows a reduced energy barrier for the isomerization resulting in a fast formation of the (*E*)-isomer. This species can then transfer its radical to another (*Z*)-isomer, thereby making the process catalytic in consideration of the electrons, expanding the space of possible isomerization catalysts of AB.[88] The group of Hecht expanded on this concept with an in-depth study of the electron-[91] and hole-[92] catalytic isomerization of ABs. Based on these results, Fuchter and Han prepared arylazopyrazole **32** that showed nearly quantitative (*E*)-to (*Z*)-isomerization ($PSS_{340\ nm}$ = 98% (*Z*)-isomer), but only limited (*Z*)- to (*E*)-photoisomerization ($PSS_{495\ nm}$ = 24% (*E*)-isomer), which drastically limits its usage as a MOST material.[169]

Due to the introduction of an ionic side chain, arylazopyrazole **32** showed conductivity in the condensed phase. Upon applying a potential above the redox potential to a thin-film of the photoswitch, after 20 h an 80% decrease in the (*Z*)-content was observed, which is a lot more than expected of the thermal back isomerization ($t_{1/2}$ = 14 years). By measuring the injected number of charges, the catalytic property of the holes was confirmed.

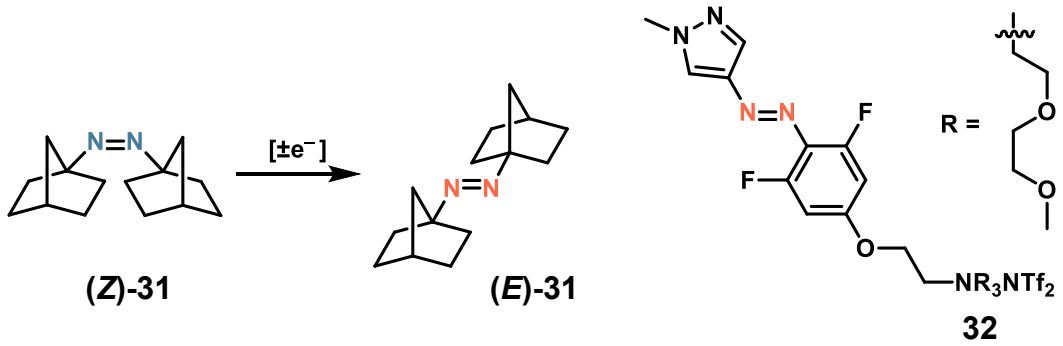

Figure 19. Electro-catalytic isomerization of (*Z*)-1,1'-azanorbornane to (*E*)-1,1'-azanorbornane **31**,[145] and the azoarene **32** that shows solid state electro-catalytic switching.[169]

In a cooperative work from our group with the groups of Libuda, Dreuw, and Wasserscheid, the electrochemical energy release of an arylazothiophene was studied.[130] DFT calculations showed a decrease in isomerization activation barrier by an order of magnitude comparing the neutral and the (positively or negatively) charged transition state, making both the reductive and oxidative pathway possible. By increasing the potential applied to a photoswitch solution at the PSS, a drastic drop of (*Z*)-isomer concentration at around 1.0 V vs. Fc was measured, but the accompanying increase in (*E*)-concentration was not observed. Instead, the *in situ* measured IR spectra revealed new signals that do not originate from the isomers, but seem to be degradation products. It appears that for the arylazothiophenes, the potential needed for the decomposition is below the onset of the isomerization potential, which is different compared to pristine AB,[92] and to other heterocycles.[169] If a reductive scan is conducted, the decline of the (*Z*)-isomer concentration correlates with the increase of (*E*)-isomer concentration, showing an efficient electrocatalytic isomerization process. As the reductive degradation potential is higher than the reductive isomerization potential, the conversion level stayed over 90% after 100 switching cycles. In a follow-up study, the effect of the electrode material on the reductive isomerization of arylazothiophene was explored.[170] Graphite and gold surfaces were concluded to be the most suitable electrolyte materials, as they themselves are catalytically inactive and do not result in decomposition. Platinum on the other hand leads to decomposition of the photoswitch, which lowers isomerization yields and poisons the electrodes surface. The liquid AB **5** we introduced earlier can act as a solvent for ammonium salts, thereby increasing the conductivity of the neat organic compound. The increased electric conductivity allows for an electron- and hole-catalytic heat release in an electrochemical flow cell using graphite electrodes. Varying the applied potential shows that for the isomerization to occur, a specific potential threshold needs to be overcome (Figure 20).

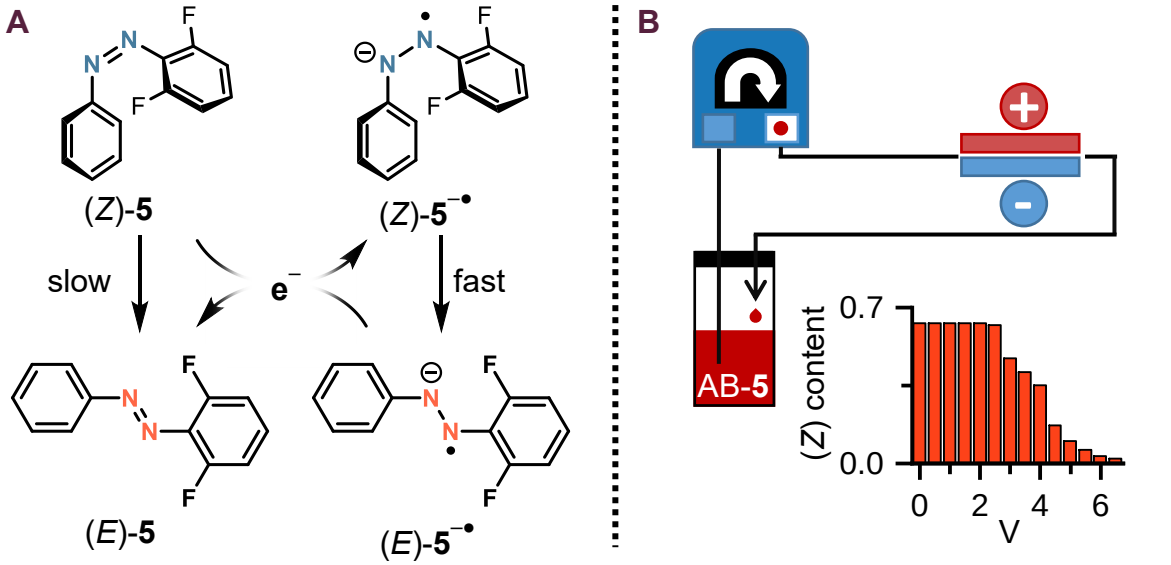

Figure 20. A) Electron-catalytical isomerization mechanism of (*Z*)-AB **5**. A similar oxidative mechanism over the radical cation is plausible as well. B) Electrochemical setup in a continuous flow apparatus and the change in the (*Z*)-isomer content during electrochemical back isomerization depending on the employed potential after one cycle.

This catalytic heat release is an improvement to a photochemical release for AB **5**. Irradiation with 405 nm leads to a PSS that still contains more than 22% (*Z*)-isomer, resembling stored thermal energy that cannot be accessed. The electrochemical isomerization on the other hand has the potential for complete back isomerization, and ensures to harvest all stored energy. Therefore, combining the electrochemistry of ABs with their application in MOST systems is a very capable way to increase the efficiency of a storage material.

4 Contributions to the Literature

4.1 *para*-Aminoazobenzenes – Bipolar Redox-Active Molecules

Reference: D. Schatz, M. E. Baumert, M. C. Kersten, F. M. Schneider, M. Brøndsted Nielsen, M. M. Hansmann, H. A. Wegner, *Angew*. *Chem*. *Int*. *Ed*. **2024**, *36*, e202405618.

DOI: 10.1002/anie.202405618

Azobenzenes (ABs) are versatile compounds featured in numerous applications for energy storage systems, such as solar thermal storages or phase change materials. Additionally, the reversible one-electron reduction of these diazenes to the nitrogen-based radical anion has been used in battery applications. Although the oxidation of ABs is normally irreversible, 4,4'-diamino substitution allows a reversible $2e^-$ oxidation, which is attributed to the formation of a stable bis-quinoidal structure. Herein, we present a system that shows a bipolar redox behaviour. In this way, ABs can serve not only as anolytes, but also as catholytes. The resulting redox potentials can be tailored by suitable amine- and ring-substitution. For the first time, the solid-state structure of the oxidized form could be characterized by X-ray diffraction.

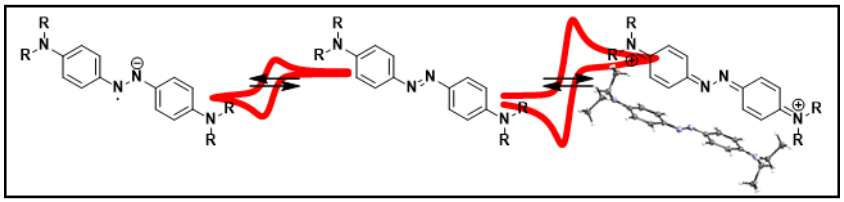

A German version of this article can be found under the following reference.

Reference: D. Schatz, M. E. Baumert, M. C. Kersten, F. Schneider, M. Brøndsted Nielsen, M. M. Hansmann, H. A. Wegner, *Angew*. *Chem*. **2024**, *36*, e202405618.

DOI: 10.1002/ange.202405618

GDCh Research Article Angewandte International Edition Chemie www.angewandte.org

Check for updates

How to cite: *Angew. Chem. Int. Ed.* **2024**, *63*, e202405618
doi.org/10.1002/anie.202405618

Electrochemistry

para-Aminoazobenzenes—Bipolar Redox-Active Molecules

*Dominic Schatz, Marcel E. Baumert, Marie C. Kersten, Finn M. Schneider, Mogens Brøndsted Nielsen, Max M. Hansmann, and Hermann A. Wegner**

Abstract: Azobenzenes (ABs) are versatile compounds featured in numerous applications for energy storage systems, such as solar thermal storages or phase change materials. Additionally, the reversible one-electron reduction of these diazenes to the nitrogen-based radical anion has been used in battery applications. Although the oxidation of ABs is normally irreversible, 4,4'-diamino substitution allows a reversible $2e^-$ oxidation, which is attributed to the formation of a stable bis-quinoidal structure. Herein, we present a system that shows a bipolar redox behaviour. In this way, ABs can serve not only as anolytes, but also as catholytes. The resulting redox potentials can be tailored by suitable amine- and ring-substitution. For the first time, the solid-state structure of the oxidized form could be characterized by X-ray diffraction.

Introduction

Since their discovery in 1834 by Mitscherlich, azobenzenes (ABs) have continuously been present in chemical research.[1] The straightforward synthesis of simple ABs, and their bright coloration sparked their application in the dye industry, where still today 70 % of the total dye production is based on these diazenes.[2] The work of Domagk at the IG Farben (German for "Dye industry syndicate stock corporation"), where the antibacterial properties of diazene dyes were studied, was awarded the Nobel Prize in 1939.[3] With the identification of the light-induced isomerization from the stable *E*- to the metastable *Z*-isomer by Hartley, the interest in these compounds has grown even more.[4] In recent years ABs have found their way into photoactivated pharmacology,[5] light induced conformation changes in biological macromolecules[6] or alignments in liquid crystalline phases,[7] as photon-driven molecular machines,[8] as a tool to reversibly change shapes of soft materials,[9] or as a Molecular Wind-up meter.[10] Another important application of ABs are energy storage systems. Here, the parent *E*-isomer is irradiated with light of a specific wavelength, and after photoisomerization, energy is stored in the resulting *Z*-state. This energy can then be released by the backreaction to the *E*-configuration. If the *Z*-isomer has a lower melting point than the *E*-isomer, solid-to-liquid phase transition can occur during the solar energy uptake.[11] This way, thermal energy from the surrounding medium is additionally stored in the phase transition, increasing the energy density of these systems further. So-called molecular solar thermal energy storage systems (MOST) rely on the storage of solar energy in bond strain, and an efficient release of this strain. There are a variety of different methods to release the strain, such as thermal activation,[12] catalysis[13] or, by electron- or hole-catalysis.[14,15] The electron catalysis of the back isomerization proceeds via the formation of a stable radical, which is located on the N–N bond. The sterically encumbered *Z*-isomer is locked in its place due to the rigid nature of the N=N double bond. If a radical is placed on the diazene subunit, the nitrogen loses its double bond character and can rotate unhindered to the *E*-form. The subsequent transfer of the electron from an already isomerized *E*- to another AB in its *Z*-state makes this process catalytic in electrons. Similar to this reductive behavior, a radical produced by the oxidation of AB undergoes the catalytic isomerization in an analogous fashion. The difference between both of these transformations is that the $1e^-$ reduction of AB is a reversible process, which means that no AB is destroyed, as shown in an electron triggered energy release from a thiophene based AB with excellent cyclability.[16]

The reversibility of the reduction of AB has led to yet another application of AB in energy storage: Recently, Zhang et al. used AB as the anolyte in redox-flow batteries (RFB),[17] and soon after a variety of RFB layouts based on AB followed,[18,19] adding to the ever-increasing space of

[*] D. Schatz, M. C. Kersten, F. M. Schneider, Prof. Dr. H. A. Wegner
Institute of Organic Chemistry
Justus Liebig University
Heinrich-Buff-Ring 17, 35392 Gießen (Germany)
E-mail: hermann.a.wegner@org.chemie.uni-giessen.de

D. Schatz, M. C. Kersten, F. M. Schneider, Prof. Dr. H. A. Wegner
Center of Materials Research (ZfM/LaMa)
Justus Liebig University
Heinrich-Buff-Ring 16, 35392 Gießen (Germany)

M. E. Baumert, Prof. Dr. M. M. Hansmann
Faculty of Chemistry and Chemical Biology (CCB)
Technical University of Dortmund
Otto-Hahn Str. 6. 44227 Dortmund (Germany)

Prof. Dr. M. B. Nielsen
Department of Chemistry
University of Copenhagen
2100 Copenhagen (Denmark)

GDCh Research Article Angewandte International Edition Chemie

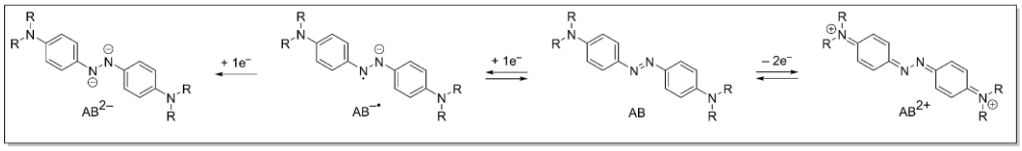

Figure 1. The reversible 1e⁻ reduction of AB to the anion radical $AB^{-\bullet}$, the irreversible 2e⁻ reduction to the dianion AB^{2-}, and the proposed 2e⁻ oxidation to a bis-quinoidal structure AB^{2+}.

organic, redox-active compounds for electrochemical energy storage.[20] These AB-based RFB rely on the redox activity of the N=N azo bond, which can reversibly be reduced to the radical anion in a 1e⁻ process, followed by an (normally) irreversible second 1e⁻ reduction to the dianion. The irreversibility of the second reduction wave was rationalized by the protonation of the rather basic, electron-rich nitrogen in the reduced form.[21] The nature of the stable radical anion has been supported by electron paramagnetic resonance spectroscopy (EPR) of azobenzene-d_{10}, where the resulting 5-line hyperfine structure confirms one electron interacting with two equivalent nitrogen atoms.[22] The product of the second reduction is diamagnetic, and does not show any EPR signal. Cyclic voltammetry of the more electron-poor 4,4'-azopyridine, however, shows reversibility of both 1e⁻ reductions, which is due to the relatively lower basicity in comparison to unsubstituted AB.[23]

Although the 2e⁻ oxidation of AB is normally irreversible, substitution in *ortho*- or *para*-position of each phenyl unit with hydroxyl or amino groups can overcome this obstacle. This change is ascribed to the formation of a stable bis-quinoid structure of the dication upon oxidation (Figure 1). The structure of the oxidation product from 4,4'-diamino AB has not been confirmed yet, although calculations are in agreement with the proposed bis-quinoid structure.[15] Combining the 1e⁻ reduction of the azo bond with the 2e⁻ oxidation to the bis-quinone offers the possibility to employ these compounds as bipolar substrates in symmetrical RFB, where the same compound is used as the anolyte and the catholyte. These symmetrical energy storage systems have advantages over conventional layouts, as they do not suffer from long-term capacity decay by transportation of active materials through the separating membrane.[24] In fact, reversal of the cell's polarity after a specific amount of cycles can effectively double the battery's lifetime. Here, the imbalance of the redox equivalents of the oxidation or reduction respectively could increase the lifetime by polarity reversal further.

As the redox behavior is highly dependent on the solvent used as well as the electrolyte, we investigated various conditions to ensure reversibility of the oxidation and the reduction. Furthermore, we evaluated the effects of changes in the chemical structure of the aromatic ring, as well as the *para*-amino group to elucidate structure–property relationships as well as to optimize the compounds for electrochemical applications. To get more insight into the structure of the oxidized form, its molecular structure was characterized by single crystal X-ray diffraction. This is, to the best of our knowledge, the first confirmation of a quinoidal AB structure obtained from oxidation. The insights into the redox properties will broaden the use of the AB scaffold in energy storage systems, expanding the already versatile profile of diazene compounds.

Results and Discussion

The 4,4'-bisamino AB motif offers two possibilities to diversify its chemical structure and to study the resulting structure-redox-properties relationship: substitution pattern on the aromatic rings, and varying substituents at the amines (Scheme 1). In this study, both possible positions (2,2'- and 3,3'-) of a symmetrical bis-substituted AB were substituted with electron-withdrawing fluorine- or electron-donating methoxy groups. Starting from either commercially available or readily synthesizable 4-bromoanilines **1a–d**,[25] 4,4'-dibromo-ABs **2a–d** were prepared in good yields by oxidation with activated MnO_2. The 4,4'-dibromo AB without additional substituents was prepared by copper catalyzed aerobic coupling of 4-bromoaniline **1e** in good yields.[26] The *para*-Br substituent conveniently allows to introduce the amino group via palladium catalyzed Buchwald–Hartwig coupling reaction.[27] For the ring-substituted AB **3a–d**, diethylamine was employed as the coupling partner of choice. The utilization of diethylamine instead of dimethylamine is due to its better solubility as well as easier and safer handling (liquid vs. gas). The electron-rich methoxy derivatives **3a–b** were isolated after column chromatography in moderate yields, while the yield of the fluorine derivatives **3c–d** was generally lower. We found evidence of products resulting from nucleophilic aromatic

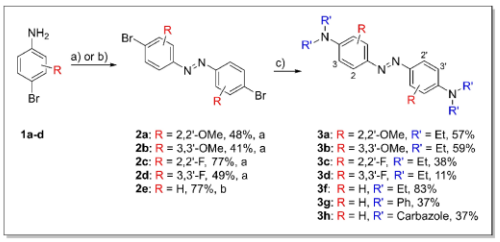

Scheme 1. Preparation of symmetric redox-active AB structures **3a–h**. a) Activated MnO_2, toluene, 70 °C, 24 h to 48 h. b) CuBr, pyridine, toluene, 60 °C, under air, 24 h. c) HNR'$_2$, $Pd_2(dba)_3$, RuPhos, Cs_2CO_3, toluene, 100 °C, 24 h to 72 h.

substitution of similar electron-poor ABs (see Supporting Information Figure S28), which results in more tedious purification and lower yields. Diversification of the amine functionality was achieved by Buchwald–Hartwig coupling of the 4,4'-dibromo compound **2e** with varying amine partners. Two aryl (**3g**–**h**) and one alkyl amine (**3f**) were synthesized in this fashion, while the dimethyl derivative **3e** was synthesized by CuBr coupling of the corresponding aniline (see Supporting Information page 18).[26]

The solvent and the electrolyte are crucial for a successful electrochemical experiment. Different combinations of both were screened. The diethyl derivative **3f** was employed as the model compound in a 2 mM concentration, with 1 mM decamethylferrocene (Fc^*) as an internal standard.

Propylene carbonate (PC), dichloromethane (DCM) and acetonitrile (ACN) were tested as solvents with 0.2 M tetra-*n*-butylammonium hexafluorophosphate ($TBAPF_6$) as electrolyte (Figure 2). For the green solvent PC, AB **3f** showed only limited solubility, as well as an irreversible reduction. Deprotonated pyridazinones are known to irreversibly open propylene carbonates, and a similar nucleophilic attack could occur with the very electron-rich radical anion, resulting in the irreversible reduction.[28] In the case of DCM, no reversible reduction was observed. On the other hand, the expected $2e^-$ oxidation peak was split into two fully reversible $1e^-$ oxidations, indicating the formation of a stable mono-cation radical. This is in accordance with titration experiments, that showed that the chemical oxidation of 4,4'-diamino AB does indeed proceed via a radical cation, and both oxidation peaks are electrochemically very close.[15] DCM was the only solvent we tested that allowed a differentiation of both $1e^-$ oxidations at slow scanning rates. Interestingly, when ACN was used as a solvent, the reduction process became more evident, but still irreversible. This is surprising, as unsubstituted AB in ACN with $TBAPF_6$ has already been employed in an asymmetric battery setup and showed good cyclability.[18] To examine the effect of electrolytes, *N*,*N*-dimethylformamide (DMF) was employed as the reference solvent. With lithium bis(trifluoromethanesulfonyl)imide (LiTFSI), the oxidation stays reversible but the reduction is irreversible. Additionally, a second oxidation peak appears that may be referenced to the initial irreversible reduction, as this peak is not present if only the oxidation is scanned (see Supporting Information Figure S5). This large peak-to-peak separation could be due to the high affinity of Li^+ cations with the $N{=}N^-$ motif that forms upon reduction.[17] This effect might be increased due to the electron rich motif of the 4,4'-diamino AB versus unsubstituted AB. Comparing the voltage profiles of tetra-*n*-butylammonium tetrafluoroborate ($TBABF_4$) and $TBAPF_6$ solutions highlights the important role of the electrolyte cation. While the PF_6^- salt shows good reversibility for the $2e^-$ oxidation, as well as for the $1e^-$ reduction of the parent compound, a low current flow was observed for the boron equivalent. One reason for that could be the deposition of insoluble BF_4^- salts on the electrode (see below), as shown by successively scanning (see Supporting Information Figure S7). Nevertheless, the DMF/$TBAPF_6$ electrolyte system allows to reversibly access three different redox states of our AB: neutral AB, the reduced radical anion, and the oxidized bis-quinoidal dication structure.

To optimize the redox activity of 4,4'-amino ABs, the influence of the amino groups was investigated (Figure 3, bottom). With the elongation of the alkyl group from methyl (**3e**) to ethyl (**3f**), no significant change of the peak potentials or the voltage window was observed, although the solubility of the ethyl derivative **3f** was superior to **3e** (32 mg/mL and 2.1 mg/mL for **3f** and **3e** in DMF, respectively). Changing the substituents from alkyl to an aromatic phenyl group (**3g**) facilitated the reduction by 400 mV, and shifted the oxidation by +300 mV. This might be explained by the more electron poor amine, leading ultimately to a lower electron density in the AB core. When the nitrogen atom was incorporated into the aromatic carbazole motif (**3h**), the redox behavior changes drastically. Compound **3h** is reduced at −1.10 V and oxidized at 1.47 V, but both of these reactions proceed irreversibly. As carbazole itself can show irreversible redox processes with complex reaction

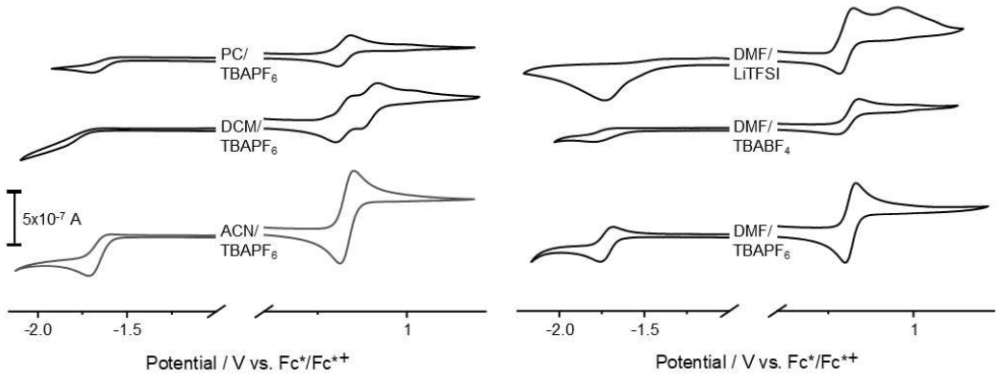

Figure 2. Cyclic voltammograms of model compound **3f** with varying conductive salts and organic solvents. Solutions were prepared with 2 mM of **3f**, 200 mM salt and 1 mM Fc^* as an internal standard. Potentials are referenced to the standard and measured with a scan rate of 100 mV/s.

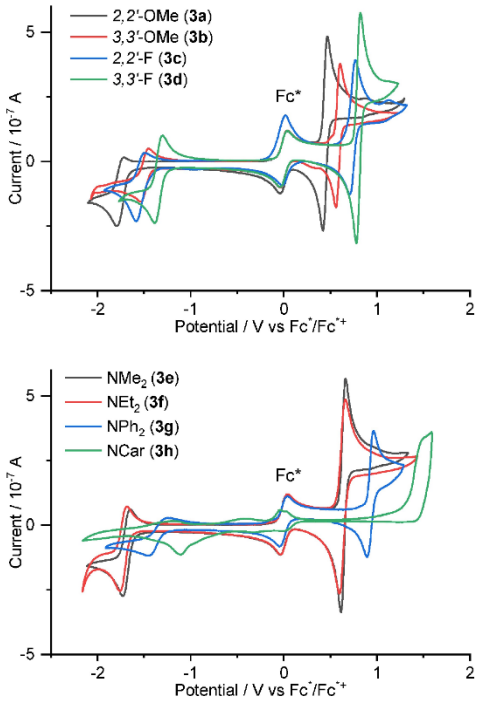

Figure 3. Influence of substitution of the 4,4'-amino AB scaffold in the cyclic voltammograms of compounds **3a–h** in DMF/$TBAPF_6$ electrolyte measured with a scan rate of 100 mV/s. Measured with and referenced to Fc*.

Table 1: Peak potentials of substituted ABs **3a–h** in DMF/$TBAPF_6$ at 100 mV/s vs Fc*.

Substitution Pattern	E_{red} /V	E_{ox} /V	$\Delta E_{ox\text{-}red}$ /V
2,2'-OMe (**3a**)	−1.74	0.62	2.36
3,3'-OMe (**3b**)	−1.49	0.59	2.08
2,2'-F (**3c**)	−1.54	0.72	2.26
3,3'-F (**3d**)	−1.34	0.80	2.14
NMe_2 (**3e**)	−1.68	0.64	2.32
NEt_2 (**3f**)	−1.73	0.63	2.36
NPh_2 (**3g**)[a]	−1.33	0.94	2.27
NCar (**3h**)[b]	−1.10	1.47	2.57

[a] Due to low solubility, only 1 mM concentration of substrate.
[b] Irreversible redox behavior.

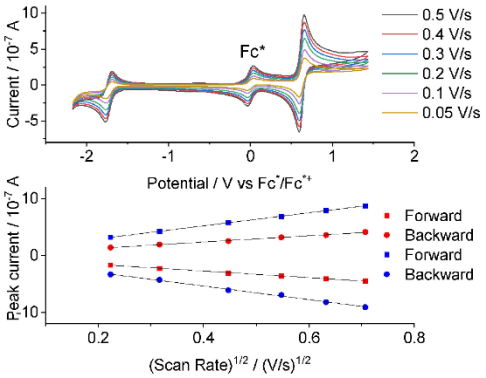

Figure 4. Electrochemical characterization of **3f**. Top: Cyclic voltammogram of **3f** in 2 mM concentration with 200 mM $TBAPF_6$ conducting salts at different scan rates from 0.5 V/s to 0.05 V/s. Bottom: Plot of the reduction and re-oxidant (red) and of the oxidation and re-reduction (blue) peak currents versus the square root of the scan rate.

products, the combination with AB might show a similar behavior.[29]

Additionally, electron-withdrawing fluorine and electron-donating methoxy groups were placed in the *ortho*- or *meta*-position of the AB core (Figure 3, top). Here, the most important observation is the decrease in the reversibility of *ortho*-substituted derivatives **3a** and **3c**. Redox peak positions can be fine-tuned by adding these groups, but the voltage window between reduction and oxidation is not larger in comparison to the unsubstituted analogs, ultimately not resulting in an improved electrochemical storage potential (Table 1).

For the diethyl derivative **3f**, which shows the largest ΔE of the tested substrates, good reversibility can be demonstrated on the CV timescale (Figure 4 top). A linear relationship between the peak currents and the square root of the scan rate reveals a diffusion-controlled behavior for the reduction, as well as for the oxidation (Figure 4 bottom). Diffusion coefficients for **3f** obtained from the Randles–Sevcik equation give different values depending on which forward redox process is monitored, with 1.36×10^{-6} cm^2s^{-1} and 8.29×10^{-7} cm^2s^{-1} for reduction and oxidation respectively. These values are comparable to other organic materials,[30] and to unsubstituted AB.[17] Diffusion coefficients of the back reactions gave 1.01×10^{-6} cm^2s^{-1} for the radical anion and 8.73×10^{-6} cm^2s^{-1} for oxidized species $\mathbf{3f^{2+}}$. Even at high concentrations of 100 mM or at saturation, reversibility is observed (SI Figures S9 and S10). According to these cyclic voltammetry studies, the bis-*para*-alkylamine substituted AB offers the possibility to be employed in symmetrical RFB as a bipolar, redox-active material.

To further explore their electrochemical properties, charge/discharge studies in an H-cell were performed. As the application of AB as the anolyte is well established, we employed compound **3f** as the catholyte (see Supporting Information page 42). AB $\mathbf{3f^{2+}}$ was electrochemically synthesized and then cycled in a symmetrical H-cell with neutral compound ($\mathbf{3f/3f^{2+}}$) under galvanostatic charge/discharge (2 C) in DMF (see Supporting Information Figure S22 and S23). Under these conditions a capacity decay of approximately 30 % was observed after 10 cycles. Additionally, the charging was performed with the chemically oxidized $\mathbf{3f^{2+}}$ in a symmetrical H-cell utilizing ACN as the solvent, which

slightly increased the performance (approximately 25% decay after 10 cycles, see Supporting Information Figure S24 and S25). Unfortunately, we were not able to cycle the $1e^-$ reduction in DMF, most probably due to the high basicity of our employed AB **3f**, leading to instability over the time-frame of our cycling experiments.

The reduction of AB has been studied thoroughly, and the $1e^-$ reduced species has been identified as the radical anion, while the $2e^-$ species corresponds to the double deprotonated hydrazine. For the oxidation of 4,4'-disubstituted AB with amines or with hydroxides, the bis-quinoidal structure is the assumed species. The formation of the stable quinone structure by bis-*para*-substitution is thought to be responsible for the fully reversible oxidation. Albeit the occurrence of the quinoidal structure is observed for "Weitz type" 4,4'-bispyridinium salts,[31] and theoretical calculation support the presence of a similar bonding type in ABs,[15] to the best of our knowledge, no experimental characterization is available. By using the chemical oxidant $NOBF_4$ in ACN solution, removing the solvent and vapor diffusion of diethyl ether from DCM, crystals suitable for X-ray diffraction were obtained. The double positively charged AB crystallized with two BF_4^- anions and one H_2O molecule in the $P_{21/n}$ space group. The low solubility of the crystallized product might explain the irreversible behavior in electrolyte solution containing a BF_4^- counter ion. The needle-like crystals appear blue or orange, depending on the viewing angle. By comparing it with the parent AB, an increase of the N_{azo}–N_{azo} bond length (1.27 to 1.36 Å), as well as a decrease of the N_{azo}–C_{aryl} bond length from 1.42 to 1.32 Å was observed (Figure 5).[32] These lengths are consistent with density functional theory (DFT) calculations.[15]

Additionally, there is a bond length alternation of C_{aryl}–C_{aryl} in the ring system. From the bond lengths c, d, e, c', d', and e', the quinoid characters[34] of $\delta_r = 0.019$ Å and 0.100 Å are obtained for **3f** and $\mathbf{3f^{2+}}$, respectively. The large value of 0.100 Å supports the fully quinoid structure of the oxidized form. To verify that the oxidized species formed by chemical oxidation equals the one formed during electrochemical analysis, **3f** was titrated with $NOBF_4$ (1.0–2.0 eq.) and the change in absorbance was analyzed. The obtained spectra were compared to measurements in a spectroelectrochemistry cell (Figure 6 and Supporting Information page 40).

The experiments show the decrease of the neutral AB **3f** π–π* band at around 470 nm, and an increase of a band at around 380 nm of $\mathbf{3f^{2+}}$. Both spectral changes pass over a species at 680 nm, which was assigned to a radical cation in previous studies.[15] This supports that the fully quinoidal structure obtained by chemical oxidation is the same as that observed during electrochemical measurements.

Conclusion

We presented the application of 4,4'-diamino ABs as bipolar redox-active materials. The combination of DMF and $TBAPF_6$ as an electrolyte allows $1e^-$ reduction of the N=N bond, as well as the stable formation of a bis-quinoidal form by a $2e^-$ oxidation process. We employed our model substrate as a redox couple $\mathbf{3f/3f^{2+}}$ in symmetric H-cell cycling experiments and observed a notable capacity decay over multiple cycles. Here, additional molecular engineering is needed to allow for a fully operational symmetrical RFB. One approach could be the shielding of the resulting Michael system. Making the whole AB less electron-rich might facilitate the $1e^-$ reduction for cycling experiments. The formation of this oxidized form in the hitherto only predicted oxidation mechanism was further elucidated by X-ray analysis, which strongly suggests the presence of an azobenzene-quinoidal structure. By attaching electron donating or withdrawing substituents, the potentials can be fine-tuned, ranging from −1.34 to −1.74 V for the reduction,

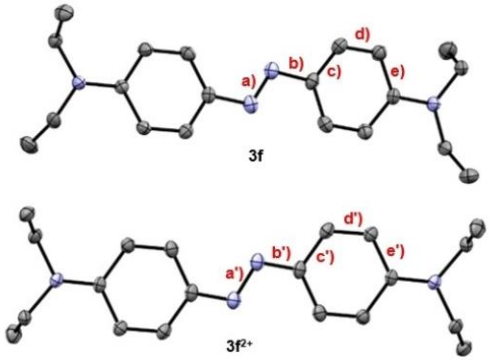

Figure 5. Solid-state structures of AB **3f** (from CCDC: 1000644)[32] and $\mathbf{3f^{2+}}$ (CCDC: 2247535) from the chemical oxidation with $NOBF_4$. Solvent molecules, hydrogens and counter anions are omitted for clarity. Thermal ellipsoids are shown at 50% probability. Bond lengths in Å: $a = 1.266$, $a' = 1.363$, $b = 1.423$, $b' = 1.321$, $c = 1.385$, $c' = 1.442$, $d = 1.382$, $d' = 1.346$, $e = 1.417$, $e' = 1.450$.[33]

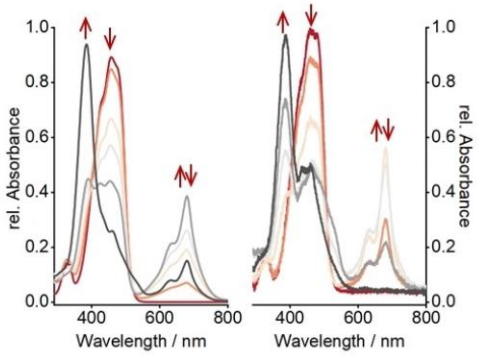

Figure 6. UV/Vis absorption spectra (left) of **3f** in ACN titrated with chemical oxidant $NOBF_4$, and spectra resulting from spectroelectrochemical analysis (right) of **3f** in ACN. Increasing oxidation from red to black.

and 0.59 to 0.80 V for the oxidation. Aryl substituents seem to influence the redox behavior the most, but show inferior redox properties, due to their irreversibility and low solubility. Elongation of alkyl substituents at the amine-nitrogen improves solubility, while retaining the redox behavior. These results provide the essential basis for application of AB derivatives in the important field of (electrochemical) energy storage.

Acknowledgements

The authors thank BMEL (Federal Ministry of Food and Agriculture) within the project FOREST (62000958) and DFG (HA-8832/2-1) for funding, Prof. Peter R. Schreiner for providing the electrochemical cell setup. Open Access funding enabled and organized by Projekt DEAL.

Conflict of Interest

The authors declare no conflict of interest.

Data Availability Statement

The data that support the findings of this study are available in the supplementary material of this article.

Keywords: azo compounds · electrochemistry · cyclic voltammetry · energy conversion · redox chemistry

[1] E. Mitscherlich, *Ann. Pharm.* **1834**, *12*, 311–314.
[2] F. A. Jerca, V. V. Jerca, R. Hoogenboom, *Nat. Chem. Rev.* **2022**, *6*, 51–69.
[3] Elsevier Publishing Company (Hrsg.) *Lex Prix Nobel*, Amsterdam, **1965**.
[4] G. S. Hartley, *Nature* **1937**, *140*, 281.
[5] a) M. M. Lerch, M. J. Hansen, G. M. van Dam, W. Szymanski, B. L. Feringa, *Angew. Chem. Int. Ed.* **2016**, *55*, 10978–10999; b) J. Broichhagen, J. A. Frank, D. Trauner, *Acc. Chem. Res.* **2015**, *48*, 1947–1960.
[6] O. Bozovic, B. Jankovic, P. Hamm, *Nat. Chem. Rev.* **2022**, *6*, 112–124.
[7] T. I. Y. Yu, *J. Photochem. Photobiol. C* **2004**, *5*, 247–265.
[8] W. R. Browne, B. L. Feringa, *Nat. Nanotechnol.* **2006**, *1*, 25–35.
[9] X. Pang, J. -Lv, C. Zhu, L. Qin, Y. Yu, *Adv. Mater.* **2019**, *31*, e1904224.
[10] C. Averdunk, K. Hanke, D. Schatz, H. A. Wegner, *Acc. Chem. Res.* **2024**, *57*, 257–266.
[11] B. Zhang, Y. Feng, W. Feng, *Nano-Micro Lett.* **2022**, *14*, 138.
[12] T. J. Kucharski, N. Ferralis, A. M. Kolpak, J. O. Zheng, D. G. Nocera, J. C. Grossman, *Nat. Chem.* **2014**, *6*, 441–447.
[13] D. Schulte-Frohlinde, *Liebigs Ann.* **1958**, *612*, 131–138.
[14] A. Goulet-Hanssens, M. Utecht, D. Mutruc, E. Titov, J. Schwarz, L. Grubert, D. Bléger, P. Saalfrank, S. Hecht, *J. Am. Chem. Soc.* **2017**, *139*, 335–341.
[15] A. Goulet-Hanssens, C. Rietze, E. Titov, L. Abdullahu, L. Grubert, P. Saalfrank, S. Hecht, *Chem* **2018**, *4*, 1740–1755.
[16] E. Franz, A. Kunz, N. Oberhof, A. H. Heindl, M. Bertram, L. Fusek, N. Taccardi, P. Wasserscheid, A. Dreuw, H. A. Wegner, O. Brummel, J. Libuda, *ChemSusChem* **2022**, *15*, e202200958.
[17] L. Zhang, Y. Qian, R. Feng, Y. Ding, X. Zu, C. Zhang, X. Guo, W. Wang, G. Yu, *Nat. Commun.* **2020**, *11*, 3843.
[18] X. Wang, J. Chai, A. Lashgari, J. J. Jiang, *ChemElectroChem* **2021**, *8*, 83–89.
[19] a) D. Xu, C. Zhang, Y. Zhen, Y. Zhao, Y. Li, *J. Power Sources* **2021**, *495*, 229819; b) X. Zu, L. Zhang, Y. Qian, C. Zhang, G. Yu, *Angew. Chem. Int. Ed.* **2020**, *59*, 22163–22170.
[20] a) J. Winsberg, T. Hagemann, T. Janoschka, M. D. Hager, U. S. Schubert, *Angew. Chem. Int. Ed.* **2017**, *56*, 686–711; b) P. Leung, A. A. Shah, L. Sanz, C. Flox, J. R. Morante, Q. Xu, M. R. Mohamed, C. Ponce de León, F. C. Walsh, *J. Power Sources* **2017**, *360*, 243–283; c) X. Wei, W. Pan, W. Duan, A. Hollas, Z. Yang, B. Li, Z. Nie, J. Liu, D. Reed, W. Wang, V. Sprenkle, *ACS Energy Lett.* **2017**, *2*, 2187–2204; d) V. Singh, S. Kim, J. Kang, H. R. Byon, *Nano Res.* **2019**, *12*, 1988–2001; e) J. Luo, B. Hu, M. Hu, Y. Zhao, T. L. Liu, *ACS Energy Lett.* **2019**, *4*, 2220–2240; f) D. G. Kwabi, Y. Ji, M. J. Aziz, *Chem. Rev.* **2020**, *120*, 6467–6489.
[21] J. L. Sadler, A. J. Bard, *J. Am. Chem. Soc.* **1967**, *90*, 1979–1989.
[22] G. H. Aylward, J. L. Garnett, J. H. Sharp, *Anal. Chem.* **1967**, *39*, 457–460.
[23] A. J. Bellamy, I. S. MacKirdy, C. E. Niven, *J. Chem. Soc. Perkin Trans. 2* **1983**, 183–185.
[24] a) M. L. Perry, J. D. Saraidaridis, R. M. Darling, *Curr. Opin. Electrochem.* **2020**, *21*, 311–318; b) M. Li, J. Case, S. D. Minteer, *ChemElectroChem* **2021**, *8*, 1215–1232; c) R. A. Potash, J. R. McKone, S. Conte, H. D. Abruña, *J. Electrochem. Soc.* **2016**, *163*, A338–A344.
[25] a) Q. Zhou, T. A. Reekie, R. H. Abbassi, D. Indurthi Venkata, J. S. Font, R. M. Ryan, L. Munoz, M. Kassiou, *Bioorg. Med. Chem.* **2018**, *26*, 5852–5869; b) M. Kohn, *J. Org. Chem.* **1953**, *18*, 530–533.
[26] C. Zhang, N. Jiao, *Angew. Chem. Int. Ed.* **2010**, *49*, 6174–6177.
[27] a) S. Samanta, A. Babalhavaeji, M. Dong, G. A. Woolley, *Angew. Chem. Int. Ed.* **2013**, *52*, 14127–14130; b) D. Wu, M. Dong, C. V. Collins, A. Babalhavaeji, G. A. Woolley, *Adv. Opt. Mater.* **2016**, *4*, 1402–1409.
[28] A. Czompa, B. L. Pásztor, J. A. Sahar, Z. Mucsi, D. Bogdán, K. Ludányi, Z. Varga, I. M. Mándity, *RSC Adv.* **2019**, *9*, 37818–37824.
[29] K. Karon, M. Lapkowski, *J. Solid State Electrochem.* **2015**, *19*, 2601–2610.
[30] Y. Yan, S. G. Robinson, M. S. Sigman, M. S. Sanford, *J. Am. Chem. Soc.* **2019**, *141*, 15301–15306.
[31] Z. Liu, M. Frasconi, W.-G. Liu, Y. Zhang, S. M. Dyar, D. Shen, A. A. Sarjeant, W. A. Goddard III, M. R. Wasielwski, J. F. Stoddart, *J. Am. Chem. Soc.* **2018**, *140*, 9387–9391.
[32] K. Gajda, B. Zarychta, Z. Daszkiewicz, A. A. Domanski, K. Ejsmont, *Acta Crys. C* **2014**, *70*, 575–579.
[33] Deposition numbers 2247535 (for **3f**$^{2+}$), 2247536 (Side product of the Buchwald–Hartwig coupling of electron poor azobenzenes, see Supporting Information Figure S28), and 2247537 (for **3h**) contains the supplementary crystallographic data for this paper. These data are provided free of charge by the joint Cambridge Crystallographic Data Centre and Fachinformationszentrum Karlsruhe Access Structures service. These data can be obtained free of charge via https://www.ccdc.cam.ac.uk/structures/.
[34] C. Dehu, F. Meyers, J. L. Brédas, *J. Am. Chem. Soc.* **1993**, *115*, 6198–6206.

Manuscript received: March 22, 2024
Accepted manuscript online: June 13, 2024
Version of record online: July 29, 2024

4.2 Amino-substituted Azoxybenzenes as Potential Redox-Active Catholyte Materials

Reference: D. Schatz, C. Burdenski, F. M. Schneider, M. M. Hansmann, H. A, Wegner, *Chem*. *Eur*. *J*. **2025**, *63*, e202404001.

DOI: 10.1002/chem.202404001

Aryl diazenes, particularly azobenzenes (AB), represent a versatile class of compounds with significant historical and practical relevance, ranging from dyes to molecular machines, solar thermal and electrochemical storage. Their oxygen-substituted counterparts, azoxybenzenes (AOB), share structural similarities but have been less explored, especially in energy storage applications. This study investigates the redox properties of AOB, comparing them to AB, and evaluates their potential as redox-active materials for energy storage systems. Through cyclic voltammetry (CV) and spectro-electrochemical analyses, we demonstrate that AOBs exhibit a distinct redox behaviour, influenced by the solvent and electrolyte environment, with a reversible oxidation process. Despite their promising redox characteristics, AOBs suffer from capacity decay during galvanostatic cycling, likely due to the instability of the radical cation intermediate. These findings suggest that while AOBs offer intriguing redox properties, further investigation into stabilization strategies are needed for their application in energy storage.

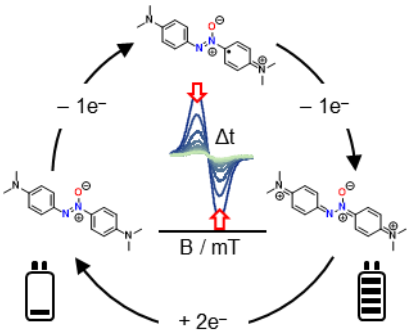

Chemistry - A European Journal

10.1002/chem.202404001

WILEY-VCH

RESEARCH ARTICLE

Amino-substituted Azoxybenzenes as Potential Redox-Active Catholyte Materials

Dominic Schatz,[a, b] Chris Burdenski,[c] Finn M. Schneider,[a, b] Max M. Hansmann,[c] and Hermann A. Wegner*[a, b]

[a] D. Schatz, F. M. Schneider, Prof. Dr. H. A. Wegner
Institute of Organic Chemistry
Justus Liebig University Giessen
Heinrich-Buff-Ring 17, 35392 Gießen (Germany)
E-mail: hermann.a.wegner@org.chemie.uni-giessen.de

[b] D. Schatz, F. M. Schneider, Prof. Dr. H. A. Wegner
Center of Materials Research (ZfM/LaMa)
Justus Liebig University
Heinrich-Buff-Ring 16, 35391 Gießen (Germany)
35392 Gießen (Germany)

[c] C. Burdenski, Prof. Dr. M. M. Hansmann
Faculty of Chemistry and Chemical Biology (CCB)
Technical University of Dortmund
Otto-Hahn Str. 6. 44227 Dortmund (Germany)

Supporting information for this article is given via a link at the end of the document.

Abstract: Aryl diazenes, particularly azobenzenes (AB), represent a versatile class of compounds with significant historical and practical relevance, ranging from dyes to molecular machines, solar thermal and electrochemical storage. Their oxygen-substituted counterparts, azoxybenzenes (AOB), share structural similarities but have been less explored, especially in energy storage applications. This study investigates the redox properties of AOB, comparing them to AB, and evaluates their potential as redox-active materials for energy storage systems. Through cyclic voltammetry (CV) and spectro-electrochemical analyses, we demonstrate that AOBs exhibit a distinct redox behaviour, influenced by the solvent and electrolyte environment, with a reversible oxidation process. Despite their promising redox characteristics, AOBs suffer from capacity decay during galvanostatic cycling, likely due to the instability of the radical cation intermediate. These findings suggest that while AOBs offer intriguing redox properties, further investigation into stabilization strategies are needed for their application in energy storage.

Introduction

Azobenzenes (AB) are gaining attention as versatile active materials for energy storage. Their reversible (*E*)- to (*Z*)-isomerization,[1] and the energy difference between the ground state isomer and the metastable state, are the major foundation for their application as molecular organic solar thermal (MOST) storage systems or as phase change materials.[2] In these storage types, solar energy is stored as bond strains, and is released as heat. A recently established application of ABs for energy storage is their usage in organic batteries due to their reversible reduction. This feature was applied in 2020 by Zhang *et al.* for constructing the first AB redox-flow battery (RFB), in which AB acts as the anolyte.[3] RFBs are a promising technology for large-scale energy storage, especially suitable for grid management with fluctuating energy production from renewables.[4,5] Further improvements based on Zhang's seminal technology increase the operating voltage or transferred the system to an aqueous medium.[6–9] These battery applications are based on the reversible formation of a radical anion, located *inter alia* on the N=N double bond.[10,11] By placement of amino or hydroxyl groups in the *para* positions, an additional reversible 2e$^-$ oxidation redox event is realized (Figure 1).[12] Recently, we were able to crystallize the oxidation product by reacting the 4,4'-diethylamine AB with $NOBF_4$, and confirmed the formation of bis-quinone type structure by single crystal XRD.[13] We applied the 4,4'-diethylamino AB as the catholyte in galvanostatic charge/discharge experiments. Although we observed noticeable degradation over multiple cycles, this was the first time AB has been employed as a catholyte.

A structurally akin compounds to AB are azoxybenzenes (AOB). Although AOB are synthetically and structurally similar to their widely utilized counterpart AB,[14] there are only a few applications, e.g. in the field of liquid crystals, polymers[15] and drugs.[16] For AOB, their reductive electrochemical behavior has been comprehensively studied. In aqueous or protic solvents, a 4e$^-$ irreversible reduction is observed.[17,18] This reduction leads to the formation of aryl hydrazines, which upon reoxidation provides AB. The removal of oxygen, therefore, represents an irreversible redox process of AOB. In aprotic solvents, the reductive redox chemistry is dependent on the supporting electrolytes.[19] A DMF solution with 0.2 M $NaNO_3$ shows a similar reduction behavior to AB, while tetra-*n*-butyl ammonium salts split the obtained reduction into three separate waves, with the first wave being reversible. The first wave is ascribed to the radical anion of AOB, as shown by *in situ* UV-VIS spectroscopy. The second wave corresponds to the formation of the AOB di-anion. This electron-rich species is protonated, and by elimination of hydroxide, AB is formed.[20] As AB is reduced to the radical anion at potentials needed for the second AOB reduction, the formed AB is directly consumed.[21] The third observed wave is therefore the formation of the hydrazine from AB radical anion. The structure of the AOB and AB have been studied by EPR studies thoroughly being stable in aprotic solvents.[22,23]

Chemistry - A European Journal

10.1002/chem.202404001

WILEY-VCH

RESEARCH ARTICLE

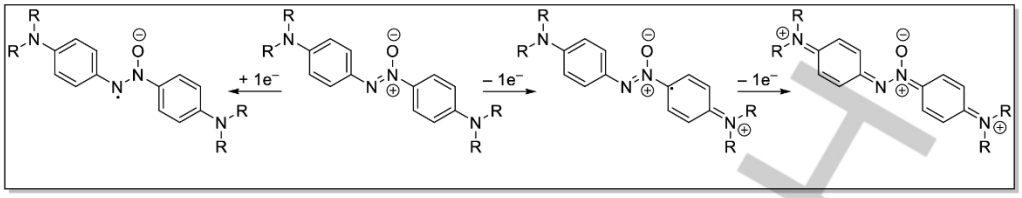

Figure 1. The 1 e⁻ reduction of AOB to a radical anion, the two subsequent 1 e⁻ oxidations affording a radical cation and the proposed bis-quinoidal structure AOB^{2+}.

Similar to 4,4'-diamino substituted AB that form quinoidal structures upon oxidation, 4,4'-diamino AOBs show reversible 2e⁻ oxidation, which proceeds *via* a radical cation (Figure 1).[24] The groups of Kubota and Hecht showed a convincing correlation between nonaqueous redox potentials with Hammett parameters for *para*- and *meta*-substituted AOB and 4-amino AB respectively.[25,24,10,12] Although a direct comparison of the obtained Hammett plots is not possible, as the oxidation mechanisms of 4-amino substituted diaza-compounds is different to AB, an interesting effect can be observed by comparing 4,4'-dimethylamino AB and AOB: The potential difference between oxidation and the first reduction process is considerably larger for AOB. Herein, we want to introduce AOB as a new class of compounds for energy storage in comparison to their widely known AB counterparts. As the larger oxidative redox potential could lead to a larger cell voltage, AOB could be a potential improvement for storage solutions based on diazenes.

Results and Discussion

Cyclic voltammetry (CV) measurements of 4,4'-dimethylamino AB **4a** and AOB **3a** under the same conditions (DMF and 0.2 M $TBAPF_6$) and setup, revealed very similar reduction potentials for both compounds, while the oxidation is shifted by 160 mV to more positive potentials for AOB (Figure 2). This might be surprising, as the radical anion formed during the reduction is mainly located on the nitrogen-nitrogen bond (where the oxygen substituent of AOB is located), while the quinoidal structure is distributed over the entire molecule.

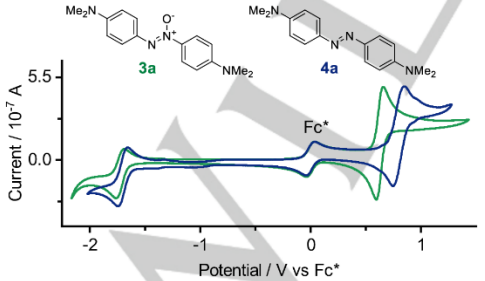

Figure 2. Cyclic voltammograms of 4,4'-dimethylamino AB **4a** (green) and AOB **3a** (blue). Solutions were prepared with 2 mM substrate, 200 mM $TBAPF_6$ and 1 mM Fc* as an internal standard in DMF. Potentials are referenced to the standard and measured with a scan rate of 100 mV/s.

To further examine AOB redox properties, CV measurements in a variety of solvents and electrolytes were conducted. The 4,4'-diethylamino AOB **3b** was employed as model substrate in 2 mM concentration with 1 mM decamethylferrocene (Fc*) as an internal standard. For solvents, propylene carbonate (PC), dichloromethane (DCM), acetonitrile (ACN) and *N*,*N*'-dimethylformamide (DMF) were tested with 0.2 M tetra-*n*-butylammonium hexafluorophosphate ($TBAPF_6$). For electrolyte salts lithium bis(trifluoromethanesulfonyl)imide (LiTFSI), tetra-*n*-butylammoium tetrafluoroborate ($TBABF_4$) and $TBAPF_6$ in DMF were investigated (Figure 3). The selection of electrolytes and solvents were based on our previous work on AB as a catholyte, in which we obtained similar results.[13] For PC, an irreversible reduction was observed, which is rationalized by the nucleophilic attack of the electron-rich radical anion to the carbonate, as observed for deprotonated pyridazinones.[26] In ACN and DCM, the reduction remains irreversible, while the oxidation is noticeably split into two consecutive 1e⁻ processes. The voltage difference between these two processes is larger in less coordinating solvents, such as DCM. In the case of AB, DCM was the only solvent that allowed the observation of the two separate oxidation steps as the redox potentials of both oxidations were very close.[13] Titration experiments also proved the stepwise oxidation in ACN, though.[12] For AOB the first and second oxidation potentials are more different. Even in DMF the second oxidation is visible as a shoulder in the CV at scan rates of 0.1 V/s. By changing the electrolyte salt from a tetra-*n*-butylammonium salt to LiTFSI an additional peak appears at positive voltages. Radical anions of AOB can form cyclic dimeric complexes with alkali metals, shown by the reduction of unsubstituted AOB with $C_8H_8K_2$ in THF solutions.[27]

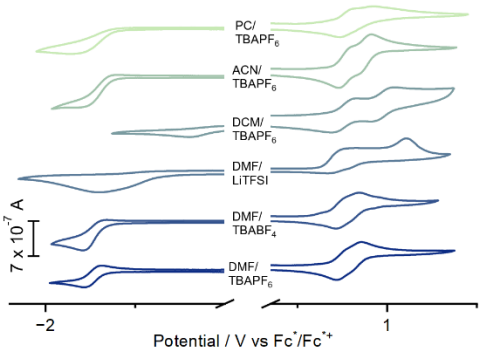

Figure 3. Cyclic voltammograms of model compound **3b** in varying solvents and with varying salts. Solutions were prepared with 2 mM **3b**, 200 mM $TBAPF_6$ and 1 mM Fc* as an internal standard. Potentials are referenced to the standard and measured with a scan rate of 100 mV/s.

Chemistry - A European Journal

10.1002/chem.202404001

WILEY-VCH

RESEARCH ARTICLE

In the case of the more electron rich 4,4'-diethylamino AOB this complexation might be facilitated and influence the redox behavior. Changing the counter anion of the ammonium salts does not alter the appearance of the CV curves.

For AB, the resulting BF_4^- salt of the oxidized species exhibit low solubility and precipitated on the electrodes.[13] Interestingly, the oxidized AOB does not seem to precipitate from solution, which can be rationalized with the higher solubility of the employed 4,4'-diethylamino AOB **3b** in comparison to AB **4b**.

As the electrolyte capacity is dependent on the amount of dissolved redox active species, solubility is an important metric to optimize.[28] To improve solubility we stepwise optimized the alkyl chains from methyl to hexyl on the amine nitrogen (Scheme 1).

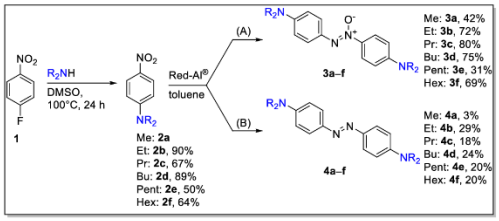

Scheme 1. Preparation of dialkylamino AOBs **3a-f** and ABs **4a-f**. A) 1.5 equiv. Red-Al®, 0 °C to r-t. B) 2.5 equiv. Red-Al®, 0 °C to reflux.

Nucleophilic aromatic substitution of commercially available 4-fluoronitrobenzene (**1**) with the corresponding alkyl amine was carried out at 100 °C in DMSO to yield 4,4'-dialkylamino nitrobenzenes **2b-f**. A reductive coupling of these nitrobenzenes using Red-Al® provided the symmetrical AOBs or ABs, depending on the reaction conditions. With the minimal required equivalents of reducing agent and stirring at 0 °C, AOBs **3a-f** were obtained in good yields. If stronger reductive conditions were used with more equivalents of Red-Al® and a short period of reflux, the AB compounds **4a-f** were obtained in moderate yields. For ethyl AB **4b** and AOB **3b**, the solubility in DMF solution is 32 mg/mL and 59 mg/mL, respectively. Here, the dipole moment could be the reason why AOB has an increased solubility compared to AB, although this effect is reversed up to C_5 chains, where AOB is an oil (SI page 52). CV measurements of alkyl AB **3a-f** and AOB **4a-f** show the expected redox behavior of one $1e^-$ reduction and two $1e^-$ oxidations (SI page 41). The maximal peak current obtained for both redox processes, decreases for longer alkyl chains. Due to the linear relationship of the peak current and the square root of the scan rate, diffusion coefficients can be estimated using the Randles-Ševčík equation. Forward and reverse scans of the oxidation process deliver different diffusion coefficients, with the diffusion coefficients of AOB being smaller than for AB (SI page 49). The diffusion coefficient is another important metric as it plays a major part in obtainable current density and can lead to large overpotentials.[29]

As AOBs show good reversibility of the redox events independently of the scan rate, we further explored the applicability in electrochemical energy storage. As we were not able to cycle the reduction of AB, we applied AOBs only as the catholyte in charge/discharge H-cell studies. We choose the ethyl derivative **3b** as a model substrate as it shows good solubility and can be compared to the 4,4'-diethylamino AB **4b** that we applied earlier in galvanostatic charging cycles.[13] AOB^{2+} $\mathbf{3b^{2+}}$ was prepared *in situ* by oxidation with $NOPF_6$ and was then galvanostaticly cycled at 2C in a symmetrical H-cell against the neutral compound (**3b**/$\mathbf{3b^{2+}}$). In ACN as solvent we observed a drastic capacity decay of approximately 29% from the second to 10th cycle (SI page 53). By electrochemical preparation of the dication, similar capacity decay was observed (SI page 55). A CV scan comparing the solution before and after cycling shows a drop in concentration of the studied compound, probably due to decomposition (SI page 54 and 56). These results are similar with the observations from AB cycling studies, indicating a related degradation mechanism for the structurally akin compounds. To evaluate the stability in ACN solution, AOB **3b** was chemically oxidized with 2.05 eq. $NOPF_6$ in d_3-ACN to obtain the dication and analyzed by time dependent ^{1}H-NMR measurements (Figure 4, and SI page 34). The ^{1}H-NMR signals shift downfield similar to the ^{1}H- and ^{13}C-NMR signals of quinones in comparison to their hydroquinones. We observed no noticeable change of the observed signals even after over 6 days of being in solution at room temperature under inert conditions. These results hint to a stable bis-quinone structure of the dication.

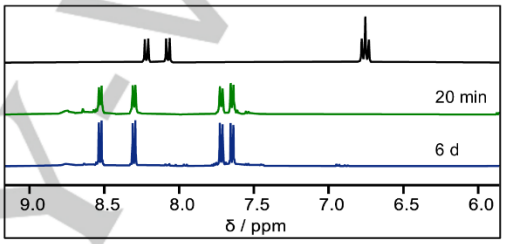

Figure 4. ^{1}H-NMR spectra of AOB **3b** (top) and after oxidation with 2.05 equiv. $NOPF_6$ in d_3-ACN over time. Depicted is only the aromatic region. (Additional spectra, see SI page 34–37)

The product shows upon oxidation with 1.00 equiv. of oxidant a broad, unresolved EPR signal (Figure 5, left). Unlike the fully oxidized (dicationic) quinone, we observed a decrease in the intensity of the EPR signal over 2 h. This suggests only a limited stability of the formed radical species. The decline of the observed signal can be fitted by an exponential function, suggesting a second or higher order kinetic for the decomposition (Figure 5, right).

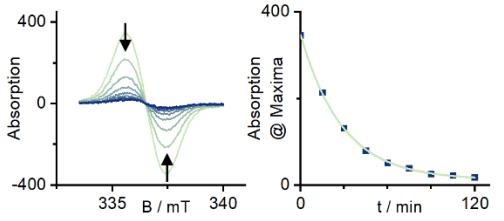

Figure 5. Left: EPR spectra of AOB **3b** after oxidation with 1.00 equiv. $NOPF_6$ in time intervals of 15 min in ACN. Right: Decay of maximum absorption of the EPR signal over time. Fitted with an exponential decay function.

AOB **3b** was titrated with $NOPF_6$, the change in absorbance was analyzed by UV-VIS spectroscopy and compared with a spectro-electrochemical measurement (Figure 6). That way it can be ensured, that the radical and the quinoidal structure obtained by chemical oxidation are the same as observed during

Chemistry - A European Journal

10.1002/chem.202404001

WILEY-VCH

RESEARCH ARTICLE

electrochemical analysis. The observed maximum at 430 nm for the neutral compound AOB can be attributed to the π-π* transition, which is red-shifted compared to the corresponding AB.[30–32] Upon oxidation, the absorbance at this maximum decreases, while two new red-shifted local maxima appear at 565 nm and 706 nm.

As the intensity of these two peaks diminishes with further oxidation, they can be assigned to a radical cation intermediate. Further oxidation results in a new maximum at 455 nm, along with multiple absorption peaks around 670 nm. The red-shifted absorption is distinctly different from the oxidized form of AB, which exhibited only an absorption maximum at 380 nm.

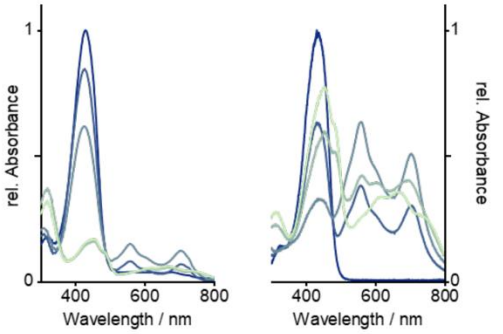

Figure 6. Left: UV-Vis absorption spectra of AOB **3b** in ACN, titrated with $NOPF_6$. Right: Spectra resulting from a slow CV scan (0.15 V to 0.9 V with 2 mV/s vs Fc) in ACN with $TBAPF_6$. Increasing oxidation from blue to green.

The instability of the intermediate cation radical could explain the observed capacity decay during galvanostatic charge/discharge cycling. As the observed capacity decay is similar to that of AB, and both structurally akin compounds show similar spectro-electrochemical responses, a comparable degradation mechanism of AOB and AB can be expected.[13] The larger capacity decay of AOB in comparison to AB can be explained by the more pronounced formation of the radical intermediate, as observed by the CV scans.

Conclusion

We showed a first example of an 4,4'-diamino substituted AOB as a catholyte in galvanostatic charge/discharge cycles, which can be oxidized at higher potentials then the structurally similar AB. Variation of the electrolyte system split the $2e^-$ oxidation process into two distinct $1e^-$ oxidations with a radical cation intermediate. We presented the diffusion and solubility properties of different *N*,*N*'-alkyl groups. AOB shows a notable capacity decay in H-cell cycling experiments, which we assigned to the instability of the radical cation intermediate. This proposal is supported by time-dependent EPR studies, while NMR studies showed prolonged stability of the fully oxidized compound under inert atmosphere. The analysis of the product after oxidization appears to be a quinoidal dication, similar to a previously isolated product of AB oxidation. Although AOB shows an oxidation potential that is +160 mV higher than of the corresponding AB, their electrochemical instability requires further optimization for their successful application in electrochemical energy storage systems.

Recently, a report presenting a skeletal rearrangement of azobenzenes to benzo[*c*]chinolines has been published, which showed increased electrochemical stability. This strategy is also very well suitable for the AOB and will be part of future endeavours to improve the performance of AOB.[33]

Experimental Part

Exemplary procedure for the electrophilic aromatic substitution: 4-Fluoro aniline (**1**, 2.82 g, 20.0 mmol, 1.00 equiv.), K_2CO_3 (4.15 g, 30.0 mmol, 1.50 equiv.) and diethylamine (3.11 mL, 30.0 mmol, 1.50 equiv.) were stirred at 100 °C in DMSO (dry, 10 mL) under N_2 for 24 h. After cooling to r.t., H_2O (100 mL) was added, the precipitate collected by filtration, washed with H_2O (250 mL), and thoroughly dried. The solid was recrystallized from cyclohexane (approx. 10 mL to yield the product **2b** as yellow crystals.

Yield: 3.49 g; 90%. ^{1}H-NMR ($CDCl_3$, 400 MHz) δ: 8.14 – 8.06 (m, 2H). 6.62 – 6.54 (m, 2H), 3.45 (q, J = 7.1 Hz, 4H), 1.23 (t, J = 7.1 Hz, 6H) ppm.

Exemplary procedure for the reductive coupling to azoxybenzenes: *N*,*N*'-Diethyl-4-nitrobenzenamin (**2b**, 991 mg, 5.00 mmol, 1.00 equiv.) was dissolved in toluene (dry, 25 mL) and cooled to 0 °C. Red-Al® (60%, 2.45 mL, 7.51 mmol, 1.50 equiv.) was added dropwise. The reaction mixture was stirred at 0 °C for 20 min, and at r.t. for 30 min. Afterwards, the mixture was quenched with Rusells solution, and the organic phase was washed with water (2x 30 mL). The aqueous phase was extracted with EtOAc (3x 60 mL) and combined with the toluene phase. Combined organic phases were washed with brine (50 mL), dried over $MgSO_4$, filtered and evaporated. The crude product was recrystallized two times from cyclohexane (approx. 15 mL) to yield the product **3b** as a crystalline orange solid. Yield: 617 mg; 72%. ^{1}H-NMR ($CDCl_3$, 400 MHz) δ: 8.31 – 8.22 (m, 2H), 8.16 – 8.08 (m, 2H), 6.75 – 6.59 (m, 4H), 3.48 – 3.37 (m, 4H), 1.25 – 1.16 (m, 6H) ppm.

Exemplary procedure for the reductive coupling to azobenzenes: *N*,*N*'-Diethyl-4-nitrobenzenamine (2b, 991 mg, 5.00 mmol, 1.00 equiv.) was dissolved in toluene (dry, 25 mL) and cooled to 0 °C. Red-Al® (60%, 2.00 mL, 6.25 mmol, 2.50 equiv.) was added dropwise. The reaction mixture was stirred at 0 °C for 20 min, at r.t. for 15 min, and then refluxed for 30 min. After cooling to r.t., the mixture was quenched with Rusells solution, and the organic phase was washed with water (80 mL). The aqueous phase was extracted with EtOAc (3x 60 mL) and combined with the toluene phase. Combined organic phases were dried over $MgSO_4$, filtered and evaporated. The crude product was purified by column chromatography (60 g Alox, toluene:cyclohexane 5:1, then 90 g SiO_2, cyclohexane:EtOAc 10:1) to yield the product 4b as red crystals. Yield: 617 mg; 72%. ^{1}H-NMR ($CDCl_3$, 400 MHz) δ: 7.75 – 7.68 (m, 24), 6.76 – 6.68 (m, 4H), 3.44 (q, J = 7.1 Hz, 8H), 1.21 (t, J = 7.1 Hz, 12H) ppm.

Chemistry - A European Journal

10.1002/chem.202404001

WILEY-VCH

RESEARCH ARTICLE

Acknowledgements

The authors thank BMEL (Federal Ministry of Food and Agriculture) within the project FOREST (62000958) for funding, Prof. Peter R. Schreiner for providing the electrochemical cell setup, and Marcel E. Baumert for his help with H-cell measurements. We thank the Fonds der chemischen Industrie (Kekulé fellowship to C. B.).

Keywords: azo compounds • electrochemistry • cyclic voltammetry • energy storage • radicals

[1] G. S. Hartley, *Nature* **1937**, *140*, 281.
[2] Z. Wang, P. Erhart, T. Li, Z.-Y. Zhang, D. Sampedro, Z. Hu, H. A. Wegner, O. Brummel, J. Libuda, M. Brøndsted Nielsen, K. Moth-Poulsen, *Joule* **2021**, *5*, 3116–3136.
[3] L. Zhang, Y. Qian, R. Feng, Y. Ding, X. Zu, C. Zhang, X. Guo, W. Wang, G. Yu, *Nat. Commun.* **2020**, *11*, 3843.
[4] A. Z. Weber, M. M. Mench, J. P. Meyers, P. N. Ross, J. T. Gostick, Q. Liu, *J. Appl. Electrochem.* **2011**, *41*, 1137–1164.
[5] W. Wang, Q. Luo, B. Li, X. Wei, L. Li, Z. Yang, *Adv. Funct. Mater.* **2013**, *23*, 970–986.
[6] X. Wang, J. Chai, A. Lashgari, J. J. Jiang, *ChemElectroChem* **2021**, *8*, 83–89.
[7] D. Xu, C. Zhang, Y. Zhen, Y. Zhao, Y. Li, *J. Power Sources* **2021**, *495*, 229819.
[8] X. Zu, L. Zhang, Y. Qian, C. Zhang, G. Yu, *Angew. Chem. Int. Ed.* **2020**, *59*, 22163–22170.
[9] D. Du, Y. Chen, H. Zhang, J. Zhao, L. Jin, W. Ji, H. Huang, S. Pang, *Angew. Chem. Int. Ed.* **2024**, *63*, e202408292.
[10] A. Goulet-Hanssens, M. Utecht, D. Mutruc, E. Titov, J. Schwarz, L. Grubert, D. Bléger, P. Saalfrank, S. Hecht, *J. Am. Chem. Soc.* **2017**, *139*, 335–341.
[11] E. Franz, A. Kunz, N. Oberhof, A. H. Heindl, M. Bertram, L. Fusek, N. Taccardi, P. Wasserscheid, A. Dreuw, H. A. Wegner, O. Brummel, J. Libuda, *ChemSusChem* **2022**, *15*, e202200958.
[12] A. Goulet-Hanssens, C. Rietze, E. Titov, L. Abdullahu, L. Grubert, P. Saalfrank, S. Hecht, *Chem* **2018**, *4*, 1740–1755.
[13] D. Schatz, M. E. Baumert, M. C. Kersten, F. M. Schneider, M. Brøndsted Nielsen, Max. M. Hansmann, H. A. Wegner, *Angew. Chem. Int. Ed.* **2024**, *63*, e202405618.
[14] E. Merino, *Chem. Soc. Rev.* **2011**, *40*, 3835–3853.
[15] J. M. Huang, J. F. Kuo, C. Y. Chen, *J. Appl. Polym. Sci.* **1995**, *55*, 1217–1229.
[16] H. Takahasi, T. Ishioka, Y. Koiso, M. Sodeoka, Y. Hasimoto, *Biol. Pharm. Bull* **2000**, *23*, 1387–1390.
[17] L. Holleck, A. M. Shams el Din, *Electrochim. Acta* **1968**, *2*, 199–206.
[18] L. Holleck, S. Vavricka, M. Heyrovsky, *Electrochim. Acta* **1970**, *15*, 645–656.
[19] M. Lipsztajn, T. M. Krygowski, E. Laren, Z. Galus, *J. Electroanal. Chem. Interf. Electrochem.* **1974**, *54*, 313–320.
[20] Y. Ogata, M. Tsuchida, Y. Takagi, *J. Am. Chem. Soc.* **1957**, *79*, 3397–3401.
[21] Y. Huang, J. Lessard, *Electroanalysis* **2016**, *28*, 2716–2727.
[22] S. Jacques, G. - S. Noëlle in *PATAI'S Chemistry of Functional Groups* (Hrsg.: S. Patai), Wiley, **1997**, S. 391–463.
[23] G. H. Aylward, J. L. Garnett, J. H. Sharp, *Anal. Chem.* **1967**, *39*, 457–460.
[24] T. Kubota, H. Miyazaki, M. Yamakawa, K. Ezumi, Y. Yamamoto, *Bull. Chem. Soc. Jpn.* **1979**, *52*, 1588–1596.
[25] T. Kubota, B. Uno, Y. Matsuhisa, H. Miyazaki, K. Kano, *Chem. Pharm. Bull.* **1983**, 373–385.
[26] A. Czompa, B. L. Pásztor, J. A. Sahar, Z. Mucsi, D. Bogdán, K. Ludányi, Z. Varga, I. M. Mándity, *RSC Adv.* **2019**, *9*, 37818–37824.
[27] Z. V. Todres, S. P. Avagyan, D. N. Kursanov, *J. Organomet. Chem.* **1975**, *97*, 139–144.
[28] Y. Yao, J. Lei, Y. Shi, F. Ai, Y.-C. Lu, *Nat. Energy* **2021**, *6*, 582–588.
[29] H. Wang, S. Youssef Sayed, E. J. Luber, B. C. Olsen, S. M. Shirurkar, S. Venkatakrishnan, U. M. Tefashe, A. L. Farquhar, E. S. Smotkin, R. L. McCreery, J. M. Buriak, *ACS nano* **2020**, *14*, 2575–2584.
[30] D. L. Webb, H. H. Jaffé, *J. Am. Chem. Soc.* **1964**, *86*, 2419–2421.
[31] A. Saupe, *Z. Naturforsch. A* **1963**, *18*, 336–347.
[32] P. H. Gore, O. H. Wheeler, *J. Am. Chem. Soc.* **1956**, *78*, 2160–2163.
[33] J. Zhao, W. Zhang, D. Du, Z. Liu, W. Ji, H. Huang, S. Pang, *Angew. Chem. Int. Ed.* **2024**, e202419887.

4.2.1 Inside Cover Feature

4.3 An Azobenzene-Based Liquid Molecular Solar Thermal (MOST) Storage System – Energy Carrier and Solvent

Reference: D. Schatz, C. Averdunk, R. Fritzius, H. A, Wegner, *ChemRxiv*, 10.26434/chemrxiv-2025-7v3ds-v2.

DOI: 10.26434/chemrxiv-2025-7v3ds-v2

The concept of molecular solar thermal (MOST) storage systems is based on capturing solar energy *via* photoisomerization, which can be released later as thermal energy. Generally, suitable compounds are irradiated and analyzed as a solution, as this facilitates isomerization and handling in general. Energy densities, though, are calculated for the neat compound. Herein, we want to introduce the low viscous, green light active, 2,6-difluoroazobenzene (AB), which can be efficiently irradiated, pumped and handled in its neat state. Synthesis as well as isomerization can be done conveniently in continuous flow set-up. Storage densities of 218 kJ kg^{-1} are the highest compared to other liquid azobenzenes. Additionally, the irradiation with green light and the processibility in the neat state make this compound a promising candidate for energy storage applications. Furthermore, the liquid AB can be employed as a MOST-active solvent. For example, we demonstrated the solvation of an electrolyte to induce a measurable conductivity, which then allows for electron-catalyzed back-isomerization to harvest the stored energy. Alternatively, it can act as a solvent for a higher energy MOST material. As a proof-of-concept a norbornadiene (NBD) has been dissolved in our AB solvent allowing to utilize the energy of the NBD as well as the AB solvent. Further optimization of the solute-solvents systems is required to fully harvest the potential of this new concept for efficient energy storage.

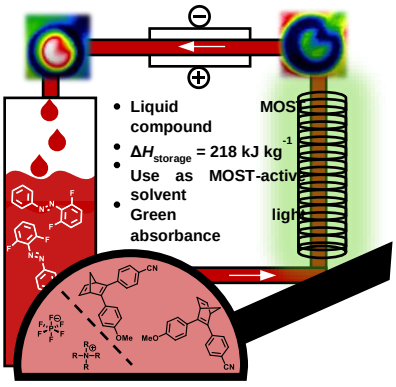

An Azobenzene-Based Liquid Molecular Solar Thermal (MOST) Storage System – Energy Carrier and Solvent

Dominic Schatz,[a, b] Conrad Averdunk,[a, b] Rouven Fritzius[a, b] and Hermann A. Wegner*[a, b]

[a] D. Schatz, C. Averdunk, R. Fritzius, Prof. Dr. H. A. Wegner
Institute of Organic Chemistry
Justus Liebig University Giessen
Heinrich-Buff-Ring 17, 35392 Gießen (Germany)
E-mail: hermann.a.wegner@org.chemie.uni-giessen.de
[b] D. Schatz, C. Averdunk, R. Fritzius, Prof. Dr. H. A. Wegner
Center of Materials Research (ZfM/LaMa)
Justus Liebig University
Heinrich-Buff-Ring 16, 35391 Giessen (Germany)
35392 Gießen (Germany)

Supporting information for this article is given via a link at the end of the document.

Abstract: The concept of molecular solar thermal (MOST) storage systems is based on capturing solar energy *via* photoisomerization, which can be released later as thermal energy. Generally, suitable compounds are irradiated and analyzed as a solution, as this facilitates isomerization and handling in general. Energy densities, though, are calculated for the neat compound. Herein, we want to introduce the low viscous, green light active, 2,6-difluoroazobenzene (AB), which can be efficiently irradiated, pumped and handled in its neat state. Synthesis as well as isomerization can be done conveniently in continuous flow set-up. Storage densities of 218 kJ kg^{-1} are the highest compared to other liquid azobenzenes. Additionally, the irradiation with green light and the processibility in the neat state make this compound a promising candidate for energy storage applications. Furthermore, the liquid AB can be employed as a MOST-active solvent. For example, we demonstrated the solvation of an electrolyte to induce a measurable conductivity, which then allows for electron-catalyzed back-isomerization to harvest the stored energy. Alternatively, it can act as a solvent for a higher energy MOST material. As a proof-of-concept a norbornadiene (NBD) has been dissolved in our AB solvent allowing to utilize the energy of the NBD as well as the AB solvent. Further optimization of the solute-solvents systems is required to fully harvest the potential of this new concept for efficient energy storage.

Introduction

As the worldwide energy demand grows, and the negative effect of fossil fuel consumption becomes prevalent, renewable energy resources become an important topic in research, as well as in politics and society. The ever increasing demand for sustainable energy production,[1,2] storage and conversion lead to a variety of promising technologies, like photovoltaic devises,[3] redox-flow batteries,[4] or efficient water splitting reactions.[5] Another enabling concept that utilizes the source of the most abundant renewable energy – the sun – are molecular solar thermal storage (MOST) systems.[6–8] The ideas behind this technology relies on the property of molecular photoswitches which can be converted from a thermodynamic stable ground state to a higher-energy metastable state by irradiation with a specific wavelength. Back-isomerization to the ground state then releases the stored thermal energy. There are multiple scaffolds that can be applied as energy storage system, each with their own advantages and disadvantages. Azobenzenes [AB, from (*E*)- to (*Z*)-isomerization] and norbornadiene [from norbornadiene (NBD) to quadricyclane (QC)] are the most explored examples (Figure 1).

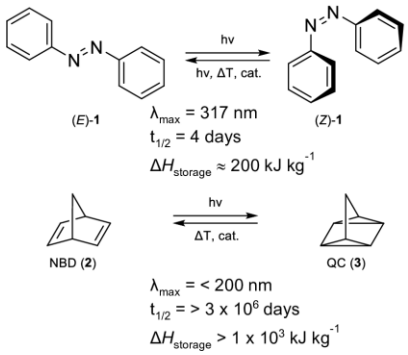

Figure 1. Selected molecular photoswitches utilized in the context of molecular organic solar thermal storage (MOST) systems.[6,9] AB **1** can be isomerized from stable (*E*)- to metastable (*Z*)-isomer, and norbornadiene (**2**, NBD) can be transformed to the quadricyclane (**3**, QC) structure.

Important parameters that need to be addressed and optimized for MOST systems are the solar spectrum match, storage time, energy density, the energy release, quantum yields and stability. In the case of AB, the higher energy (*Z*)-state can be reached by exciting the π–π* transition by irradiation at the absorption maxima. To achieve isomerization with visible light and increase the solar match, red-shifting of the π–π* band is needed. Due to the prevalent use of AB in photopharmacology, these properties have been studied in depth.[10–12] Introduction of a push-pull system across the diazo unit can shift the absorption maxima into the red region, but usually result in very fast thermal relaxation time.[13] As a large half-life is needed for most storage applications of the absorbed energy, a different way to induce green light absorption is required. An additional possibility for photoisomerization is irradiation into the n–π* band. Usually, the n–π* bands of (*E*)- and (*Z*)-AB are superimposed, so that the resulting photostationary state (PSS) does not result in adequate (*Z*)-isomer formation. This overlap can be decreased by *ortho* substitution. Wooley introduced methoxy groups in all four *ortho* positions, and observed a shift in the n–π* maxima of both isomers by 28 nm. This is due to the repulsion of the methoxy groups and the nitrogen lone pairs, which is more pronounced in the (*E*)-state, thus red-shifting the n–π* band of the (*E*)-isomer,

https://doi.org/10.26434/chemrxiv-2025-7v3ds-v2 **ORCID:** https://orcid.org/0000-0001-7260-6018

while the (*Z*)-isomer is less effected. Hecht and Bléger pioneered the *ortho* substitution with electron withdrawing fluorine substituents, which stabilize the n-orbital of the (*Z*)-isomer, as well as the π*-orbitals of both isomers, resulting in efficient net separation of the absorption of both isomers. An additional effect of the stabilized (*Z*)-n orbital is a long half-live, which is important for MOST materials. The effect of an electron-rich substituent in *ortho*-position for red shifting has been exploited by the Li group for 1,3-bis-hetero AB,[14] and for mono-hetero AB.[15]

Next to the isomerization wavelength, a large energy density, low molecular-weight compounds that show good solubility are important for efficient energy storage. If the application of interest allows solid-state photoswitches to be used, the photoisomerization can be accompanied by a phase transition.[16] The liquefication upon irradiation stores additional energy in form of the phase transition, while the crystallization upon back isomerization releases isomerization energy as well as lateral heat. Another way to increase the energy density is to stabilize the (*E*)-isomer, e.g. through intermolecular attractive interactions,[17] such as London dispersion.[18] Additionally, multiple AB units can be fused to a single aromatic ring, therefore lowering the molecular mass per switching unit.[19]

One of the reasons that prevents MOST molecules from achieving their full potential is their application in solution. This introduces often toxic and expensive solvents that, while allowing easy handling of the MOST compound, is lowering the energy density tremendously and diminishing the maximum obtainable thermal energy. Therefore, it would be important to avoid unnecessary solvents completely. The first example of such a compound was reported by Kimizuka in 2014, which is based on branched 2-ethylhexoxy AB **4** (Figure 2).[20] In their seminal paper they showed that the isomerization of AB can efficiently occur in the solvent-free, condensed phase. DSC measurements revealed, after irradiation with UV light, an energy density of 52 kJ mol^{-1}, or 183 kJ L^{-1} [for presumed 100% (*E*)-isomer]. In subsequent work from the Moth-Poulsen group the same AB **4** has been used in a device, which allows the *in fluxu* irradiation, as well as the *in fluxu* catalytic energy release with a copper(I) complex.[21] Unfortunately, the liquid AB was again employed in μM concentration, probably to facilitate irradiation and transportation through a chip reactor. Additionally, most liquid AB rely on the introduction of long, sometimes branched, alkyl chains, by adding flexibility, breaking the symmetry and to hinder π–π interactions of the phenyl units. These additional groups increase the synthetic effort, lower efficiency of the storage material, and decrease the energy density due to the additional molecular weight (Figure 2). There is tremendous effort to obtain higher energy densities, but most devices still require a solvent for efficient solar harvest and transport, thereby lowering the applicability. Additionally, the usage of toxic organic solvents is not in compliance with these greener, solar technologies.

In 2014, Hecht and Bléger introduced the *ortho*-fluoro AB as green light, high quantum yield, long half-life photoswitchable molecules, and reported the non-symmetric 2,6-difluoro AB (**10**, *o*F-AB, MW = 218 g mol^{-1}) as an oil.[22] Herein, we investigate this liquid AB as a visible light photoswitch in a solvent-free solar thermal storage application. A focus here will be on the performance of the complete MOST cycle, from irradiation to heat release, without additional solvent. Moreover, we investigate the ability of the liquid AB to act as solvent to dissolve MOST compounds with higher energy density such as NBDs. With this new strategy, a better spectral overlap and a higher energy density could be achieved, while still having an easy to handle, low viscous liquid MOST material.

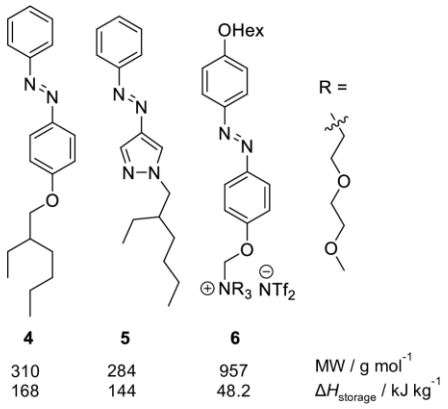

Figure 2. Properties of liquid state AB compounds **4**–**6** reported by Kimizuka in the literature.[23,20,24,25] Energy densities are calculate for 100% (*Z*)-isomer.

Results and Discussion

Synthesis: An efficient way to prepare non-symmetric AB is the condensation of an aniline and a nitrosobenzene in a Baeyer-Mills reaction.[26,27] This reaction proceeds *via* a nucleophilic attack of the aniline on the nitrosobenzene under acidic or basic conditions,[28] which explains why electron-rich anilines and electron-poor nitrosobenzenes provide high yields with mild reaction conditions and short reaction times. The *o*F-AB **10** was prepared by oxidation of 2,6-difluoroaniline (**7**) to the corresponding difluoro-nitrosobenzene (**8**) with Oxone® in a biphasic CH_2Cl_2/H_2O mixture, which, after extraction and removal of the solvent, was employed in a Baeyer-Mills reaction in acetic acid (Scheme 1).[22]

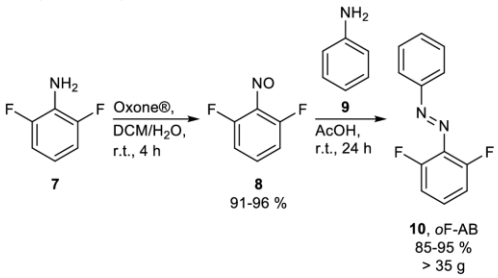

Schema 1. Biphasic oxidation of difluoro aniline **7** using Oxone® to the nitrosobenzene **8**, followed by Baeyer-Mills reaction with aniline to yield the liquid AB **10** after distillation.

Instead of a column chromatography compound **10** was purified by fractional distillation resulting in a yield of 95 %. The use of distillation as the main purification step allows easy up-scaling for large scale preparation of *o*F-AB **10**. We were able to prepare up to 38 g of *o*F-AB **10** in a single batch, albeit using higher

concentration of starting material resulted in a slightly lower yield of 85 %.

A continuous flow setup offers advantages to batch synthesis especially for large scale synthesis. We focused on the Baeyer-Mills reaction,[29] as the oxidation from aniline to nitroso is limited by the solubility of Oxone®. Nevertheless, it is also feasible to do both steps in flow by using a phase separator.[30] As 2,6-difluoro nitrosobenzene (**8**) is only slightly soluble in AcOH, we dissolved compound **8** in DCM and aniline (**9**) in AcOH. By increasing the reaction temperature to 50 °C, a flow-rate of 2 mL min^{-1} (1 ml min^{-1} for compound **7** and **8** respectively) can be achieved with a 10 mL coiled tube reactor (Figure 3). Higher temperature results in the formation of phenazine derivative as a side product (SI Figure 11).[31] That way, continues flow yielded 24.8 g of clean *o*F-AB **10** after distillation (runtime 400 min). This corresponds to a yield of 81%, and a throughput of purified compound of 3.7 g h^{-1}. This yield is in accordance with the one we obtained by using higher concentrations in batch reactions. As flow synthesis is easy to upscale by either running the experiment longer, or by increasing the reactor volume, large-scale synthesis of the AB can be assured.

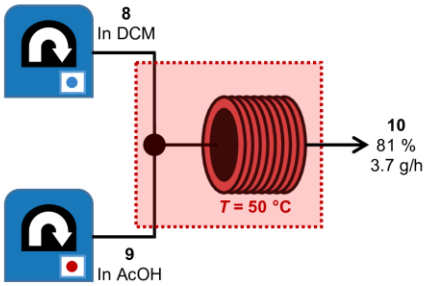

Figure 3. Schematic presentation of the continuous flow Baeyer-Mills reaction of aniline (**9**) and 2,6-difluoronitrosobenzene (**8**) in a tubular reactor. A throughput of 3.7 g pure AB **10** was obtained after distillation.

Photophysical properties: The UV/Vis absorption spectrum of *o*F-AB **10** in acetonitrile (ACN) solution shows an absorption maximum of the π–π* transition at 310 nm and a broad n–π* transition centered at 450 nm (Figure 4, left). Upon irradiation with green light, the expected separation of the latter band is observed, accompanied by decrease in absorption at 310 nm. A neat sample of *o*F-AB **10** was prepared as a thin-film between two quartz plates (Figure 4, right).

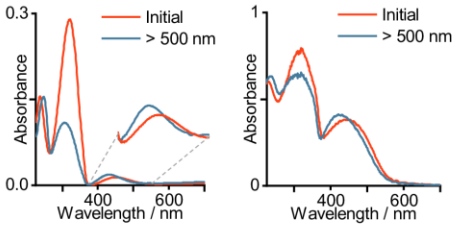

Figure 4. UV/Vis absorption spectra of *o*F-AB **10** in ACN (left) solution and in the neat liquid state (right).

The peak positions in the neat or dissolved state are very similar. The main difference is the much larger intensity of the formally forbidden n–π* transition, which usually shows lower absorbance. This observation could be due to the difference in the transition dipole moments of both absorptions, and a preferred alignment between the quartz plates.[32,33]

Thermal properties: The heat storage potential of *o*F-AB **10** was investigated by differential scanning calorimetry (DSC). A sample of neat *o*F-AB **10** was irradiated with a 530 nm LED, the content of the (*Z*)-isomer was analyzed by HPLC, and measured from -100 °C to 200 °C. The obtained DSC thermogram shows a broad exothermic peak centered at around 150 °C (SI Figure 9), which is not present in the second heating/cooling procedure of the same sample (SI Figure 9). We assigned this irreversible process to the thermal (*Z*)- to (*E*)-isomerization of the *o*F-AB **10**. At the PSS reachable with our green LED [$PSS_{530\ nm}$ = 63 % (*Z*)-isomer], a heat storage of 137 kJ kg^{-1} can be achieved, which corresponds to 218 kJ kg^{-1} for 100 % (*Z*)-isomer. This is considerably higher than the discussed liquid AB derivatives **4**–**6**, which again highlights advantage of the small molecular weight of our employed *o*F-AB **10**. The group of Hecht reported a PSS of 74 % with their green LED,[22] which would correspond to a thermal energy storage of 161 kJ kg^{-1}. The here obtained enthalpies are directly correlated to the maximum obtainable heat release, as no additional solvent is needed.

Irradiation: The irradiation of neat samples can be inefficient and tedious, in the solid state but also in the neat liquid state, mainly due to the inner filter effect and diffusion. We chose to rely on flow chemistry to tackle these difficulties. As the maximum flow rate and the back pressure of pumps depend on the viscosity of the employed liquid, it was important to quantify the viscosity of *o*F-AB **10**. We measured the viscosity of (*E*)-*o*F-AB **10** and of the (*E*/*Z*)-mixture at the PSS at 530 nm (Figure 5).

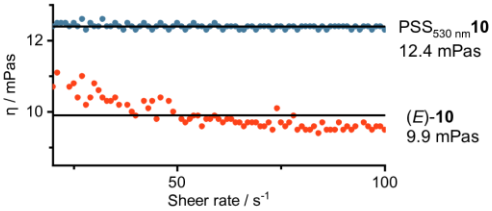

Figure 5. Rheology measurements of neat *o*F-AB **10** in the ground state (*E*)-isomer, and with 63 % (*Z*)-isomer at the PSS.

Interestingly, the *o*F-AB **10** shows a larger shear viscosity at the $PSS_{530\ nm}$ then the (*E*)-isomer. As the viscosity of liquids arise from friction between clustered molecules, and is therefore dependent on the size, shape and intermolecular interactions, there seems to be larger interactions within the metastable isomer. This is in contrast to the numerous examples of solid to liquid phase change AB, as well as to Kimizuka's liquid alkoxy AB **4**.[20] Furthermore, the (*E*)-isomer shows non-Newtonian behavior at slow low shear rats. The obtained pseudoplastic flow is indicative of structural formations, which are disrupted by stress introduced with higher shear rates.[34] The obtained viscosities are well within the range transportable liquids, and a magnitude smaller than of an already used liquid energy AB[20,21] or liquid NBDs.[35] Due to the low viscosity, high fluidity nature of *o*F-AB **10**, we can employ it in a photochemical flow setup for irradiation.

Conducting photochemistry in flow has significant advantages compared to batch reactions. For example a uniform irradiation, shorter reaction times, easy and efficient scale-up, and less degradations due to better reaction control can be achieved.[36–38] Especially the combination of flow chemistry with solar generators or collectors offers interesting possibilities for liquid MOST systems (Figure 6).[39]

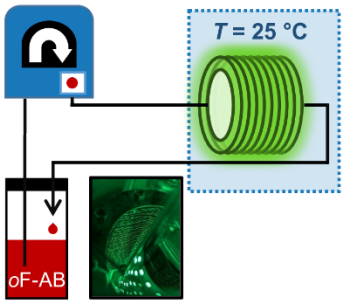

Figure 6. Continuous flow irradiation of neat *o*F-AB **10** in a 10 mL tube reactor.

Depending on the residence time inside the irradiation chamber, different (*Z*)-isomer ratios can be obtained. After around 200 min, neat *o*F-AB **10** was switched to the PSS of 63 % (*Z*)-isomer. Although the PSS is not ideal, it has been shown that a PSS up to 74 % can be achieved by using a different green light source.[22] Interestingly, we obtained even shorter irradiation times using a cheap commercially available LED strip, used for ambient light installations, and a simple home-made weaved flow reactor (Figure 6). This highlights the easiness of real-life implementations of this MOST system. With the chosen dimension of our reactor, this irradiation time would correspond to a throughput of 3.3 mL of charged *o*F-AB **10** per hour. Due to the scalability of flow chemistry, increase of the reactor length and volume would linearly scale with our obtained throughput.

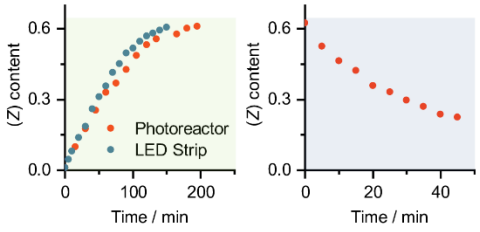

Figure 7. Change in the (*Z*)-isomer content in the PSS during green light (left) and blue light (right) irradiation of neat *o*F-AB **10** pumped through a 10 mL tube reactor. The irradiation was either conducted by a commercial photoreactor (530 nm and 405 nm), or by a simple home-made setup using a LED strip intended for ambient light irradiation. During each run, 10 mL AB **10** was used to ensure a completely filled reactor. The (*Z*)-content was measured *via* offline HPLC of aliquots integrated at the isosbestic point.

Energy release: Irradiation with 405 nm leads to the back isomerization with a PSS of 78 % of the (*E*)-isomer (Figure 7, right). As the PSS resulting from blue light irradiation is a limiting factor for the heat release, other triggers for the back reaction are necessary to harvest the maximum stored energy. One possibility is the electron-catalyzed isomerization.[40] In order to realize electrochemical back-conversion, we were able to dissolved approximately 5 % by weight of the organic salt tetra-*n*-butyl ammonium hexafluorophosphate ($TBAPF_6$) in the neat *o*F-AB **10** (Figure 8 A). $TBAPF_6$ is a salt often used for electrochemical measurements in organic solvents to increase conductivity.[41] Using a simple multimeter circuit analyzer, neat *o*F-AB **10** did not show any conductivity, which increased to a measurable quantity with $TBAPF_6$ (SI Figure 3). The observable electric conductivity results in a significant current through the liquid when applying a potential. If a potential close to the redox potential of the employed photoswitch is applied, a $1e^-$ reduction to a radical anion is generally observed.[42] As the formed radical is *inter alia* located on the N=N bonds, a significant decrease in the bond order is observed.[43] This results in a very low inversion barrier of (*Z*)- to (*E*)-AB radical, and therefore a fast thermal isomerization.[44] A subsequential electron transfer from the formed (*E*)-isomer to a (*Z*)-isomer, results in an electron catalytic isomerization behavior.[40] This represents an alternative trigger to irradiation, acids or catalysis, which can be used to induce the heat release in MOST materials,[45] and can be started either reductively or oxidatively.[40,46,47] Azoheteroarenes with ionic side chains showed electro catalytic switching in the condensed phase, but the large isomerization barrier of these T-shaped (*Z*)-isomers make on demand heat release not feasible.[48] We tested the electro catalytic isomerization of neat *o*F-AB **10** with $TBAPF_6$ *in fluxu* using a continuous flow electro-cell. The cell had an inner volume of around 1 mL, and with a flow rate of 1 mL min^{-1}, resulted in a residence time of 1 min. Depending on the applied potential, a significant decrease in the (*Z*)-isomer can be observed (Figure 8 B).

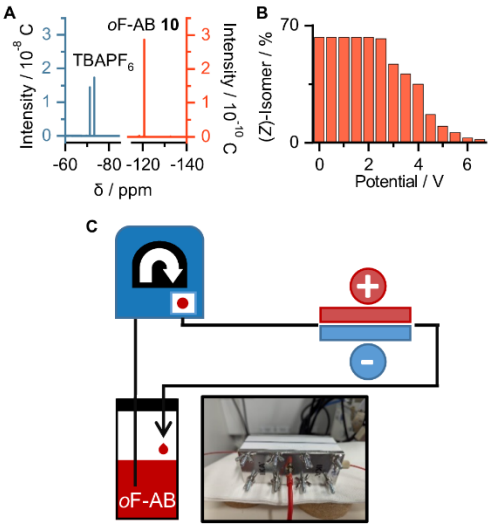

Figure 8. A) ^{19}F-NMR of a saturated $TBAPF_6$ solution in *o*F-AB **10**. B) Change in the (*Z*)-isomer content during electrochemical back isomerization. C) Electrochemical set-up.

The isomerization does not take place below 3 V. At higher potentials, a nearly complete back-isomerization is observed, although these high potentials might lead to side reactions. Nevertheless, complete isomerization can be obtained by this electrochemical setup. In comparison to the photochemical back reaction, that resulted in still 22 % (*Z*)-isomer after irradiation, this improvement allows harvesting of the total stored thermal energy.

To demonstrate the applicability of *o*F-AB **10**, we isomerized around 1 mL of the compound with a green LED. Complete heat release was achieved by addition of a catalytic amount of acid, and the resulting isomerization to the ground state was observed by infrared (IR) camera and an *in situ* thermometer. Upon addition of the acid (at 3 s), a drastic increase in the internal temperature was observed, and the maximal temperature of 66 °C was reached within 34 s (Figure 9). A second addition of acid did not result in any change in the thermal behavior, which indicates that the heat was released completely, and originated in the relaxation of the (*Z*)-isomer, and not by the acid-base reaction enthalpy.

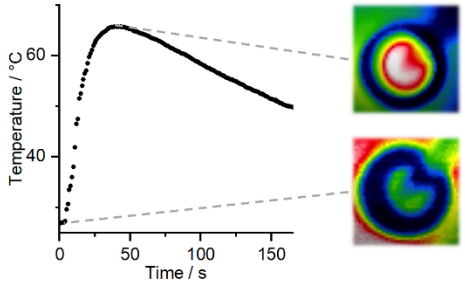

Figure 9. Macroscopic heat release of 1 mL *o*F-AB **10** after addition of a catalytic amount of acid measured by an *in situ* thermometer and visualized using an IR camera.

Liquid MOST as solvent: One additional scope of application for the low viscous *o*F-AB **10** is to use it as a MOST-active solvent. Besides additional additives, which can be added to *o*F-AB **10** to further enhance its properties, it can be used as a solvent for higher-energy density photoswitches. One of the disadvantages of AB for MOST storages is the relatively low stored energy in the nitrogen-nitrogen bond isomerization, in comparison to other MOST materials, that rely on bond formation, like azaborines or NBDs.[6,49] We used the solvent properties of AB **10** to dissolve a high energy density NBD within the AB **10**. Thereby, we can harvest the higher energy density of NBD moieties, while still handling a pumpable and easy to irradiate, low viscous liquid. In other words, we can substitute the generally employed death-weight organic solvents with a MOST-active solvent that does not influence the obtainable energy density negatively. As a proof-of-concept we tested this new strategy by preparing an asymmetric di-aryl NBD, as they show absorption maxima between the π-π* and the n-π* absorption bands of *o*F-AB **10**.[50] The 4-methoxyphenyl-4'-benzonitrile NBD **11** derivative was chosen, as it showed a good compromise between maximum absorption and half live.[50] We dissolved 10% of NBD **11** in the *o*F-AB **10**, without any observable change in the viscosity. The UV/Vis spectrum is overshadowed by the absorption of the AB moiety, which has a rather high extinction coefficient. To demonstrate that the NBD **10** is dissolved and switching in the *o*F-AB, the mixture was irradiated first with 530 nm to switch only the AB, then with 340 nm to switch AB and NBD, followed by 530 nm again. A differential spectrum of both green light PSS spectra shows the expected absorption of NBD **11** which correlated to the measured spectra in organic solvents (Figure 10 A).[50] Exact quantification can be achieved using ^{1}H-NMR, and PSS measurement using HPLC. A diluted sample of this mixture show a $PSS_{340\ nm}$ of around 95% (*Z*)-AB **10** and 92% QC-**11** (SI Figure 6).

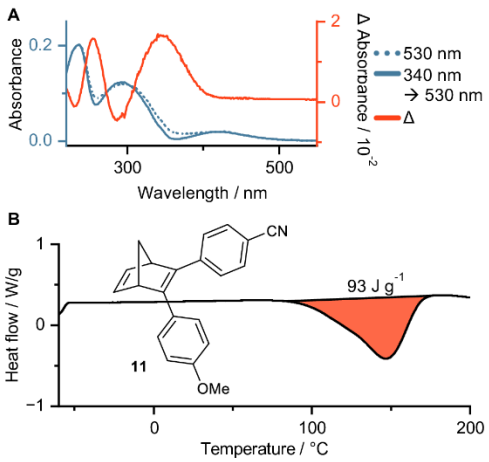

Figure 10. A) Absorption of the AB **10** and NBD **11** mixture in ACN. Irradiation at 530 nm switches only AB **10** while 340 nm switches both compounds. The differential spectra between the PSS at 530 nm before and after a 340 nm irradiation corresponds to the absorption spectra of NBD **11**,[50] and supports the dissolution and the ability to switch of the mixture. B) DSC curve of AB **10** and NBD **11** mixtures with 58 % (*Z*)-**10**, and 18 % QC-**11**. Higher PSS were not obtainable due to decomposition of compound **11** during irradiation with 340 nm. A small peak shoulder shows the heat release of the NBD **11** (SI Figure 10). The mixture contained NBD **11** decomposition products.

For DSC measurements, we irradiated the sample neat with a 340 nm LED in a vial under stirring. Here we observed only slow isomerization of both photoswitches, and were not able to achieve a PSS state before the NBD **11** showed degradation during HPLC measurements (SI Figure 8). This highlights the importance of *vide supra* described *in fluxu* irradiation using a flow setup. Nevertheless, we performed DSC measurements of our mixture containing only 58 % (*Z*)-*o*F-AB **10**, and 18 % QC of compound **11**. On the first glance one large exothermic peak is observed (Figure 10, B). Upon closer examination, a small peak shoulder at the lower temperature region can be observed, which can be assigned to the isomerization of compound **11**. This shoulder is more pronounced in the first derivative of the DSC curve (SI Figure 10). The smaller obtained heat release can be explained by the inefficient isomerization using 340 nm, and by degradation products which do not contribute to the energy release. Nevertheless, we herein employed a high energy density MOST material in our MOST-active *o*F-AB **10** as a solvent. This adds another possibility to enhance the energy density of MOST materials, alongside approaches such as introduction of a phase change,[51] stabilization of the (*E*)-isomer by e.g. London

dispersion interactions[17] and destabilization of the (*Z*)-isomer by templating on crowded nanocarbons.[52]

Conclusion

Herein, we introduced 2,6-difluoro AB **10** as a liquid storage material for MOST systems. The compound shows isomerization upon green light irradiation, and has an energy density of 218 kJ kg^{-1} This corresponds to an energy content of 137 kJ kg^{-1} at the PSS [(*Z*)-content 63 %] with 530 nm. The storage capacity of 218 kJ kg^{-1} is considerably higher than comparable liquid AB materials, due to low molecular mass of the employed compound. The most important feature is the low viscosity of the photoswitch of only around 10 mPas, which allows a very efficient isomerization, handling and storing in the neat state. Especially the isomerization *in fluxu* using a peristaltic pump, a home-made weaved tubular reactor and a cheap commercial LED strip used for ambient light irradiation, demonstrates the ease of use of *o*F-AB **10**. To showcase the large-scale applicability of this switch, an efficient *in fluxu* preparation *via* Baeyer-Mills reaction of difluoro nitrosobenzene **8** and aniline **9** in a continuous flow setup was established. After destillative purification, a throughput of 3.7 g h^{-1} pure AB **10** can be achieved. To further increase its applicability as an energy storage material, AB **10** was investigated as a MOST-active solvent. We were able to dissolve approx. 5 wt% $TBAPF_6$ conductive salt in neat AB **10**, which increased its electrical conductivity to a measurable quantity. This improvement resulted in an efficient electron-catalyzed back isomerization using a flow electrochemical cell, which resulted in a complete back conversion to the (*E*)-isomer. This is an improvement in comparison to the photochemical back isomerization. Here, PSS still contains considerable amounts of (*Z*)-isomer [$PSS_{405\,nm}$ = 78 % (*E*)-isomer]. Additionally, we prepared the higher energy density NBD **11**, which we dissolved in the liquid AB **10** (10 wt%) while still having a low viscous liquid. Complete isomerization of this mixture with 340 nm was not achieved, as the employed NBD **10** showed decomposition before PSS states could be reached. This could be improved by choosing a more stable NBD derivative with suitable absorption properties and a long half live. Nevertheless, as a proof-of-concept we demonstrated the strategy to dissolve and irradiate a MOST candidate dissolved in a neat MOST-active solvent. This way, we can avoid the usage of additional solvents maintaining the processibility keeping a high absolute storage density.

Acknowledgements

The authors acknowledge financial support by the European and Hessian Government within the “Innovationslabor Prozessdiagnostik” (EFRE 21031934) and by the Deutsche Forschungsgemeinschaft (DFG) within the Research Unit FOR 5499 “Molecular Solar Energy Management - Chemistry of MOST Systems”. We thank Natalia Haibel and Apl. Prof. Dr. Dr. Dirk Walter for providing and helping with DSC measurements. Additionally, we thank Dr. Christian Würtele and Lisa-Marie Wagner for help with the XRD analysis. We thank Dr. Rafael Meinusch and Prof. Dr. Bernd Smarsly for providing and helping with viscosity measurements. We thank Vapourtec for borrowing their photoreactor. Furthermore, we thank Dr. Leonie Lieber and Prof. Dr. Nicole Graulich for the IR camera.

Keywords: azo compounds • electrochemistry • photochemistry • energy storage • solvent

References

[1] S. Chu, A. Majumdar, *Nature* **2012**, *488*, 294–303.
[2] S. Chu, Y. Cui, N. Liu, *Nat. Mater.* **2016**, 16–22.
[3] J.-L. Brédas, E. H. Sargent, G. D. Scholes, *Nat. Mater.*, *2017*, 35–44.
[4] A. Z. Weber, M. M. Mench, J. P. Meyers, P. N. Ross, J. T. Gostick, Q. Liu, *J. Appl. Electrochem.* **2011**, *41*, 1137–1164.
[5] V. R. Stamenkovic, D. Strmcnik, P. P. Lopes, N. M. Markovic, *Nat. Mater.* **2017**, *16*, 57–69.
[6] Z. Wang, P. Erhart, T. Li, Z.-Y. Zhang, D. Sampedro, Z. Hu, H. A. Wegner, O. Brummel, J. Libuda, M. Brøndsted Nielsen, K. Moth-Poulsen, *Joule* **2021**, *5*, 3116–3136.
[7] R. J. Salthouse, K. Moth-Poulsen, *J. Mater. Chem. A* **2024**, *12*, 3180–3208.
[8] Z. Wang, H. Hölzel, K. Moth-Poulsen, *Chem. Soc. Rev.* **2022**, *51*, 7313–7326.
[9] F. J. Hernández, J. M. Cox, J. Li, R. Crespo-Otero, S. A. Lopez, *J. Org. Chem.* **2023**, *88*, 5311–5320.
[10] A. A. Beharry, O. Sandovski, G. A. Wooley, *J. Am. Chem. Soc.* **2011**, *133*, 19684–19687.
[11] H. A. Wegner, *Angew. Chem. Int. Ed.* **2012**, *51*, 4787–4788.
[12] M. Dong, A. Babalhavaeji, S. Samanta, A. A. Beharry, G. A. Wooley, *Acc. Chem. Res* **2015**, *48*, 2662–2670.
[13] J. Garcia-Amorós, M. Díaz-Lobo, S. Nonell, D. Velasco, *Angew. Chem. Int. Ed.* **2012**, *51*, 12820–12823.
[14] D. Dong, Z.-Y. Zhang, T. Dang, T. Li, *Angew. Chem. Int. Ed.* **2024**, *63*, e202407186.
[15] Z.-Y. Zhang, D. Dong, T. Bösking, T. Dang, C. Liu, W. Sun, M. Xie, S. Hecht, T. Li, *Angew. Chem. Int. Ed.* **2024**, *63*, e202404528.
[16] X. Li, S. CHo, G. G. D. Han, *ACS Mater. Au* **2023**, *3*, 37–42.
[17] A. Kunz, A. H. Heindl, A. Dreos, Z. Wang, K. Moth-Poulsen, J. Becker, H. A. Wegner, *ChemPlusChem* **2019**, *84*, 1145–1148.
[18] C. Averdunk, K. Hanke, D. Schatz, H. A. Wegner, *Acc. Chem. Res* **2024**, *57*, 257–266.
[19] D. Dong, T. Li, *ChemPhotoChem* **2024**, *8*.
[20] K. Masutani, M. Morikawa, N. Kimizuka, *Chem. Commun.* **2014**, *20*, 15803–15806.
[21] Z. Wang, R. Losantos, D. Sampedro, M. Morikawa, K. Börjesson, N. Kimizuka, K. Moth-Poulsen, *J. Mater. Chem. A* **2019**, *7*, 15042–15047.
[22] C. Knie, M. Utecht, F. Zhao, H. Kulla, S. Kovalenko, A. M. Brouwer, P. Saalfrank, S. Hecht, D. Bléger, *Chem. Eur. J.* **2014**, *20*, 16492–16501.
[23] Q. Qiu, Y. Shi, G. G. D. Han, *J. Mater. Chem. C* **2021**, *9*, 11444–11463.
[24] M. Morikawa, H. Yang, K. Ishiba, M. Masutani, J. K.-H. Hui, N. Kimizuka, *Chem. Lett.* **2020**, *49*, 736–740.
[25] K. Ishiba, M. Morikawa, C. Chikara, T. Yamada, K. Iwase, M. Kawakita, N. Kimizuka, *Angew. Chem. Int. Ed.* **2015**, *54*, 1532–1536.
[26] C. Mills, *J. Am. Chem. Soc.* **1895**, *67*, 925–933.
[27] A. Baeyer, *Dtsch. Chem. Ges.* **1874**, *7*, 1638–1640.
[28] K. Ueno, S. Akiyoshi, *J. Am. Chem. Soc.* **1954**, *76*, 3615–3868.
[29] J. H. Griwatz, A. Kunz, H. A. Wegner, *Beilstein J. Org. Chem.* **2022**, *18*, 781–787.
[30] J. H. Griwatz, C. E. Campi, A. Kunz, H. A. Wegner, *ChemSusChem* **2024**, *17*, e202301714.

[31] L. Vaghi, M. Coletta, P. Coghi, I. Andreosso, L. Beverina, R. Ruffo, A. Papagni, *Arkivoc* **2020**, *5*, 340–351.
[32] Y. Yu, T. Ikeda, *J. Photochem. Photobiol. C* **2004**, *5*, 247–265.
[33] S. Y. Grebenkin, V. M. Syutkin, D. S. Baranov, *J. Photochem. Photobiol. A* **2017**, *344*, 1–7.
[34] M. M. Cross, *J. Colloid. Sci.* **1965**, *20*, 417–437.
[35] A. Dreos, Z. Wang, J. Udmark, A. Ström, P. Erhart, K. Börjesson, M. Brøndsted Nielsen, K. Moth-Poulsen, *Adv. Energy Mater.* **2018**, *8*, 1703401.
[36] K. Gilmore, P. H. Seeberger, *Chem. Rec.* **2014**, *14*, 410–418.
[37] C. Sambiagio, T. Noël, *Trends Chem.* **2020**, *2*, 92–106.
[38] L. Buglioni, F. Raymenants, A. Slattery, S. D. A. Zondag, T. Noël, *Chem. Rev.* **2022**, *122*, 2752–2906.
[39] D. Cambié, T. Noël, *Top. Curr. Chem.* **2018**, *376*, 1–27.
[40] A. Goulet-Hanssens, M. Utecht, D. Mutruc, E. Titov, J. Schwarz, L. Grubert, D. Bléger, P. Saalfrank, S. Hecht, *J. Am. Chem. Soc.* **2017**, *139*, 335–341.
[41] D. L. Goldfarb, M. P. Longinotti, H. R. Corti, *J. Solut. Chem.* **2001**, *30*, 307–322.
[42] J. L. Sadler, A. J. Bard, *J. Am. Chem. Soc.* **1968**, *90*, 1979–1989.
[43] P. Nandadulal, S. Subhas, G. Sreebrata, *Inorg. Chem.* **2010**, *49*, 2649–2655.
[44] E. Laviron, Y. Mugnier, *J. Electroanal. Chem.* **1978**, *93*, 69–73.
[45] D. Schulte-Frohlinde, *Justus Liebigs Ann. Chem.* **1958**, *612*, 138–152.
[46] A. Goulet-Hanssens, C. Rietze, E. Titov, L. Abdullahu, L. Grubert, P. Saalfrank, S. Hecht, *Chem* **2018**, *4*, 1740–1755.
[47] E. Franz, A. Kunz, N. Oberhof, A. H. Heindl, M. Bertram, L. Fusek, N. Taccardi, P. Wasserscheid, A. Dreuw, H. A. Wegner, O. Brummel: J. Libuda, *ChemSusChem* **2022**, *15*, e202200958.
[48] J. L. Greenfield, M. A. Gerkman, R. S. L. Gibson, G. G. D. Han, M. J. Fuchter, *J. Am. Chem. Soc.* **2021**, *143*, 15250–15257.
[49] K. Edel, X. Yang, J. S. A. Ishibashi, A. N. Lamm, C. Maile-Mössmer, Z. X. Giustra, S.-Y. Liu, H. F. Bettinger, *Angew. Chem. Int. Ed.* **2018**, *57*, 5296–5300.
[50] V. Gray, A. Lennartson, P. Ratanalert, K. Börjesson, K. Moth-Poulsen, *Chem. Commun.* **2014**, *50*, 5330–5332.
[51] M. Le, G. G. D. Han, *Acc. Mater. Res.* **2022**, *3*, 634–643.
[52] A. M. Kolpak, J. C. Grossman, *Nano. Lett.* **2011**, *11*, 3156–3162.

4.4 Electrochemistry of Azobenzenes and Its Potential for Energy Storage

Reference: D. Schatz, H. A, Wegner, *J*. *Org*. *Chem*. **2025**, *accepted*.

DOI: 10.1021/acs.joc.5c00315

Azobenzenes are promising materials for energy storage due to their reversible photoisomerization and redox properties. Given the critical role of redox behavior in the latter application, an investigation of their redox processes is essential. We propose a classification of azobenzenes into two categories: benzenoid-type and quinoid-type, based on the mechanism of their oxidation. Benzenoid-type compounds have been extensively studied due to their reversible reduction. Quinoid-type compounds exhibit oxidative and reductive versatility, making them promising for further research in energy storage.

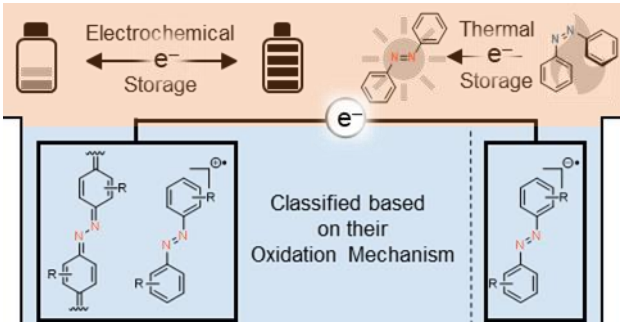

JOC The Journal of Organic Chemistry

Open Access

pubs.acs.org/joc

JOCSynopsis

Electrochemistry of Azobenzenes and Its Potential for Energy Storage

Published as part of The Journal of Organic Chemistry special issue "Physical Organic Chemistry: Never Out of Style".

Dominic Schatz and Hermann A. Wegner*

Cite This: https://doi.org/10.1021/acs.joc.5c00315

Read Online

ACCESS | Metrics & More | Article Recommendations

ABSTRACT: Azobenzenes are promising materials for energy storage due to their reversible photoisomerization and redox properties. Given the critical role of redox behavior in the latter application, an investigation of their redox processes is essential. We propose a classification of azobenzenes into two categories: *benzenoid*-type and *quinoid*-type, based on the mechanism of their oxidation. *Benzenoid*-type compounds have been extensively studied due to their reversible reduction. *Quinoid*-type compounds exhibit oxidative and reductive versatility, making them promising for further research in energy storage.

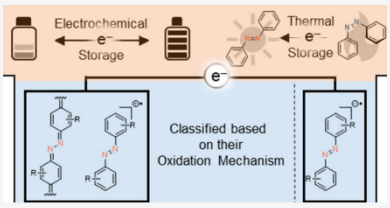

Undoubtedly, azobenzenes (AB) belong to a class of privileged structures, which have extensively been studied since their discovery by Mitscherlich in the middle of the 19th century.[1] The versatile applications in many different fields can be traced back to mainly three properties: Their bright coloration,[2] their reversible photoisomerization,[3] and their redox chemistry.[4] By focusing on their photophysical properties, AB can be divided into three different classes depending on their n-π^* and π-π^* transitions, and various overviews deal with the respective dye or photoswitch properties of these classes.[5] Generally, the incorporation of nitrogen atoms into a molecular scaffold significantly alters the electronic nature.[6] For example, the first reduction wave of AB is more facile by 800 mV in comparison to stilbene (−1.4 V vs −2.2 V, respectively vs saturated calomel electrode).[7,8] Additionally, π-delocalization changes the electronic behavior.[9] Therefore, AB as a nitrogen-containing π-extended compound offers interesting opportunities to control its redox chemistry via structural variation. ABs show distinct reductive and oxidative redox performance and can be divided into two categories, depending on the mechanism of their oxidation. Most AB show irreversible oxidation, which we assign to the first, the *benzenoid*-type category. We categorize AB that can form a quinoidal system upon oxidation into the second, *quinoid*-type group (Figure 1). Herein we want to introduce the underlying redox properties of both of these classes and showcase current applications based on their respective reductive and oxidative behavior. A comprehensive assessment and comparison of the performances in AB-based battery solutions can be found in a review by Shimizu, Tanifuji and Yoshikawa.[4]

***Benzenoid*-Type ABs.** The redox chemistry of *benzenoid*-type AB was already investigated by Schlenk and Wittig, who studied the addition of metal to different double bonds. Addition of sodium to pristine AB **1** results in a dark purple solid, which, after quenching with water, yields equimolar hydrazobenzene and neutral AB.[10] The result was, therefore, not the expected 1e⁻ reduction product as a monosodium radical anion but a mixture of neutral compound and the 2e⁻ reduction product. Addition of 2 equiv of methyllithium, on the other hand, formed bis-lithiated hydrazobenzene, which formed a radical anion after addition of a second equivalent of AB.[11]

This comproportionation of deprotonated hydrazobenzene was further studied and showed a strong dependence on the employed countercation, as well as an electron paramagnetic resonance (EPR) signal that is influenced by hyperfine splitting of the alkali metal.[12] Even just the mixture of AB and hydrazobenzene yields a radicaloid species observable by EPR, indicating an electron transfer between the compounds with oxidation state −2 and −1 (Figure 2, A).[13] In electrochemical experiments, AB behaves differently depending on solvent, electrolyte, and electrode material. During polarography in aprotic, polar solvents, AB is reduced in two consecutive 1e⁻

Received: February 11, 2025
Revised: March 24, 2025
Accepted: April 8, 2025

The Journal of Organic Chemistry pubs.acs.org/joc JOCSynopsis

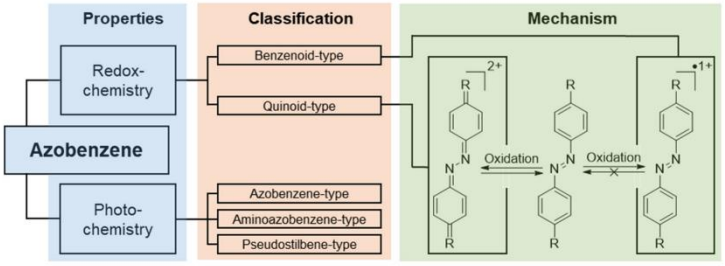

Figure 1. Classification of AB in *benzenoid*-type and *quinoid*-type, depending on the reversibility and mechanism of the oxidation process. The formed radical cation of *benzenoid* compounds decomposes rapidly, while the benzoquinone imine structure of *quinoid* AB is stable.

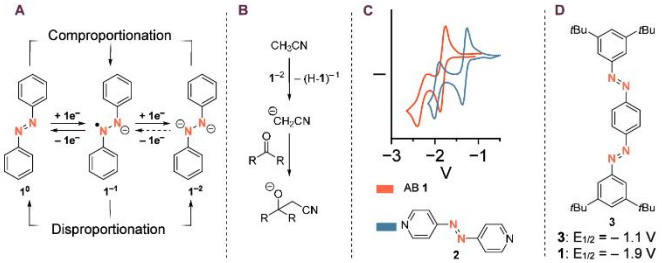

Figure 2. A) The two consecutive reductions of AB to the anion radical and the bis-deprotonated hydrazine, and their interconversion via comproportionation and disproportionation reactions. B) Electrogenerated AB $\mathbf{1}^{-2}$ base yields a reactive cyanomethyl anion. C) Cyclic voltammogram (CV) measured with ferrocene (Fc) and referenced vs Fc/Fc^+ of pristine azobenzene (**1**) and 4,4′-azopyridine (**2**) highlighting the pseudoreversible second reduction of the electron poor derivative.[16,21] Copyright © 2024, American Chemical Society. D) Structure of bis-AB **3** and its reduction potential vs Fc/Fc^+ compared to the reduction potential of AB **1**.[22,23]

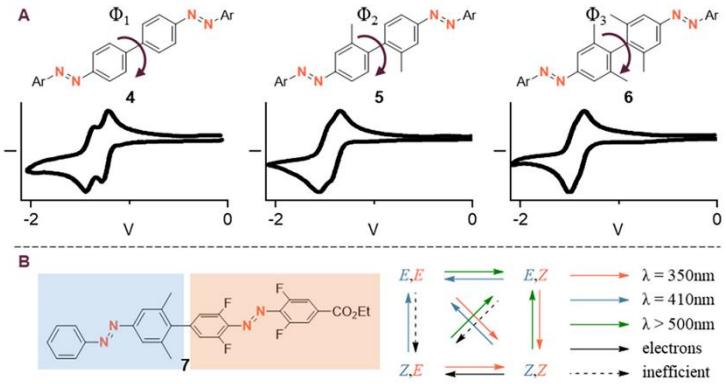

Figure 3. A) Dependence of the peak-to-peak separation in the CV of bis-azobenzenes **4**–**6** based on the dihedral angle between both photoswitches. CVs are referenced vs Fc/Fc^+ The higher the dihedral angle, the smaller the peak separation, as the independent redox behavior increases with increasing angle.[23] Copyright © 2011, American Chemical Society. B) Asymmetric bis-azobenzene **7** and the pathways to achieve orthogonal switching, with the different reduction potential allowing selective (*Z*) to (*E*) switching of the more electron poor switch.[24]

waves.[14] The first wave produces the radical anion, as observed by EPR and UV–vis measurements, and the second wave produces the bis-anion. Under most conditions, the first wave appears reversible on the time-scale of the electrochemical measurements, while the second wave appears to be irreversible. The irreversibility of the second wave can be explained with the aforementioned comproportionation, as well as the significant basicity of the electron-rich bis-anion, leading to side reactions (Figure 2, B).[15] An example of this is the semireversible second 1e⁻ reduction of electron poor 4,4′-azopyridine **15**, which is more reversible then for the pristine AB **1** (Figure 2, C).[16] Elucidation of the structure and

https://doi.org/10.1021/acs.joc.5c00315
J. Org. Chem. XXXX, XXX, XXX–XXX

geometry of the reduced AB species was obtained by single crystal XRD. In earlier studies the electron transfer from two ABs to Re(0) yielded a paramagnetic Re(II) complex of two AB radicals.[17] In the obtained crystal, an elongation of the N−N bond in comparison to pristine AB was observed as well as a shift in the ν(N−N) IR band to lower wavenumbers, indicating a decrease in the double bond character of the radical in comparison to the neutral compound. The observed bond elongation and the obtainable EPR signals are in agreement with the location of the radical on and over the azo nitrogen atoms. Similar results have been obtained in osmium[18] and ruthenium[19] complexes, or with imidazole based AB.[20] In 2020, the free radical and bis-anion of an AB derivative were isolated after reduction with alkali metals in the presence of crown ether (N−N bond lengths of neutral, radical, and bis-anion are 1.252 1.326, and 1.391 Å, respectively).[25] Due to the free N−N bond in these anions, they were able to coordinate and activate CO_2, yielding oxalic acid. A radical anion structure based on a quinoidal system is also proposed.[26]

By extending the π system in *para* connected bis-AB, their reduction proceeds more facilely in comparison to pristine AB (Figure 2, D).[23] The *para* bis-AB **3** shows two clearly distinct reversible 1e$^-$ reductions for each azo unit that are separated by 0.5 V. This clearly shows the strong electronic communication in *para* ABs, as also demonstrated by ultrafast isomerization dynamic experiments.[27] If the azo units are separated by a biphenyl linker, the first two 1e$^-$ reductions proceed at more similar potentials, as they behave more independently of each other. Increasing the dihedral angle between the biphenyl moieties (from **4** to **6**) by adding steric bulk results in one indistinguishable redox wave for both redox processes (Figure 3, A). This charge delocalization of quasi planar *para*-bridged oligo-AB has also been visualized by EPR.[28] The observed delocalization is smaller than that in the structurally akin stilbene compounds, which is attributed to the large degree of spin density on the nitrogen bridge. Furthermore, *para* biphenylene connected asymmetric bis-AB **7** was able to switch orthogonally by a mixture of photochemical and electrochemical stimuli (Figure 3, B).[24] The reason for that is the discussed loss of electronic communication due to rotationally hindered biphenyl bridges as well as two clearly different redox potentials due to different substitution on the AB rings. The oxidative behavior of *benzenoid*-type compounds is less explored, mainly due to the reason that most AB derivatives show irreversible and destructive oxidation behavior.[29] Nevertheless, an EPR spectrum of AB **1** was obtained after bombardment with γ-rays of AB in a frozen $CFCl_3$ matrix,[30] and later in a frozen cryofluorane matrix at 77 K.[31] The formed radical cation can also be observed in the isomerization of a bulk solution of AB after addition of oxidation reagent, albeit with destructive behavior.[29]

***Quinoid*-Type ABs.** The second class of redox-active AB consists of bis *ortho*- and *para*-connected amino- or hydroxyl-substituted compounds. They are distinct from the first class, as they show a stable 2e$^-$ oxidized quinoidal structure, that allows reversible oxidative behavior.[32,33] Although earlier studies observed only a 1e$^-$ oxidation of 4,4′-diamino ABs by electron poor quinodimethanes, forming the corresponding 1:1 salts,[34] more recent electrochemical studies and redox titrations by the group of Hecht confirmed the 2e$^-$ oxidation, of, for example, AB **8** (Figure 4).[35] Spectro-electro measurements demonstrated a red-shifted intermediate, which hints to

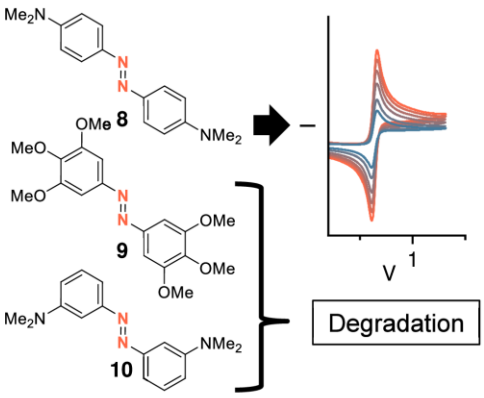

Figure 4. Reversible oxidation of 4,4′-dimethylamino AB **8** is based on the formed quinoidal oxidized species, as neither the electron-rich hexamethoxy AB **9** nor the 3,3′-dialkylamino AB **10** show reversibility.[35,36] CV is measured with decamethylferrocene (Fc*) and referenced vs Fc*/Fc*$^+$. Copyright © 2024 The Author(s). Angewandte Chemie International Edition published by Wiley-VCH GmbH.

the formation of an radical cation by 1e$^-$ oxidation, followed by an fast consecutive 1e$^-$ oxidation to the quinoidal system.[35,36] 3,3′,4,4′,5,5′-Hexamethoxy AB **9** and 3,3′-dimethylamino AB **10** were prepared to demonstrate that the origin of the reversibility lies in the formation of the quinoidal structure, and not just on the electron-density of these compounds, as both showed oxidative degradation (Figure 4).[35]

The stabilizing two electron process was rationalized with the formation of a benzoquinone imine azine structure by comparing ^{1}H NMR signals before and after oxidation of AB containing hydroxyl groups at both *para* positions.[33] The obtained signals are shifted downfield in contrast to the neutral compound and are different from the signals of the corresponding azoxy compound, eliminating azoxy compounds as possible oxidation products. To get further evidence into the structure of the oxidized species and the mechanisms of the reversible oxidation, we crystallized the product **11**$^{2+}$ obtained after oxidation of 4,4′-diethylamino AB **11** with 2 equiv of $NOBF_4$ (Figure 5).[36] The obtained solid-state structure revealed that the predicted quinoidal structure is valid. A bond elongation of the N−N bond, a shortening of the N−C_{aryl} bond, and a bond alternation in the ring systems all indicate quinoidal character over the whole AB core. Furthermore, calculation of the δr[38] value, a value used for quantification of quinoidal character, of 0.100 Å verifies fully quinoidal rings.

One of the most prominent features of AB is the ability to isomerize from the stable (*E*)- to the metastable (*Z*)-isomer by irradiation with the appropriate wavelength. Isomerization leads to changes in properties, such as basicity, end-to-end distance, solubility, and dipole moment, and this raises the question of whether the electrochemical properties are also affected. Unfortunately, *quinoid* ABs usually show short half-lives in comparison to their *benzenoid*-type analogs, so that mostly *benzenoid*-type (*Z*)-switches have been studied electrochemically.[5] Polarograms of *para*-methoxy AB **12** in aqueous

https://doi.org/10.1021/acs.joc.5c00315
J. Org. Chem. XXXX, XXX, XXX−XXX

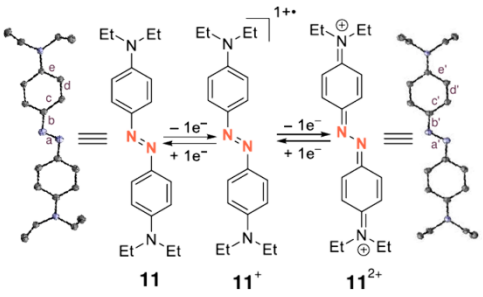

Figure 5. Oxidation of *quinoidal* AB **11** (CCDC: 1000644)[37] via a cation radical, observable by spectro-electro measurements, and the formed stable 2e- oxidized species. Geometry of the oxidized compound was confirmed by single crystal XRD (CCDC: 2247535).[36] Solid state structures are depicted without solvent molecules and anions. Bond lengths in Å: a = 1.266, a′ = 1.363, b = 1.423, b′ = 1.321, c = 1.385, c′ = 1.442, d = 1.382, d′ = 1.346, e = 1.417, e′ = 1.450.

dioxane electrolyte gave an additional signal after irradiation of the sample with UV light (Figure 6).[39] The height ratio of both

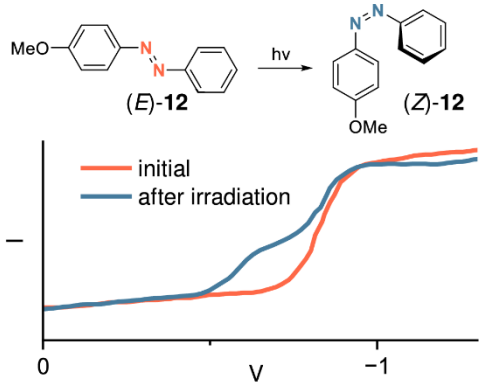

Figure 6. Difference between the polarograms of *para* methoxy AB **12** in 70% aqueous dioxane before and after photoisomerization. The new signal corresponding to the (*Z*)-isomer is shifted to more positive potentials and corresponds to the polarogram of a pure (*Z*)-isomer sample.[39] Copyright © 1974, American Chemical Society.

peaks was dependent on the irradiation duration, but the sum stayed constant, which correlates with photoisomerization. The metastable isomer can be more easily reduced by nearly 200 mV. The result of the observed 2e$^-$ reduction is the same starting from the (*E*)- or (*Z*)-isomer. If similar experiments are carried out in DMF solutions, no difference in the redox potential of both isomers at room temperature is observed.[40] Cooling the electrolyte to −22 °C and using very high sweep rates results in distinguishable cyclic voltammograms of (*E*)- and (*Z*)-AB. Photomodulated voltammetry, a technique typically used for elusive radical species,[41,42] of in situ generated (*Z*)-AB in a variety of organic solvents revealed also a difference between both isomers.[43]

The underlying challenge of electrochemical analysis of the (*Z*)-isomer is the formation of the anion radical, which has an activation energy for the isomerization of only around 8 kJ mol^{-1}.[40] Pairing the fast kinetic constant with a radical transfer to (*Z*)-AB in the vicinity of the electrochemically generated radical, the metastable isomer can only be observed in voltammograms if the sweep rate is higher than the rate of isomerization.

Nevertheless, Hecht and Herges found ways to demonstrate the change in the redox potential upon isomerization. Hecht prepared a cyclic AB (**13**) and compared it to an analogous linear compound (**14**).[22] He observed no difference of the (*E*)- and (*Z*)-isomer of **14** in the voltammograms, while the cyclic derivative showed a difference of around 250 mV to more negative potentials for the 1e$^-$ reduction (Figure 7, bottom).

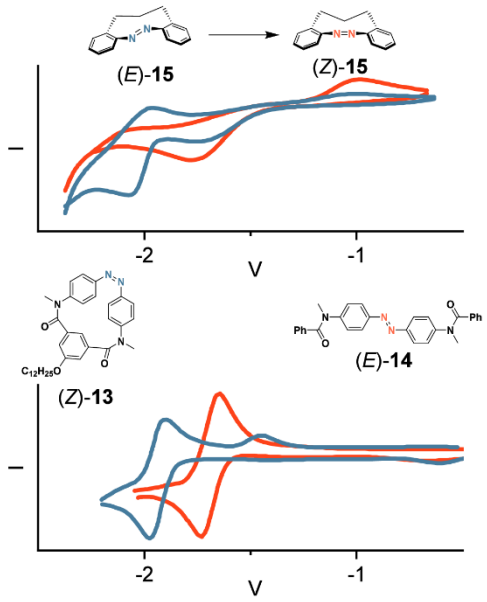

Figure 7. Top: Herges' diazonines **15** where the (*Z*)-isomer (thermodynamically stable, red) and (*E*)-isomer (metastable, blue) show different redox potentials observable by CV measurements, due to the stability of the formed radical anion that only undergoes slow radical transfer.[44] Copyright © 2023 The Authors. Chemistry - A European Journal published by Wiley-VCH GmbH. Bottom: A cyclic derivative **13** of (*E*)-AB **14** (blue) as a model for the (*Z*)-isomer with different redox potentials. (*Z*)-AB **14** isomerizes due to fast radical transfer on the time scale of the CV experiment.[22] CVs are referenced to Fc/Fc$^+$. Copyright © 2017, American Chemical Society.

The former observation was rationalized with the catalytic back isomerization during scanning. By addition of a small amount of generated AB anion radical to a bulk solution containing (*Z*)-AB, fast isomerization to (*E*)-AB was observed. Using a spectro-electrochemical setup, the fast isomerization of the (*Z*)-isomer to its stable isomer was observable by its change in the UV−vis spectra during cyclic voltammetry, even before the onset of the (*E*)-isomer redox potential was reached. Herges investigated other cyclic diazo derivatives, the

https://doi.org/10.1021/acs.joc.5c00315
J. Org. Chem. XXXX, XXX, XXX−XXX

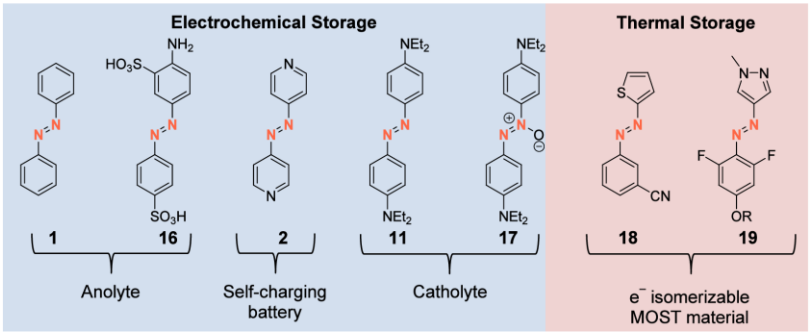

Figure 8. Some derivatives of AB applied in energy storage solutions. Most of these compounds (**1**, **16**, **2**, **18**, **19**) show *benzenoid*-type redox chemistry.

1,2-diazocines. Their redox behavior is strongly dependent on the length of their alkyl chains, although all show the expected 1e⁻ reduction of azo compounds.[44] If the linker is increased to a C3-chain (diazonine **15**), yielding a nine member central cycle, reduction of the metastable (*E*)-isomer does not yield the (*Z*)-isomer in a catalytic fashion, while C1- and C2-chains isomerize upon reduction. The obtained redox potentials of the (*E*)-isomer are shifted 130 mV to more positive potentials, demonstrating a clear difference between both photoisomers (Figure 7, top).

Storage Applications. Both classes of AB have found their way into electrochemical or thermal energy storage applications (Figure 8). Due to the reversible reduction of most AB from the *benzenoid*-type class, as well as only marginal solubility in employed solvents, they show great performance as electrodes in metal-based batteries.[45] Thanks to a relatively easy access to derivatives, their properties can be fine-tuned to succeed in aqueous (compound **16**) or organic (compound **1**) applications.[46] An additional battery technology that employs *benzenoid*-type compounds is redox-flow batteries, where their reversibility allows them to be employed as the active anolyte.[47] Moreover, the catalytic isomerization upon addition of either oxidant or reductant to produce radical cation or anion, respectively, can be used in molecular organic solar thermal storage (MOST). For MOST, a molecular photoswitch like AB absorbs light and transforms this energy into chemical energy.[48] The thereby stored thermal energy can be later released and used. For an efficient MOST material, the heat release needs to be triggered to allow for on-demand applications. The redox chemistry of the employed photoswitches is perhaps one of the most efficient and promising triggers. The lowering of the isomerization barrier by radical formation, and the radical transfer to other photoswitches results in the complete isomerization of the (*Z*)-isomer (Figure 9).

Hereby, the reductive pathway via anion radicals, as well as an oxidative pathway via the radical cation with hetero AB similar to azothiophene **18** have been explored.[29,49]

The oxidative pathway shows lower cyclability due to the instability of the formed radical in comparison to that of the reduced species. By derivatization of azoheteroarenes with ionic side chains (compound **19**), an efficient electrocatalytic heat release can be realized even in the condensed phase.[50]

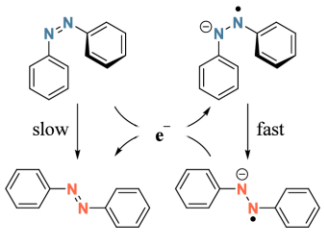

Figure 9. Proposed reaction mechanism for the electrocatalytic (*Z*)- to (*E*)-isomerization of ABs, that is based on a smaller isomerization energy barrier for the radical anion compared to the neutral compound. Intermolecular electron transfer from isomerized (*E*)- to (*Z*)-AB makes this process catalytic in electrons.

Quinoid ABs, on the other hand, can be employed as the catholyte in redox flow batteries.[36] Hereby a larger capacity decay is observed over multiple cycles, possibly due to the instability of intermediate radical cations. Full symmetric RFB based on the oxidation and reduction of a single *quinoid* AB could not yet been established, as the reduction appears to be not reversible on the time scale of charge/discharge cycles. This might be due to the electron-rich nature of the employed 4,4′-diethylamino AB (**11**). Similar results were obtained by employing the structurally related *para*-amino azoxybenzenes (compound **16**) as the catholyte.[51]

Although the redox chemistry of AB has been known for quite some time, its applications in electrical and thermal energy storage are currently studied, mostly as electrodes in metal batteries, as the redox active material in flow batteries, or as a release trigger for MOST materials. In these cases, most employed structures belong to the class of *benzenoid*-type ABs due to their reversible reductive behavior. The potential of the reversible oxidation of *quinoid* AB has yet only been demonstrated as redox active materials in catholytes although we hope that further research will increase the stability and reversibility of *quinoid* AB for comparable energy storage technologies.

Conclusion. The redox chemistry of AB offers multiple features for applications. The structure of the intermediated radical can be used to catalytically induce a thermal heat release in MOST energy storage systems, and the reversibility

https://doi.org/10.1021/acs.joc.5c00315
J. Org. Chem. XXXX, XXX, XXX−XXX

of this redox process can be used for electrochemical energy storage in metal-based batteries or in redox-flow batteries. Nevertheless, the high electron density in the reduced form of AB needs to be controlled to increase electrochemical stability, as side reactions with solvent or electrophiles are possible and, in the case of electron generated bases, even desired.

The oxidative behavior of AB, on the other hand, is a less established field, possibly due to the instability of formed radical cations, and only the further formation of a quinoidal oxidation product after a two electron process makes the oxidative side reversible. As the quinone formation results in a different oxidation mechanism, we classified AB based on their redox properties into *benzenoid* and *quinoid* like classes. With this categorization based on the underlying oxidation mechanism, we hope to increase the visibility of the versatility and applicability of AB redox chemistry and to facilitate and accelerate further research endeavors.

■ ASSOCIATED CONTENT

Data Availability Statement

The data underlying this study are available in the published article. Data for Figures 2, 3, 4, 6 and 7 have been extracted from their respective publications using https://automeris.io/.

■ AUTHOR INFORMATION

Corresponding Author

Hermann A. Wegner − *Institute of Organic Chemistry, Justus Liebig University, 35392 Gießen, Germany; Center of Materials Research (ZfM/LaMa), Justus Liebig University, 35392 Gießen, Germany;* orcid.org/0000-0001-7260-6018; Email: hermann.a.wegner@org.chemie.uni-giessen.de

Author

Dominic Schatz − *Institute of Organic Chemistry, Justus Liebig University, 35392 Gießen, Germany; Center of Materials Research (ZfM/LaMa), Justus Liebig University, 35392 Gießen, Germany*

Complete contact information is available at: https://pubs.acs.org/10.1021/acs.joc.5c00315

Author Contributions

The manuscript was written through contributions of all authors. All authors have given approval to the final version of the manuscript.

Funding

The authors thank European and Hessian Government for funding the "Innovationslabor Prozessdiagnostik" (EFRE 21031934).

Notes

The authors declare no competing financial interest.

■ ABBREVIATIONS

AB = azobenzene; EPR = electron paramagnetic resonance; CV = cyclic voltammetry or cyclic voltammogram; MOST = molecular organic solar thermal storage

■ REFERENCES

(1) Mitscherlich, E. Ueber das Stickstoffbenzid. *Ann. Pharm.* **1834**, *12* (2−3), 311−314.

(2) Bafana, A.; Devi, S. S.; Chakrabarti, T. Azo dyes: past, present and the future. *Environ. Rev.* **2011**, *19*, 350−371.

(3) Mahimwalla, Z.; Yager, K. G.; Mamiya, J.; Shishido, A.; Priimagi, A.; Barrett, C. J. Azobenzene photomechanics: prospects and potential applications. *Polym. Bull.* **2012**, *69* (8), 967−1006.

(4) Shimizu, T.; Tanifuji, N.; Yoshikawa, H. Azo Compounds as Active Materials of Energy Storage Systems. *Angew. Chem., Int. Ed.* **2022**, *61* (36), No. e202206093.

(5) Bandara, H. M. D.; Burdette, S. C. Photoisomerization in different classes of azobenzene. *Chem. Soc. Rev.* **2012**, *41* (5), 1809−1825.

(6) Kotwica, K.; Wielgus, I.; Proń, A. Azaacenes Based Electroactive Materials: Preparation, Structure, Electrochemistry, Spectroscopy and Applications-A Critical Review. *Materials* **2021**, *14* (18), 5155.

(7) Uno, B.; Matsuhisa, Y.; Kano, K.; Kubota, T. Relation between the First and the Second Nonaqueos Reduction Potentials of Substituted Silbenes. *Chem. Pharm. Bull.* **1984**, *32* (32), 1−10.

(8) Sadler, J. L.; Bard, A. J. Electrochemical reduction of aromatic azo compounds. *J. Am. Chem. Soc.* **1968**, *90* (90), 1979−1989.

(9) Zade, S. S.; Bendikov, M. From oligomers to polymer: convergence in the HOMO-LUMO gaps of conjugated oligomers. *Org. Lett.* **2006**, *8* (23), 5243−5246.

(10) Schlenk, W.; Appenrodt, J.; Michael, A.; Thal, A. Über Metalladditionen an mehrfache Bindungen. *Ber. Dtsch. Chem. Ges.* **1914**, *47* (1), 473−490.

(11) Wittig, G. 1. Synthesen mit lithiumorganischen Verbindungen. *Angew. Chem.* **1940**, *53* (23−24), 241−247.

(12) Evans, A. G.; Evans, J. C.; Emes, P. J.; James, C. L.; Pomery, P. J. Reactions of Radical Anions. *J. Chem. Soc. B* **1971**, *0* (0), 1484−1493.

(13) Russell, G. A.; Janzen, E. G.; Strom, E. T. The Formation of Radical-Anions by Electron Transfer Between Anions and Their Unsaturated Analogs in Dimethyl Sulfoxide Solution. *J. Am. Chem. Soc.* **1962**, *84* (84), 4155−4157.

(14) Aylward, G. H.; Garnett, J. L.; Sharp, J. H. Electrochemistry of Azobenzene in Dimethylformamide. *J. Am. Chem. Soc.* **1966**, No. 73, 137−138.

(15) Bellamy, A. J. Observation by cyclic voltammetry of the addition of electrogenerated − CH2CN to aromatic carbonyl compounds. *J. Chem. Soc., Chem. Commun.* **1975**, No. 23, 944−945.

(16) Bellamy, A. J.; MacKirdy, I. S.; Niven, C. E. Cyclic voltammetry of azopyridines, phenylazopyridines, and azobenzene in acetonitrile and dimethylformamide. *J. Chem. Soc., Perkin Trans.* **1983**, *2*, 183−185.

(17) Nandadulal, P.; Subhas, S.; Sreebrata, G. Redox induced electron transfer in doublet azo-anion diradical rhenium(II) complexes. Characterization of complete electron transfer series. *Inorg. Chem.* **2010**, *49* (6), 2649−2655.

(18) Roy, S.; Pramanik, S.; Patra, S. C.; Adhikari, B.; Mondal, A.; Ganguly, S.; Pramanik, K. Ambient-Stable Bis-Azoaromatic-Centered Diradical (L·)M(L·) Complexes of Rh(III): Synthesis, Structure, Redox, and Spin-Spin Interaction. *Inorg. Chem.* **2017**, *56* (21), 12764−12774.

(19) Shivakumar, M.; Pramanik, K.; Bhattacharyya, I.; Chakravorty, A. Chemistry of metal-bound anion radicals. A family of mono- and bis(azopyridine) chelates of bivalent ruthenium. *Inorg. Chem.* **2000**, *39* (19), 4332−4338.

(20) Chakraborty, I.; Sengupta, S.; Das, S.; Banerjee, S.; Chakravorty, A. Chemistry of monovalent and bivalent rhenium: synthesis, structure, isomer specificity and metal redox of azoheterocycle complexes. *Dalton Trans.* **2003**, No. 1, 134−140.

(21) Xie, Y.; Li, M.; Ma, Y.; Lin, F.; Zhu, H.; Li, W.; Jiang, S.; Shen, C.; Jia, Z.; Zhang, K. Azopyridine Aqueous Electrochemistry Enables Superior Organic AZIBs. *ACS Appl. Mater. Interfaces.* **2024**, *16* (44), 60132−60141.

(22) Goulet-Hanssens, A.; Utecht, M.; Mutruc, D.; Titov, E.; Schwarz, J.; Grubert, L.; Bléger, D.; Saalfrank, P.; Hecht, S. Electrocatalytic Z → E Isomerization of Azobenzenes. *J. Am. Chem. Soc.* **2017**, *139* (1), 335−341.

(23) Bléger, D.; Dokic, J.; Peters, M. V.; Grubert, L.; Saalfrank, P.; Hecht, S. Electronic decoupling approach to quantitative photo-

https://doi.org/10.1021/acs.joc.5c00315
J. Org. Chem. XXXX, XXX, XXX−XXX

switching in linear multiazobenzene architectures. *J. Phys. Chem. B* **2011**, *115* (33), 9930−9940.
(24) Zhao, F.; Grubert, L.; Hecht, S.; Bléger, D. Orthogonal switching in four-state azobenzene mixed-dimers. *Chem. Commun.* **2017**, *53* (23), 3323−3326.
(25) Wang, W.; Tan, G.; Feng, R.; Fang, Y.; Chen, C.; Ruan, H.; Zhao, Y.; Wang, X. Stable, yet "naked", azo radical anion ArNNAr and dianion ArNNAr2 (Ar = 4-CN-2,6-iPr2-C6H2)with selective CO2 activation. *Chem. Commun.* **2020**, *56* (56), 3285−3288.
(26) He, L.; Wang, G.; Tang, Q.; Fu, X.; Gong, C. Synthesis and characterization of novel electrochromic and photoresponsive materials based on azobenzene-4,4′-dicarboxylic acid dialkyl ester. *J. Mater. Chem. C* **2014**, *2* (38), 8162−8169.
(27) Slavov, C.; Yang, C.; Schweighauser, L.; Boumrifak, C.; Dreuw, A.; Wegner, H. A.; Wachtveitl, J. Connectivity matters - ultrafast isomerization dynamics of bisazobenzene photoswitches. *Phys. Chem. Chem. Phys.* **2016**, *18* (22), 14795−14804.
(28) Moneo, Á.; Justino, G. C.; Carvalho, M. F. N. N.; Oliveira, M. C.; Antunes, A. M. M.; Bléger, D.; Hecht, S.; Telo, J. P. Electronic communication in linear oligo(azobenzene) radical anions. *J. Phys. Chem. A* **2013**, *117* (51), 14056−14064.
(29) Franz, E.; Kunz, A.; Oberhof, N.; Heindl, A. H.; Bertram, M.; Fusek, L.; Taccardi, N.; Wasserscheid, P.; Dreuw, A.; Wegner, H. A.; Brummel, O.; Libuda, J. Electrochemically Triggered Energy Release from an Azothiophene-Based Molecular Solar Thermal System. *ChemSusChem* **2022**, *15* (18), No. e202200958.
(30) Rhodes, C. J. An ESR Study of the Radical Cation of trans-Azobenzene. *J. Chem. Soc.* **1990**, *11*, 799−801.
(31) Rhodes, C. J.; Agirbas, H.; Lindgren, M.; Antzutkin, O. N. An EPR and Theoretical Investigation of Azoalkane and Azobenzene Radical Cations. *J. Chem. Soc., Perkin Trans.* **1993**, *2*, 2135−2139.
(32) Eriksson, A.; Nyholm, L. A comparison of the electrochemical properties of some azosalicylic acids at glassy carbon electrodes by cyclic and hydrodynamic voltammetry. *Electrochim. Acta* **1999**, *44* (23), 4029−4040.
(33) Eriksson, A.; Nyholm, L. Coulometric and spectroscopic investigations of the oxidation and reduction of some azosalicylic acids at glassycarbon electrodes. *Electrochim. Acta* **2001**, *46* (8), 1113−1129.
(34) Kaplan, M. L.; Haddon, R. C.; Raghavachari, K.; Menezes, S.; Schilling, F. C.; Hauser, J. J.; Marshall, J. H. Electrical Conductivity in TCNQ Salts of Bis(4-dimethylaminophenylimino) sulfur and its Structural Analogues. *Mol. Cryst. Liq. Cryst.* **1982**, *80* (1), 51−66.
(35) Goulet-Hanssens, A.; Rietze, C.; Titov, E.; Abdullahu, L.; Grubert, L.; Saalfrank, P.; Hecht, S. Hole Catalysis as a General Mechanism for Efficient and Wavelength-Independent Z → E Azobenzene Isomerization. *Chem.* **2018**, *4* (7), 1740−1755.
(36) Schatz, D.; Baumert, M. E.; Kersten, M. C.; Schneider, F. M.; Nielsen, M. B.; Hansmann, M. M.; Wegner, H. A. para-Amino-azobenzenes - Bipolar Redox-Active Molecules. *Angew. Chem., Int. Ed.* **2024**, *63*, No. e202405618.
(37) Gajda, K.; Zarychta, B.; Daszkiewicz, Z.; Domanski, A. A.; Ejsmont, K. Substituent effects in trans-p,p'-di-substituted azobenzenes: X-ray structures at 100 K and DFT-calculated structures. *Acta Crys. C* **2014**, *70* (70), 575−579.
(38) Dehu, C.; Meyers, F.; Brédas, J. L. Donor-Acceptor Diphenylacetylenes: Geometric Structure, Electronic Structure, and Second-Order Nonlinear Optical Properties. *J. Am. Chem. Soc.* **1993**, *115* (115), 6198−6206.
(39) Klopman, G.; Doddapaneni, N. Electrochemical behavior of cis and trans azobenzenes. *J. Phys. Chem.* **1974**, *78*, 1825−1828.
(40) Laviron, E.; Mugnier, Y. A Study of The Isomerization of cis-Azobenzene Anion Radical in Dimethylformamide. *J. Electroanal. Chem.* **1978**, *93* (93), 69−73.
(41) Wayner, D. D. M.; Griller, D. Oxidation and reduction potentials of transient free radicals. *J. Am. Chem. Soc.* **1985**, *107*, 7764−7765.
(42) Wayner, D. D. M.; Houmam, A. Redox Properties of Free Radicals. *Acta Chem. Scand.* **1998**, *52*, 377−384.
(43) Grampp, G.; Mureşanu, C.; Landgraf, S. Solvent influence on the electrochemical reduction of photochemically generated cis-azobenzene. *J. Electroanal. Chem.* **2005**, *582* (1−2), 171−178.
(44) Glotz, G.; Knaipp, K.; Maier, M. S.; Hüll, K.; Novak, A.; Kelterer, A.-M.; Griebenow, T.; Herges, R.; Trauner, D.; Gescheidt, G. To Isomerize or not to Isomerize? E/Z Isomers of Cyclic Azobenzene Derivatives and Their Reactivity Upon One-Electron Reduction. *Chem.—Eur. J.* **2023**, *29* (35), No. e202300146.
(45) Luo, C.; Ji, X.; Chen, J.; Gaskell, K. J.; He, X.; Liang, Y.; Jiang, J.; Wang, C. Solid-State Electrolyte Anchored with a Carboxylated Azo Compound for All-Solid-State Lithium Batteries. *Angew. Chem., Int. Ed.* **2018**, *57* (28), 8567−8571.
(46) Park, J.; Kim, M.; Choi, J.; Lee, S.; Kim, J.; Han, D.; Jang, H.; Park, M. Recent Progress in High-voltage Aqueous Zinc-based Hybrid Redox Flow Batteries. *Chem.—Asian J.* **2023**, *18* (2), No. e202201052.
(47) Zhang, L.; Qian, Y.; Feng, R.; Ding, Y.; Zu, X.; Zhang, C.; Guo, X.; Wang, W.; Yu, G. Reversible redox chemistry in azobenzene-based organic molecules for high-capacity and long-life nonaqueous redox flow batteries. *Nat. Commun.* **2020**, *11* (1), 3843.
(48) Wang, Z.; Erhart, P.; Li, T.; Zhang, Z.-Y.; Sampedro, D.; Hu, Z.; Wegner, H. A.; Brummel, O.; Libuda, J.; Nielsen, M. B.; Moth-Poulsen, K. Storing energy with molecular photoisomers. *Joule* **2021**, *5* (12), 3116−3136.
(49) Franz, E.; Jung, J.; Kunz, A.; Wegner, H. A.; Brummel, O.; Mollenhauer, D.; Libuda, J. How Adsorption Affects the Energy Release in an Azothiophene-Based Molecular Solar-Thermal System. *J. Phys. Chem. Lett.* **2023**, *14* (6), 1470−1477.
(50) Greenfield, J. L.; Gerkman, M. A.; Gibson, R. S. L.; Han, G. G. D.; Fuchter, M. J. Efficient Electrocatalytic Switching of Azoheteroarenes in the Condensed Phases. *J. Am. Chem. Soc.* **2021**, *143* (37), 15250−15257.
(51) Schatz, D.; Burdenski, C.; Schneider, F. M.; Hansmann, M. M.; Wegner, H. A. Amino-substituted Azoxybenzenes as Potential Redox-Active Catholyte Materials. *Chem.—Eur. J.* **2025**, *31*, No. e202404001.

https://doi.org/10.1021/acs.joc.5c00315
J. Org. Chem. XXXX, XXX, XXX−XXX

5 Additional Contributions

5.1 An Incremental System to Predict the Effect of London Dispersion Donors in All-*meta*-Substituted Azobenzenes

Reference: C. Di Berardino[+], M. A. Strauss[+], D. Schatz, H. A. Wegner *Chem*. *Eur*. *J*. **2022**, *28*, e202104284.

DOI: 10.1002/chem.202104284

[+]These authors contributed equally.

Predictive models based on incremental system exist for many chemical phenomena, thus allowing easy estimates. Despite their low magnitude in isolated systems London dispersion interactions are ubiquitous in manifold situations raging from solvation to catalysis or in biological systems. Based on our azobenzene systems, we systemically determined the London dispersion donor strength of the alkyl substitutes Me, Et, *i*Pr up to *t*Bu. Based on this data, we were able to implement an incremental system for London dispersion for the azobenzene scheme. We propose an equation that allows the prediction of the effect of change of substituents on London dispersion interactions in azobenzenes, which has to be validated in similar molecular arrangements in the future.

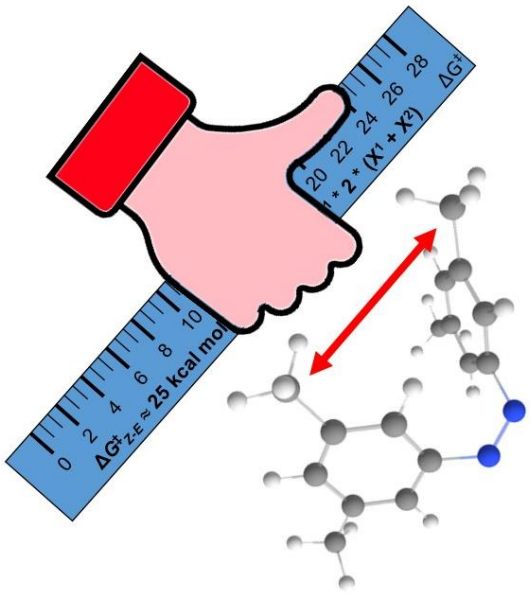

5.2 Investigation of Alkyl–Aryl Interactions Using the Azobenzene Switch – The Influence of the Electronic Nature of Aromatic London Dispersion Donors

Reference: D. Schatz[+], A. Kunz[+], A. R. Raab, H. A. Wegner, *Synlett* **2023**, *34*, 1153–1158.

DOI: 10.1055/a-1951-2833

[+]These authors contributed equally.

Herein we report the synthesis of nonsymmetrically substituted azobenzene derivatives with *meta*-alkyl substituents on one side and *meta*-aryl moieties with electron-donating or electron-withdrawing groups on the other side. The half-lives for the thermal (*Z*)- to (*E*)-isomerization of these molecules were measured in *n*-octane, which allows investigation of the strength of the aryl–alkyl interactions between their substituents. It was found that the London dispersion donor strength of the alkyl substrate is the decisive factor in the observed stabilization, whereas the electronic structure of the aryl fragment does not influence the isomerization in a significant way.

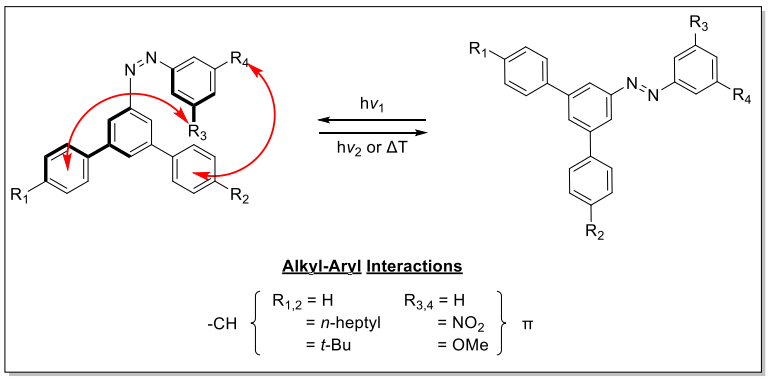

5.3 Synthesis and investigation of a *meta*[6]cycloparaphenylene gold(I) *N*-heterocyclic carbene complex

Reference: F. Bernt, C. M. Leonhardt, D. Schatz, H. A. Wegner, *Chem*. *Commun*. **2024**, *60*, 3055–3058

DOI: 10.1039/D3CC06225B

Meta[n]cycloparaphenylenes (*m*[n]CPPs) as well as N-heterocyclic carbene (NHC) gold(I)-complexes are intriguing building blocks for material and life sciences due to their extraordinary structures resulting in unique photophysical properties. Herein, we report the combination of a *m*[6]CPP with a N-heterocyclic carbene serving as a ligand in a linear gold(I)-complex possessing the form [AuBr(NHC)]. Solid-state structures of both the precursor and the complex are presented and discussed. Moreover, we investigated the luminescence properties of both the imidazolium intermediate and the corresponding gold(I)-complex.

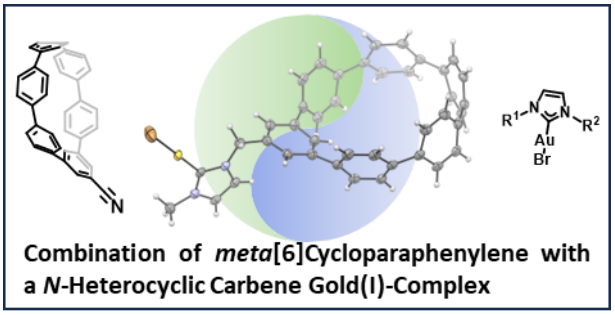

Combination of *meta*[6]Cycloparaphenylene with a *N*-Heterocyclic Carbene Gold(I)-Complex

5.4 Molecular Wind-Up Meter for the Quantification of London Dispersion Interactions

Reference: C. Averdunk[+], K. Hanke[+], D. Schatz[+], H. A. Wegner, *Acc*. *Chem*. *Res*. **2024**, *2*, 257–266.

DOI: 10.1021/acs.accounts.3c00616

[+]These authors contributed equally.

The experimental quantification of interactions on the molecular level provides the necessary basis for the design of functional materials and chemical processes. The interplay of multiple parameters and the small quantity of individual interactions pose a special challenge for such endeavors. The common method is the use of molecular balances, which can exist in two different states. Thereby, a stabilizing interaction can occur in one of the states, favoring its formation and thus affecting the thermodynamic equilibrium of the system. One challenge is determining the change in this equilibrium since various analytical methods could not be applied to fast-changing equilibria. A new and promising method for quantifying molecular interactions is the use of Molecular Wind-up Meters (MWM) in which the change in kinetics, rather than the effect on thermodynamics, is investigated. An MWM is transformed with an energy input (e.g. irradiation) into a metastable state. Then, the rate of thermal transformation back to the ground state is measured. The strength of interactions present in the metastable state controls the kinetics of the back reactions, allowing direct correlation. The advantage of this approach lies in the high sensitivity (energy differences can be larger by 1 order of magnitude) and, in general, allows the use of a broader range of solvents and analytical methods. An Azobenzene-based MWM has been established as a powerful tool to quantify London dispersion interactions. London dispersion (LD) represents the attractive part of the van der Waals potential. Although neglected in the past due to its weak character, it has been shown that the influence of LD on the structure, stability, and reactivity of matter can be decisive. Especially in larger molecules, its energy contribution increases overproportionately with the number of atoms, which has sparked increasing interest in the use of so-called dispersion energy donors (DED) as a new structural element. Application of the azobenzene-based MWM not only allowed the differentiation of bulkiness, but also systematically addressed the influence of the length of n-alkyl chains. Additionally, the solvent influence on LD was studied. Based on the azobenzene MWM, an increment system has been proposed, allowing a rough estimate of the effect of a specific DED.

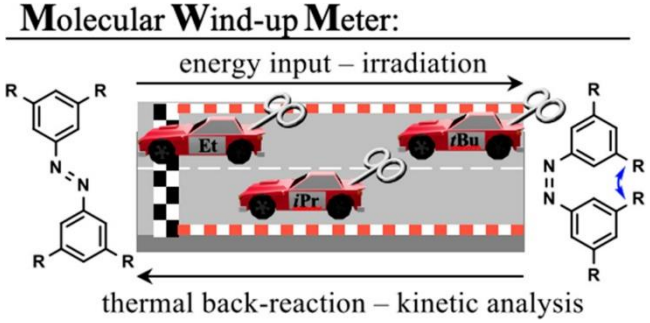

5.5 Expanding the Clip-and-Cleave Concept: Approaching Enantioselective C–H Hydroxylations by Copper Imine Complexes Using O_2 and H_2O_2 as Oxidants

Reference: A. Petrillo, K. F. Kirchgeßner-Prado, D. Hiller, K. A. Eisenlohr, G. Rubin, C. Würtele, R. Goldberg, D. Schatz, M. C. Holthausen, I. Garcia-Bosch, S. Schindler, *J. Am. Chem. Soc.* **2024**, *37*, 25689–25700.

DOI: 10.1021/jacs.4c07777

Copper-mediated aromatic and aliphatic C–H hydroxylations using benign oxidants (O_2 and H_2O_2) have been studied intensively in recent years to meet the growing demand for efficient and green C–H functionalizations. Herein, we report an enantioselective variant of the so-called clip-and-cleave concept for intramolecular ligand hydroxylations by the application of chiral diamines as directing groups. We tested the hydroxylation of cyclohexanone and 1-acetyladamantane under different oxidative conditions (Cu^I/O_2; Cu^I/H_2O_2; Cu^{II}/H_2O_2) in various solvents. As an outstanding example, we obtained (R)-1-acetyl-2-adamantol with a yield of 37% and >99:1 enantiomeric excess from hydroxylation in acetone using Cu^I and O_2. Low-temperature stopped-flow UV–Vis measurements in combination with density functional theory (DFT) computations revealed that the hydroxylation proceeds *via* a bis(μ-oxido) dicopper intermediate. The reaction product represents a rare example of an enantiopure 1,2-difunctionalized adamantane derivative, which paves the way for potential pharmacological studies. Furthermore, we found that 1-acetyladamantane can be hydroxylated in a one-pot reaction under air with isolated yields up to 36% and enantiomeric ratios of 96:4 using Cu^{II}/H_2O_2 in MeOH.

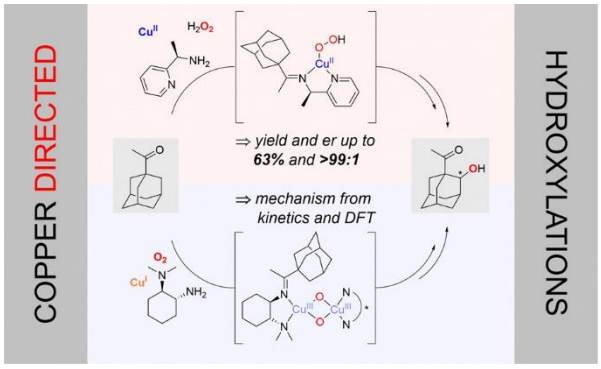

6 Abbreviations

AB	Azobenzene
AOB	Azoxybenzenes
MOST	Molecular solar thermal energy storage
PSS	Photostaionary state
UV	Ultraviolet
VIS	Visible
LED	Light-emitting diode
IR	Infrared
HOMO	Highest occupied molecular orbital
LUMO	Lowest unoccupied molecular orbital
Fc	Ferrocene
EPR	Electron paramagnetic resonance
ACN	Acetonitrile
CV	Cyclic voltammetry
SC-XRD	Single-crystal X-ray diffraction
CCDC	Cambridge crystallographic data centre
RFB	Redox-flow battery

7 Acknowledgement

No acknowledgments are included in this version of the thesis.

No acknowledgments are included in this version of the thesis.

8 References

[1] E. Mitscherlich, *Ann. Pharm.* **1834**, *12*, 311–314.
[2] A. Bafana, S. S. Devi, T. Chakrabarti, *Environ. Rev.* **2011**, *19*, 350–371.
[3] G. Domagk, *Dtsch. Med. Wochenschr.* **1935**, *61*, 250–253.
[4] M. Wainwright, J. E. Kristiansen, *Dyes Pigment.* **2011**, *88*, 231–234.
[5] G. S. Hartley, *Nature* **1937**, *140*, 281.
[6] M.-M. Russew, S. Hecht, *Adv. Mater.* **2010**, *22*, 3348–3360.
[7] M. A. Strauss, H. A. Wegner, *Angew. Chem. Int. Ed.* **2019**, *58*, 18552–18556.
[8] J. Garcia-Amorós, M. Díaz-Lobo, S. Nonell, D. Velasco, *Angew. Chem. Int. Ed.* **2012**, *51*, 12820–12823.
[9] N. Eleya, S. Ghosh, E. Lork, A. Staubitz, *J. Mater. Chem. C* **2021**, *9*, 82–87.
[10] M. Ishikawa, T. Ohzono, T. Yamaguchi, Y. Norikane, *Sci. Rep.* **2017**, 6909.
[11] C. Brown, S. K. Rastogi, S. L. Barrett, H. E. Anderson, E. Twichell, S. Gralinski, A. McDonald, *J. Photochem. Photobiol. A* **2017**, 140–145.
[12] G. S. Hartley, R. J. W. Le Févre, *J. Chem. Soc.* **1939**, 531–535.
[13] A. Samanta, A. Babalhavaeji, M.-x. Dong, G. A. Wooley, *Angew. Chem. Int. Ed.* **2013**, *52*, 14127–14130.
[14] C. E. Weston, R. D. Richardson, M. J. Fuchter, *Chem. Commun.* **2016**, *52*, 4521–4524.
[15] C. J. Brown, *Acta Cryst.* **1966**, *21*, 146–152.
[16] A. Mostad, C. Rømming, *Acta Chem. Scand.* **1971**, *25*, 3561-3568.
[17] S. Lee, H. S. Kang, J.-K. Park, *Adv. Mater.* **2012**, *24*, 2069–2103.
[18] H. Kumar, G. Parthiban, A. Velloth, J. Saini, R. De, S. K. Pal, K. S. Hazra, S. Venkataramani, *Chem. Eur. J.* **2024**, *30*, e202401836.
[19] Z. Mahimwalla, K. G. Yager, J. Mamiya, A. Shishido, A. Priimagi, C. J. Barrett, *Polym. Bull.* **2012**, *69*, 967–1006.
[20] Z. Deng, K. Li, A. Priimagi, H. Zeng, *Nat. Mater.* **2024**, *23*, 1728-1734.
[21] K. Hüll, J. Morstein, D. Trauner, *Chem. Rev.* **2018**, *118*, 10710–10747.
[22] P. Kobauri, F. J. Dekker, W. Szymanski, B. L. Feringa, *Angew. Chem. Int. Ed.* **2023**, *62*, e202300681.
[23] L. Schweighauser, M. A. Strauss, S. Bellotto, H. A. Wegner, *Angew. Chem. Int. Ed.* **2015**, *54*, 13436–13439.
[24] C. Di Berardino, M. A. Strauss, D. Schatz, H. A. Wegner, *Chem. Eur. J.* **2022**, *28*, e202104284.
[25] D. Schatz, A. Kunz, A. R. Raab, H. A. Wegner, *Synlett* **2023**, *34*, 1153–1158.
[26] C. Averdunk, K. Hanke, D. Schatz, H. A. Wegner, *Acc. Chem. Res.* **2024**, *57*, 257–266.
[27] B. L. Feringa, *Noble Lecture*, *2016*.
[28] B. L. Feringa, *Angew. Chem. Int. Ed.* **2017**, *56*, 11060–11078.
[29] S. Ould Amrouche, D. Rekioua, T. Rekioua, S. Bacha, *Int. J. Hydrogen Energy.* **2016**, *41*, 20914–20927.
[30] W. S. Ho, S. Macchietto, J. S. Lim, H. Hashim, Z. A. Muis, W. H. Liu, *Renew. Sustain. Energy Rev.* **2016**, *58*, 1100–1107.
[31] X. Zhang, L.-D. Zhao, *J. Materiomics.* **2015**, *1*, 92–105.

[32] K. Moth-Poulsen, D. Coso, K. Börjesson, N. Vinokurov, S. K. Meier, A. Majumdar, K. P. C. Vollhardt, R. A. Segalman, *Energy Environ. Sci.* **2012**, *5*, 8534.
[33] R. Luther, F. Weigert, *Z. Physik. Chem.* **1905**, *53*, 385–427.
[34] F. Weigert, *Z. Physik. Chem.* **1908**, *63*, 458-466.
[35] F. Weigert, *Ber. Dtsch. Chem. Ges.* **1909**, *42*, 850–862.
[36] A. Lennartson, A. Roffey, K. Moth-Poulsen, *Tetrahedron Lett.* **2015**, *56*, 1457–1465.
[37] C.-L. Sun, C. Wang, R. Boulatov, *ChemPhotoChem* **2019**, *3*, 268–283.
[38] R. Losantos, D. Sampedro, *Molecules* **2021**, *26*, 3796.
[39] Z. Wang, P. Erhart, T. Li, Z.-Y. Zhang, D. Sampedro, Z. Hu, H. A. Wegner, O. Brummel, J. Libuda, M. Brøndsted Nielsen, K. Moth-Poulsen, *Joule* **2021**, *5*, 3116–3136.
[40] A. Gimenez-Gomez, L. Magson, B. Peñin, N. Sanosa, J. Soilán, R. Losantos, D. Sampedro, *Photochem.* **2022**, *2*, 694–716.
[41] Z. Wang, H. Hölzel, K. Moth-Poulsen, *Chem. Soc. Rev.* **2022**, *51*, 7313–7326.
[42] J. Usuba, G. D. Han, *Trends Chem.* **2023**, *5*, 577–580.
[43] A. Gimenez-Gomez, L. Magson, C. Merino-Robledillo, S. Hernáez-Troya, N. Sanosa, D. Sampedro, I. Funes-Ardoiz, *React. Chem. Eng.* **2024**, *9*, 1629–1640.
[44] M. Dong, A. Babalhavaeji, S. Samanta, A. A. Beharry, G. A. Wooley, *Acc. Chem. Res.* **2015**, *48*, 2662–2670.
[45] A. A. Beharry, O. Sadovski, G. A. Wooley, *J. Am. Chem. Soc.* **2011**, *133*, 19684–19687.
[46] A. Samanta, T. M. McCormick, S. K. Schmidt, D. S. Seferos, G. A. Wooley, *Chem. Commun.* **2013**, *49*, 10314–10316.
[47] D. Bléger, J. Schwarz, A. M. Brouwer, S. Hecht, *J. Am. Chem. Soc.* **2012**, *134*, 20597–20600.
[48] C. Knie, M. Utecht, F. Zhai, H. Kulla, S. Kovalenko, A. M. Brouwer, P. Saalfrank, S. Hecht, D. Bléger, *Chem. Eur. J.* **2014**, *20*, 16492–16501.
[49] D. B. Konrad, G. Savasci, L. Allmendinger, D. Trauner, C. Ochsenfeld, A. M. Ali, *J. Am. Chem. Soc.* **2020**, *142*, 6538–6547.
[50] M. J. Hansen, M. M. Lerch, W. Szymanski, B. L. Feringa, *Angew. Chem. Int. Ed.* **2016**, *55*, 13514–13518.
[51] C. E. Weston, R. D. Richardson, A. J. P.White, M. J. Fuchter, *J. Am. Chem. Soc.* **2014**, *136*, 11878–11881.
[52] J. Calbo, C. E. Weston, A. J. P.White, H. S. Rzepa, J. Contreras-García, M. J. Fuchter, *J. Am. Chem. Soc.* **2017**, *139*, 1261–1274.
[53] C. Slavov, C. Yang, A. H. Heindl, H. A. Wegner, A. Dreuw, J. Wachtveitl, *Angew. Chem. Int. Ed.* **2020**, *59*, 380–387.
[54] A. H. Heindl, H. A. Wegner, *Chem. Eur. J.* **2020**, *26*, 13730–13737.
[55] M. Kathan, S. Hecht, *Chem. Soc. Rev.* **2017**, *46*, 5536–5550.
[56] Z.-Y. Zhang, D. Dong, T. Bösking, T. Dang, C. Liu, W. Sun, M. Xie, S. Hecht, T. Li, *Angew. Chem. Int. Ed.* **2024**, *63*, e202404528.
[57] C. R. Crecca, A. E. Roitberg, *J. Phys. Chem. A* **2006**, *110*, 8188–8203.
[58] O. Sadovski, A. A. Beharry, F. Zhang, G. A. Wooley, *Angew. Chem. Int. Ed.* **2009**, *48*, 1484–1486.

[59] Z. Ahmed, A. Siiskonen, M. Virkki, A. Priimagi, *Chem. Commun.* **2017**, *53*, 12520–12523.
[60] C. Boumrifak, C. Yang, S. Bellotto, H. A. Wegner, J. Wachtveitl, A. Dreuw, C. Slavov, *ChemPhotoChem* **2019**, *3*, 411–417.
[61] D. Dong, Z.-Y. Zhang, T. Dang, T. Li, *Angew. Chem. Int. Ed.* **2024**, *63*, e202407186.
[62] V. A. Bren', A. D. Dubonosov, V. I. Minkin, V. A. Chernoivanov, *Russ. Chem. Rev.* **1991**, *60*, 451–469.
[63] E. Durgun, J. C. Grossman, *J. Phys. Chem. Lett.* **2013**, *4*, 854–860.
[64] A. H. Heindl, J. Becker, H. A. Wegner, *Chem. Sci.* **2019**, *10*, 7418–7425.
[65] R. Siewertsen, H. Neumann, B. Buchheim-Stehn, R. Herges, C. Näther, F. Renth, F. Temps, *J. Am. Chem. Soc.* **2009**, *131*, 15594–15595.
[66] M. Hammerich, C. Schütt, C. Stähler, P. Lentes, F. Röhricht, R. Höppner, R. Herges, *J. Am. Chem. Soc.* **2016**, *138*, 13111–13114.
[67] A. M. Kolpak, J. C. Grossman, *Nano. Lett.* **2011**, *11*, 3156–3162.
[68] W. Luo, Y. Feng, C. Cao, M. Li, E. Liu, S. Li, C. Qin, W. Hu, W. Feng, *J. Mater. Chem. A* **2015**, *3*, 11787–11795.
[69] W. Pang, J. Xue, P. Hua, *Sci. Rep.* **2019**, *9*, 5224.
[70] A. Kunz, A. H. Heindl, A. Dreos, Z. Wang, K. Moth-Poulsen, J. Becker, H. A. Wegner, *ChemPlusChem* **2019**, *84*, 1145–1148.
[71] R. Reuter, H. A. Wegner, *Chem. Commun.* **2013**, *49*, 146–148.
[72] Y. Shi, M. A. Gerkman, Q. Qiu, S. Zhang, G. G. D. Han, *J. Mater. Chem. A* **2021**, *9*, 9798–9808.
[73] K. Wang, H. Yu, J. Gao, Y. Feng, W. Feng, *J. Mater. Chem. C* **2024**, *12*, 3811–3837.
[74] M. A. Gerkman, R. S. L. Gibson, J. Calbo, Y. Shi, M. J. Fuchter, G. G. D. Han, *J. Am. Chem. Soc.* **2020**, *142*, 8688–8695.
[75] Q. Qiu, M. A. Gerkman, G. G. D. Han, *Chem. Commun.* **2021**, *57*, 9458–9461.
[76] K. Griffiths, N. R. Halcovitch, J. M. Griffin, *New J. Chem.* **2022**, *46*, 4057–4061.
[77] X. Li, S. Cho, G. G. D. Han, *ACS Mater. Au* **2023**, *3*, 37–42.
[78] A. Dreos, Z. Wang, J. Udmark, A. Ström, P. Erhart, K. Börjesson, M. Brøndsted Nielsen, K. Moth-Poulsen, *Adv. Energy Mater.* **2018**, *8*, 1703401.
[79] Z. Wang, R. Losantos, D. Sampedro, M. Morikawa, K. Börjesson, N. Kimizuka, K. Moth-Poulsen, *J. Mater. Chem. A* **2019**, *7*, 15042–15047.
[80] Z. Wang, A. Roffey, R. Losantos, A. Lennartson, M. Jevric, A. U. Petersen, M. Quant, A. Dreos, X. Wen, D. Sampedro, K. Börjesson, K. Moth-Poulsen, *Energy Environ. Sci.* **2019**, *12*, 187–193.
[81] S. K. Panigrahi, A. K. Mishura, *J. Photochem. Photobiol. C* **2019**, *41*, 100318.
[82] K. Masutani, M. Morikawa, N. Kimizuka, *Chem. Commun.* **2014**, *50*, 15803–15806.
[83] K. Ishiba, M. Morikawa, C. Chikara, T. Yamada, K. Iwase, M. Kawakita, N. Kimizuka, *Angew. Chem. Int. Ed.* **2015**, *54*, 1532–1536.
[84] M. Morikawa, H. Yang, K. Ishiba, K. Masutani, J. K.-H. Hui, N. Kimizuka, *Chem. Lett.* **2020**, *49*, 736–740.
[85] D. Schatz, C. Averdunk, R. Fritzius, H. A. Wegner, *ChemRxiv* **2025**, 10.26434/chemrxiv-2025-7v3ds-v2.
[86] J. Hu, S. Huang, M. Yu, H. Yu, *Adv. Energy Mater.* **2019**, *9*, 1901363.

[87] C. Szolnoky, *Characterisation of Molecular Solar Thermal (MOST) Energy Storage Materials in Miniature Windows*, Chalmers University, Sweden, **2022**.
[88] D. Schulte-Frohlinde, *Liebigs Ann. Chem.* **1958**, *1*, 131–138.
[89] S. Ciccione, J. Halpern, *Can. J. Chem.* **1959**, *37*, 1903–1910.
[90] L. Dong, Y. Chen, F. Zhai, L. Tang, W. Gao, J. Tang, Y. Feng, W. Feng, *J. Mater. Chem. A* **2020**, *8*, 18668–18676.
[91] A. Goulet-Hanssens, M. Utecht, D. Mutruc, E. Titov, J. Schwarz, L. Grubert, D. Bléger, P. Saalfrank, S. Hecht, *J. Am. Chem. Soc.* **2017**, *139*, 335–341.
[92] A. Goulet-Hanssens, C. Rietze, E. Titov, L. Abdullahu, L. Grubert, P. Saalfrank, S. Hecht, *Chem* **2018**, *4*, 1740–1755.
[93] D. Schatz, H. A. Wegner, *J. Org. Chem.* **2025**, *accepted*.
[94] K. Kotwica, I. Wielgus, A. Proń, *Materials* **2021**, *14*, 5155.
[95] M. Winkler, K. N. Houk, *J. Am. Chem. Soc.* **2007**, *129*, 1805–1815.
[96] X.-D. Tang, Y. Liao, H. Geng, Z.-G. Shuai, *J. Mater. Chem.* **2012**, *22*, 18181.
[97] T. Koopmans, *Physica* **1934**, *1*, 104–113.
[98] N. Heinrich, W. Koch, G Frenking, *Chem. Phys. Letters* **1986**, *124*, 20–25.
[99] J. D. Hofmann, F. L. Pfanschilling, N. Krawczyk, P. Geigle, L. Hong, S. Schmalisch, H. A. Wegner, D. Mollenhauer, J. Janek, D. Schröder, *Chem. Mater.* **2018**, *30*, 762–774.
[100] B. Uno, Y. Matsuhisa, K. Kano, T. Kubota, *Chem. Pharm. Bull.* **1984**, *32*, 1–10.
[101] J. L. Sadler, A. J. Bard, *J. Am. Chem. Soc.* **1968**, *90*, 1979–1989.
[102] S. S. Zade, M. Bendikov, *Org. Lett.* **2006**, *8*, 5243–5246.
[103] R. Schenk, H. Gregorius, K. Meerholz, J. Heinze, K. Müllen, *J. Am. Chem. Soc.* **1991**, *113*, 2634–2646.
[104] T. Shimizu, N. Tanifuji, H. Yoshikawa, *Angew. Chem. Int. Ed.* **2022**, *61*, e202206093.
[105] M. Ishidate, Y. Hashimoto, *Chem. Pharm. Bull.* **1962**, *10*, 125–133.
[106] J. A. Miller, C. A. Baumann, *Cancer Res.* **1945**, *5*, 227–234.
[107] S. Zbaida, A. M. Stoddart, W. G. Levine, *Chem. Biol. Interactions* **1989**, *69*, 61–71.
[108] A. Stolz, *Appl. Microbiol. Biotechnol.* **2001**, *56*, 69–80.
[109] W. G. Levine, *Drug Metab. Rev.* **1991**, *23*, 253–309.
[110] W. Schlenk, J. Appenrodt, A. Michael, A. Thal, *Ber. Dtsch. Chem. Ges.* **1914**, *47*, 473–490.
[111] G. Wittig, *Angew. Chem.* **1940**, *53*, 241–247.
[112] A. G. Evans, J. C. Evans, P. J. Emes, C. L. James, P. J. Pomery, *J. Chem. Soc. B* **1971**, *0*, 1484–1493.
[113] G. A. Russell, E. G. Janzen, E. T. Strom, *J. Am. Chem. Soc.* **1962**, *84*, 4155–4157.
[114] L. Gattermann, *Ber. Dtsch. Chem. Ges.* **1896**, *29*, 3040–3042.
[115] F. Haber, *Bunsenges. Phys. Chem.* **1898**, *4*, 506–514.
[116] F. Haber, C. Schmidt, *Z. Physik. Chem.* **1801**, *32*, 271-287.
[117] G. H. Aylward, J. L. Garnett, J. H. Sharp, *J. Am. Chem. Soc.* **1966**, *73*, 137–138.
[118] A. J. Bellamy, *J. Chem. Soc., Chem. Commun.* **1975**, *23*, 944–945.
[119] A. J. Bellamy, I. S. MacKirdy, C.E. Niven, *J. Chem. Soc., Perkin Trans. 2* **1983**, *2*, 183–185.

[120] Y. Xie, M. Li, Y. Ma, F. Lin, H. Zhu, W. Li, S. Jiang, C. Shen, Z. Jia, K. Zhang, *ACS Appl. Mater. Interfaces.* **2024**, *16*, 60132–60141.
[121] D. Bléger, J. Dokic, M. V. Peters, L. Grubert, P. Saalfrank, S. Hecht, *J. Phys. Chem. B* **2011**, *115*, 9930–9940.
[122] C. Slavov, C. Yang, L. Schweighauser, C. Boumrifak, A. Dreuw, H. A. Wegner, J. Wachtveitl, *Phys. Chem. Chem. Phys.* **2016**, *18*, 14795–14804.
[123] Á. Moneo, G. C. Justino, M. F. N. N. Carvalho, M. C. Oliveira, A. M. M. Antunes, D. Bléger, S. Hecht, J. P. Telo, *J. Phys. Chem. A* **2013**, *117*, 14056–14064.
[124] F. Zhao, L. Grubert, S. Hecht, D. Bléger, *Chem. Commun.* **2017**, *53*, 3323–3326.
[125] P. Nandadulal, S. Subhas, G. Sreebrata, *Inorg. Chem.* **2010**, *49*, 2649–2655.
[126] K. Pramanik, M. Shivakumar, P. Ghosh, A. Chakravorty, *Inorg. Chem.* **2000**, *39*, 195–199.
[127] M. Shivakumar, K. Pramanik, I. Bhattacharyya, A. Chakravorty, *Inorg. Chem.* **2000**, *39*, 4332–4338.
[128] I. Chakraborty, S. Sengupta, S. Das: S. Banerjee, A. Chakravorty, *Dalton Trans.* **2003**, *1*, 134–140.
[129] W. Wenqping, T. Gengwen, F. Rui, F. Yong, C. Chao, R. Huapeng, Z. Yue, W. Xinping, *Chem. Commun.* **2020**, *56*, 3285–3288.
[130] E. Franz, A. Kunz, N. Oberhof, A. H. Heindl, M. Bertram, L. Fusek, N. Taccardi, P. Wasserscheid, A. Dreuw, H. A. Wegner, O. Brummel, J. Libuda, *ChemSusChem* **2022**, *15*, e202200958.
[131] C. J. Rhodes, *J. Chem. Soc.* **1990**, *11*, 799–801.
[132] C. J. Rhodes, H. Agirbas, M. Lindgren, O. N. Antzutkin, *J. Chem. Soc. Perkin Trans. 2* **1993**, *11*, 2135–2139.
[133] E. Alf, N. Leif, *Electrochim. Acta* **1999**, *44*, 4029–4040.
[134] E. Alf, N. Leif, *Electrochim. Acta* **2001**, *496*, 1113–1129.
[135] M. L. Kaplan, R. C. Haddon, K. Raghavachari, S. Menezes, F. C. Schilling, J. J. Hauser, J. H. Marshall, *Mol. Cryst. Liq. Cryst.* **1982**, *80*, 51–66.
[136] D. Schatz, M. E. Baumert, M. C. Kersten, F. M. Schneider, M. Brøndsted Nielsen, M. M. Hansmann, H. A. Wegner, *Angew. Chem. Int. Ed.* **2024**, *63*, e202405618.
[137] C. Dehu, F. Meyers, J. L. Brédas, *J. Am. Chem. Soc.* **1993**, *115*, 6198–6206.
[138] K. Gajda, B. Zarychta, Z. Daszkiewicz, A. A- Domański, K. Ejsmont, *Acta Cryst. C* **2014**, *70*, 575–579.
[139] G. M. Badger, R. G. Buttery, G. E. Lewis, *J. Chem. Soc.* **1953**, *0*, 2143–2147.
[140] G. Klopman, N. Doddapaneni, *J. Phys. Chem.* **1974**, *78*, 1825–1828.
[141] E. Laviron, Y. Mugnier, *J. Electroanal. Chem.* **1978**, *93*, 69–73.
[142] D. D. M. Wayner, D. Griller, *J. Am. Chem. Soc.* **1985**, *107*, 7764–7765.
[143] D. D. M. Wayner, A. Houman, *Acta. Chem. Scand.* **1988**, *52*, 377–384.
[144] G. Grampp, C. Mureşanu, S. Landgraf, *J. Electroanal. Chem.* **2005**, *582*, 171–178.
[145] G. Glotz, K. Knaipp, M. S. Maier, K. Hüll, A. Novak, A.-M- Kelterer, T. Griebenow, R. Herges, D. Trauner, G. Gescheidt, *Chem. Eur. J.* **2023**, *29*, e202300146.
[146] C. Luo, X. Ji, S. Hou, N. Eidson, X. Fan, Y. Liang, T. Deng, J. Juang, C. Wang, *Adv. Mater.* **2018**, *30*, e1706498.

[147] C. Luo, G.-L. Xu, X. Ji, S. Hou, L. Chen, F. Wang, J. Jiang, Z. Chen, Y. Ren, K. Amine, C. Wang, *Angew. Chem. Int. Ed.* **2018**, *57*, 2879–2883.
[148] Y. Liang, C. Luo, F. Wang, S. Hou, S.-C. Liou, T. Qing, Q. Li, J. Zheng, C. Cui, C. Wang, *Adv. Energy Mater.* **2019**, *9*, 1802986.
[149] K. Qin, S. Tan, M. Mohammadiroudbari, Z. Yang, X.-Q. Yang, E. Hu, C. Luo, *Nano Energy* **2022**, *101*, 107554.
[150] Y. Zhu, P. Chen, Y. Zhou, W. Nie, Y. Xu, *Electrochim. Acta* **2019**, *318*, 262–271.
[151] Q. Li, H. Wang, Z. Si, C. Li, J. Bai, *ChemSusChem* **2020**, *13*, 2449–2456.
[152] A. V. Desai, V. R. Seymour, R. Ettlinger, A. Pramanik, A. G. Manche, D. N. Rainer, P. S. Wheatley, J. M. Griffin, R. E. Morris, A. R. Armstrong, *Chem. Commun.* **2023**, *59*, 1321–1324.
[153] G. Zhao, Y. Zhang, Z. Gao, H. Li, S. Liu, S. Cai, X. Yang, H. Guo, X. Sun, *ACS Energy Lett.* **2020**, *5*, 1022–1031.
[154] A. E. Baumann, D. A. Burns, B. Liu, V. S. Thoi, *Commun. Chem.* **2019**, *2*, 86.
[155] V. Singh, J. Kim, B. Kang, J. Moon, S. Kim, W. Y. Kim, H. Y. Byon, *Adv. Energy Mater.* **2021**, *11*, 2003735.
[156] T. Shimizu, T. Mameuda, H. Toshima, R. Akiyoshi, Y. Kamakura, K. Wakamatsu, D. Tanaka, H. Yoshikawa, *ACS Appl. Energy Mater.* **2022**, *5*, 5191–5198.
[157] C. Luo, O. Borodin, X. Ji, S. Hou, K. J. Gaskell, X. Fan, J. Chen, T. Deng, R. Wang, J. Jiang, C. Wang, *PNAS* **2018**, *115*, 2004–2009.
[158] Y. Wang, Z. Yang, T. Xia, G. Pan, L. Zhang, H. Chen, J. Zhang, *ChemElectroChem* **2019**, *6*, 5080–5085.
[159] C. Luo, X. Ji, J. Chen, K. J. Gaskell, X. He, Y. Liang, J. Jiang, C. Wang, *Angew. Chem. Int. Ed.* **2018**, *57*, 8567–8571.
[160] C. Luo, X. Ji, J. Chen, K. J. Gaskell, X. He, Y. Liang, J. Jiang, C. Wang, *Angew. Chem.* **2018**, *130*, 8703–8707.
[161] Y. Zhou, M. Wu, Y. Luo, B. Pang, X. Su, M. Zhou, L. Han, *New J. Chem,* **2019**, *43*, 1710–1715.
[162] D. Du, Y. Chen, H. Zhang, J. Zhao, L. Jin, W. Ji, H. Huang, S. Pang, *Angew. Chem. Int. Ed.* **2024**, *63*, e202408292.
[163] L. Zhang, Y. Qian, R. Feng, Y. Ding, X. Zu, C. Zhang, X. Guo, W. Wang, G. Yu, *Nat. Commun.* **2020**, *11*, 3843.
[164] D. Xu, C. Zhang, Y. Zhen, Y. Zhao, Y. Li, *J. Power Sources* **2021**, *495*, 229819.
[165] X. Zu, L. Zhang, Y. Qian, C. Zhang, G. Yu, *Angew. Chem. Int. Ed.* **2020**, *59*, 22163–22170.
[166] X. Wang, J. Chai, A. Lashgari, J. J. Jiang, *ChemElectroChem* **2020**, *8*, 83–89.
[167] S. Singh, J. Tami, C. Gruich, B. Nguyen, J. Smith, B. Goldsmith, A. McNeil, D. Kwabi, *ChemRxiv* **2024**, 10.26434/chemrxiv-2024-zrt0b.
[168] D. Schatz, C. Burdenski, F. M. Schneider, M. M. Hansmann, H. A. Wegner, *Chem. Eur. J.* **2025**, e202404001.
[169] J. L. Greenfield, M. A. Gerkman, R. S. L. Gibson, G. G. D. Han, M. J. Fuchter, *J. Am. Chem. Soc.* **2021**, *143*, 15250–15257.
[170] E. Franz, J. Jung, A. Kunz, H. A. Wegner, O. Brummel, D. Mollenhauer, J. Libuda, *J. Phys. Chem. Lett.* **2023**, *14*, 1470–1477.